

# **Applicability of the Semi-Structured Mass Movement Mechanism for Rockfall Runout Modelling**

OM PRASAD DHAKAL


June 2021

SUPERVISORS:

Assistant Professor Dr. Bastian van den Bout

Professor Dr. Cees van Westen





# Applicability of the Semi-Structured Mass Movement Mechanism for Rockfall Runout Modelling

OM PRASAD DHAKAL

Enschede, The Netherlands, June 2021

Thesis submitted to the Faculty of Geo-Information Science and Earth Observation of the University of Twente in partial fulfilment of the requirements for the degree of Master of Science in Geo-information Science and Earth Observation.

Specialization: Natural Hazard and Disaster Risk Reduction

## SUPERVISORS:

Assistant Professor Dr. Bastian van den Bout  
Professor Dr. Cees van Westen

## ADVISOR:

Dr. Olga Mavrouli

## THESIS ASSESSMENT BOARD:

Professor Dr. Mark van der Meijde (Chair)

Professor. Dr. Martin Mergili, (External Examiner, University of Graz, Austria)

#### DISCLAIMER

This document describes work undertaken as part of a programme of study at the Faculty of Geo-Information Science and Earth Observation of the University of Twente. All views and opinions expressed therein remain the sole responsibility of the author, and do not necessarily represent those of the Faculty.

# ABSTRACT

Rockfall and avalanche processes of various scales are a major natural hazard in mountainous areas throughout the world. There is a lack of clear methodology that could approach both simulating a small scale rockfall and large scale rock avalanche. The requirement of this single method is crucial when incorporating rockfall phenomena into a multi-hazard modelling framework. During such events, flow and fall processes of various scales occur and require a generalized model to capture complex interactions and transitions during runout. This research looks at the functionality of the newly developed semi-structured mass movement model by applying it to three case study sites. The selected case study sites provide enough variability when it comes to the runout extent, initiation volumes, and slope morphology.

The models in use are Rockyfor3D to represent trajectory rockfall modelling. This industry-standard tool for rockfall dynamics was calibrated for two of the three study sites. OpenLISEM hazard 1.0 and OpenLISEM hazard 2.0 represent granular flow mechanism and structured mass flow mechanism, respectively. The OpenLISEM models are compared to the reference data from Rockyfor3D in order to assess the accuracy and applicability of generalized semi-structured mass movement models to rockfall and rock avalanche dynamics.

Using a gradient descent algorithm, extensive calibration and sensitivity analysis was carried out. Simulation accuracies were calculated in terms of kinetic energies and impact pressure for each model compared to the Cohens Kappa inter reliability index. The accuracy calculated in reference to the validated model gave Kappa value of 0.66, 0.47 and 0.57 for the study case of Acheron, Andorra and Barcelonnette, respectively. Since the spatial accuracy was not enough to delineate the model's applicability, analysis based on the simulated velocities, impact to elements at risk and fragmentation behaviour of each model were carried out. The results showed at least a two-fold underestimation of velocities by the OpenLISEM hazard 2.0 model compared to the RF3D when the runout slope is greater than 40 degrees. Further, the estimation based on elements at risk showed at least a three-fold underestimation of kinetic energy values by the OpenLISEM hazard 2.0 model.

On the contrary, the OpenLISEM hazard 2.0 model accurately simulates the fragmentation behaviour. Furthermore, the non-diffusive transport of the solid and breakage based on the stress-strain relationship led to realistic results compared to a field inventory.

In conclusion, the research suggests further research and improvement of the OpenLISEM hazard 2.0 model. The design and planning for rockfall phenomena based on the model output are not suggested within the current framework. The part for improvement would be 1) modelling of the free fall, tumbling and rolling phenomena. 2) non averaged frictional forces. 3) Third impact against trees.

## ACKNOWLEDGEMENTS

Firstly, I would like to thank NUFFIC and the government of The Netherlands for this wonderful opportunity to enrol in the master's degree here at ITC. I feel grateful and privileged to be a part of the OKP scholarship, which helped maintain the quality of life during my two years stay in Enschede. I would like to mention my mentor Dr. Ranjan Kumar Dahal, for helping me find the scholarship and my workplace, Geotech Solutions International for helping me attain the scholarship.

My sincere appreciation towards my first supervisor, Assistant Professor Dr. Bastian van den Bout, for support throughout my research. From being super helpful to construct a research topic to being critical during the write up, this thesis would have been incomplete without Dr. Bastian. I would remember Dr. Olga Mavrouli for connecting me with Dr. Bastian and helping generate a proper research direction. I would also like to acknowledge Dr. Olga in support of generating the first idea of this research. Finally, I would like to thank Professor Dr. Cees van Westen for his helpful role as a second supervisor. Suggestions from Dr. Cees to line up the research and during write up was of great help. I will remember his cheerful attitude and humble personality yet being in a role of a teacher.

I'm grateful towards my family for believing in me. I'd like to thank my sister Prapti for always having my back. My mother Indira, for the love and care and Sneha for always being there.

I would like to thank all my fellow friends for assisting me during my research. Few names I cannot forget- Ashok, the super talented friend/brother of mine, I will be in debt for the help and support. Sachi, for all the motivation during the write-up phase.

I would also like to remember all my classmate from the NHR class of 2021. The journey would not have been better without you all.

# TABLE OF CONTENTS

---

1.	Introduction.....	1
1.1.	Background.....	1
1.2.	Literature review.....	2
1.3.	Problem statement.....	6
1.4.	Research objectives and research questions.....	7
1.5.	Organization of the thesis and workflow.....	8
2.	Description of the models.....	9
2.1.	Rockyfor3D.....	9
2.2.	OpenLISEM Hazard 1.0.....	9
2.3.	OpenLISEM Hazard 2.0.....	11
2.4.	Major dissimilarities seen within the flow models in respect to trajectory rockfall runout modelling.....	12
3.	Methodology.....	15
3.1.	Modelling.....	15
3.2.	Calibration.....	17
3.3.	Accuracy assessment.....	18
4.	Case study sites.....	20
4.1.	Case study 1: Acheron rock avalanche.....	21
4.2.	Case study 2: Sola de Andorra.....	24
4.3.	Case study 3: Barcelonnette.....	29
5.	Results.....	33
5.1.	Analysis associated with the overall accuracy of the models based on Cohens Kappa reliability index ..	33
5.2.	Analysis associated with the velocity of a rock mass along a runout axis.....	34
5.3.	Analysis associated with impact on the elements at risk.....	38
5.4.	Fragmentation analysis and reach distance.....	39
6.	Discussion and conclusion.....	41
6.1.	Discussion.....	41
6.2.	Conclusion.....	46
	Annexes.....	51

## LIST OF FIGURES

---

Figure 2-1 Schematic diagram of the RF3D model functionality.....	9
Figure 2-2 Schematic diagram of the OPH2 model functionality.....	11
Figure 2-3 Schematic diagram showing the conversion of trajectory vector to output raster. Source- Manual RF3D.....	12
Figure 2-4 Schematic diagram showing the major model functionality. Major observations on the schematic diagram to understand the model dissimilarities include. First, the initiating pixel is given in the colour red. Second, the runout propagation for each model $i$ is given in the colour orange. The rock mass structure and its tendency during runout in each modelling domain given as blue cubes. Details are described under separated headings below.....	13
Figure 2-5 Probabilistic assumption of the deviation in a runout trajectory (in degrees) when a runout mass collides with particular part of a tree. Source- Dorren, 2016.....	14
Figure 3-1 Flowchart conceptualizing the methodological details of the research.....	15
Figure 4-1 Elevation profile along the runout axis of the case study sites.....	20
Figure 4-2 Study area of the Acheron rock avalanche, Canterbury, New Zealand. ....	21
Figure 4-3 Convergence graph showing the calibration of the parameters within iterations .....	22
Figure 4-4 Runout inventory simulated by the three models for the case study of Acheron.....	23
Figure 4-5 Study area of rockfall prone area in Andorra. Location map of the Forat Negre (Left). The right map gives the country's perspective lying between France and Spain to the capital Andorra La Vella. Photo-Andrea (2014) .....	24
Figure 4-6 Rockfall inventory data available for the 2004 event (left) and 2008 event (right) .....	25
Figure 4-7 Delineation of a realistic detachment of rock mass (blue)- the image showing the hypothetical 150m <sup>3</sup> detachment occurred in 2008.....	26
Figure 4-8 Convergence graph showing the calibration of the parameters within iterations .....	27
Figure 4-9 Runout inventory simulated by the three models for the case study of Andorra .....	28
Figure 4-10 Study area of the Barcelonnette rock fall area.....	29
Figure 4-11 The assumed rockfall zone showing the specific volumes of detachment (in 3D).....	30
Figure 4-12 Convergence graph showing the calibration of the parameters within iterations .....	31
Figure 4-13 Runout inventory simulated by the three models for the case study of Barcelonnette.....	32
Figure 5-1 Effect of trees in modelling, yellow line showing the parts where OpenLISEM model need to fragment and spread in collision with trees.....	33
Figure 5-2 Selected runout axis for the analysis within the case study sites. ....	34
Figure 5-3 Description of the methodology to compare the model results from the trajectory models to the flow models .....	35
Figure 5-4 Simulated solid velocities by the representing models for each runout axis .....	37
Figure 5-5 Delineation of the elements at risk and the selected transect within the runout axis .....	38
Figure 5-6 Fragmentation of the rock block during the first major collision.....	39
Figure 5-7 Distal end of the runout propagation showing the final deposition of the rock volume (m <sup>3</sup> )....	40
Figure 6-1 Sensitivity analysis of two input parameters- IFA of the rockmass and the value of Mannings N .....	41



## LIST OF TABLES

---

Table 1 Review of trajectory models according to the modelling dimension and kinematics .....	4
Table 2 Review of Flow models according to the modelled phases .....	5
Table 3 Differences in the initial rock mass configuration .....	12
Table 4 Maps required for the OpenLISEM software package to run for this research .....	16
Table 5 Schematic categorization of the case study sites in respect to the type of movements .....	20
Table 6 Values of the calibrated parameters for the case study site of the Acheron rock avalanche. ....	23
Table 7 Simulation details for RF3D for Andorra .....	25
Table 8 Values of the calibrated parameters for the case study of Andorra .....	27
Table 9 Simulation details (RF3D) for Andorra .....	31
Table 10 Values of the calibrated parameters for the case study site of Barcelonnette .....	32
Table 11 Calculated Cohens Kappa values for each case study sites .....	33
Table 12 Details of the runout axis with the given name for simplicity .....	35
Table 13 Kinetic energies stimulated by the RF3D and OPH2 models .....	38
Table 14 Total runtime taken by each model .....	43

## LIST OF ABBREVIATIONS

---

OPH1- OpenLISEM Hazard 1.0  
OPH2- OpenLISEM Hazard 2.0  
OpenLISEM- generic name for OPH1 and OPH2  
FINT- Fint Individual Trees  
RF3D- Rockyfor3D  
DEM- Digital Elevation Model  
DSM- Digital Surface Model  
LIDAR- Light Detection and Ranging  
MPM- Material Point Method  
DBH- Diameter and Brest Height  
GUI- Graphical User Interface  
SPH- Smooth Particle Hydrodynamics  
GIS- Geographical Information System  
IFA- Angle of Internal Friction  
ESRI- Environmental System Research Institute  
ASCII- American Standard Code for Information Interchange  
PDF- Portable Document Format  
LINUX- Lovable Intellect Not Using XP  
2D- Two-dimension  
3D- Three dimension

# 1. INTRODUCTION

---

## 1.1. Background

Rock slope failures are classified broadly based on the type of movement as falls, topples, slides, spreads, flow and creep (Carson and Kirkby 1972; Hantz et al. 2021; Selby 1993). Among the four types of movements, falls are distinct from other movements as they are associated by freely moving masses of rock from a steep slope or a cliff (Bourrier, Dorren, and Hungr 2013; Cruden and Varnes 1996; Dorren 2003; Selby 1993; Varnes 1978). Falling movements of a rock slope are highly complex in terms of probability of occurrence and magnitude (Dorren 2003). These movements are mostly seen during the initiation and are short-lived high-energy events occurring randomly in susceptible areas (Cruden and Varnes 1996). These high energy movements may cause high impact collisions that can fatally impact assets in a rockfall-prone zone. Compared to other natural hazards, rockfalls are less destructive when it comes to monetary value. The lower degree of destruction is due to their occurrence in steep mountain terrain with fewer elements at risk.

A rock mass falling down a slope could further break up into smaller fragments that generate a stream or avalanche of debris, which could become catastrophic and more hazardous than the rockfall event itself (Hsü 1975). The damage caused by these cascading hazards when a rockfall event initiates a debris flow can either be direct or deferred. Examples of such direct cascades are from site-specific blockage of a stream to the generation of a tsunami by falling rocks on a glacial lake (Hsü 1975). Additionally, in a deferred setting, there could be a formation of a landslide dam, prone to reactivate later during monsoon ((Evans et al. 2006). Further classification of rock movements such as rockfalls or rock avalanches could be made based on the involved volume of detaching materials (Cruden and Varnes 1996). Although the scientific community still debates on the particular characterization of rockfall based on the dimension. (Corominas, Mavrouli, and Ruiz-Carulla 2017). There have been attempts characterizing rockfalls based on the maximum kinetic energy (Spang and Rautenstrauch 1988) or volumetric terms (Bourrier et al. 2013; Whalley 1984). The classification by Bourrier is given as an unambiguous definition where the classification criteria are based on the transport and depositional mechanism of the rock mass. As classified by Bourrier et al. (2013) based on the volume of the deposited rock mass after a failure, falling movement of rocks are categorized as particle fall ( $vol < 100m^3$ ), rock mass fall ( $vol \geq 100m^3$ ), and rock avalanche ( $vol \geq 10000 m^3$ ). This classification by Bourrier et al. (2013) is based on experience where the numerical values can only be taken to create classes. Based on these classes, the author also proposes a classification focused on the transport mechanism. A particle fall is falling as a fragmental rockfall with low interaction with other particles (from the detached rock mass) but a significant interaction with the substrate rock wall. When large rock volumes are detached, they result in a rock avalanche, considered a flowing mass of rock down the slope. The rock mass fall behaves intermediate between the fall and the flow movements.

Various numerical models have been developed to capture the dynamic runout of either fall or flow rock-mass movements. Modelling tools are useful as they can incorporate the physics of particular movements in a computerized environment (van den Bout, van Asch, and Hu 2020; Dorren 2003; Selby 1993; Tai and Kuo 2012). As understanding the process by a real-life event could be impractical and uncertain, modelling approaches are used to analyze, simplify, describe, and display various hillslopes systems (Selby 1993) and predict future events.

Various natural hazards are interlinked and may be triggered by one another. The concept of multi-hazard modelling, therefore, is prevalent and advancing. Multi-hazard tools are seen to be significant as various hazards, if modelled together, have larger impacts with amplified hazard intensities (Barrantes 2018; Marzocchi et al. 2009). Rock slopes fall itself can initiate a secondary hazard. Therefore, the significance to

integrate rockfalls into multi-hazard modelling prevails. A recent example by Khatiwada and Dahal (2020) on the Imja glacier lake shows that falling of rock block on the glacier lake is prominent and could create a surge, possibly resulting in a glacial lake outburst flood (GLOF).

## 1.2. Literature review

Modelling and predicting the dynamics/mechanisms of rock mass movement and their propagation is essential to understand how a rock mass descends a slope. Based on Dorren (2003), the three basic and important modes of motion a rockfall could take is 1) Freefall through the air- which mostly happens when the slope gradient exceeds 76 degrees (Ritchie 1963). 2) Bouncing- when the slope gradient is approximately from 70 degrees to 45 degrees, the first bounce after a free fall is thought to break incompetent rocks (Bozzolo and Pamini 1986), releasing almost 75-86% (Broilli 1974; Evans and Hungr 1993) of the energy gained during the fall. 3) Rolling- if the slope gradient is not high enough to keep up the energy of the trajectory, the rock then seems to roll, losing the rest of the energy until it finally comes to a stop. Therefore, the preliminary factors that play a vital role in the propagation of rockfall down a slope are mean slope gradient, rock size, slope condition (vegetation, soil, scree) (Dorren 2003).

However, with the change in terminology from rock particle fall to rock avalanche, there will also be a change in propagation from a single particle of rock only interacting to slope to a rock mass where there is inter-particle interaction. In other words, with the increase of rock mass propagating down a slope, there is a gradual transition from independently falling blocks of rocks to semi-coherent granular mass moving similar to frictional fluids (Bourrier et al. 2013). To keep the fall movement separate from other movements like sliding, the nature governed to the mass flow movement has to be contemplated with rapid mobility and comparatively large intensity of the event (Nemčok, Pašek, and Rybář 1972; Selby 1993)

The mechanism of the flow phenomena, although, is not as straightforward as the discreet particle propagation. Over the years, there has been extensive research to understand the complex rheology of the geological materials, which is dependent on the scale of the movement (Pitman and Long 2005). The flow phenomenon is described by mass and momentum balance law which uses the Coulomb constitutive description of dry granular materials. The advancement in the modelling practice will be explained in the following section.

As opposed to the discrete impact being considered for rock mass falls, granular flows and rock avalanches are commonly analyzed by means of a continuous process. A volume of perfectly mixed material is considered to provide a set of internal stresses and external forces. This assumption of continuity allows for the derivation of equations of movement. These can be a set of one, two, or three-phase equations (where phases indicate the different types of material that make up the moving mass). Single-phase equations describe the flow of one material mixture with one set of properties (van Asch et al. 2014; Luna et al. 2012; Rickenmann et al. 2006). The second category would be the mixture of two phases, solid and liquid, into a combined equation of interaction, these model advance in providing details of the process (George and Iverson 2014; Mergili et al. 2017; Pitman and Long 2005; Pudasaini 2012; Sheridan et al. 2005). The two-phase model assumes that the flow materials are fully mixed and are fragmented, which is generally invalid when modelling any structural mass (van den Bout et al. 2020). To address the uncertainty in the fraction of solid and liquid and an arbitrarily structured Mohr-Coulomb material, a generalized mass movement model is presented to function on both unstructured mixtures of flows and structured movements of materials. The addition of these theories is seen to be of great importance. First, modelling of cohesive material, ideally a rock block is seen as an important subset of any mass movement.

The cohesive structure during the movement phase shows solid dynamics, which could not be achieved by an unstructured, non-cohesive material. Further, during the movement of this structured, cohesive material, the local acceleration induces stress and strain phenomena upon the material, which might result

in fragmentation. Fragmentation of a structured mass depending on the impact caused during the runout can be of great importance (Davies and McSaveney 2009; Delaney and Evans 2014) also, the vitality that each particle after fragmentation follows its independent trajectory, which is often divergent (Corominas, Matas, and Ruiz-Carulla 2019). Moreover, the runout distance and velocities are significantly changed with the lubricating effect due to basal fragmentation. (Tang et al. 2009). Finally, there has also been the development of a multiphase equation by Pudasaini and Mergili (2019), where the idea of a complex geophysical flow is addressed by three-phase flow equations including coarse solid, fine solids, and viscous fluid (Pudasaini and Mergili 2019). The equation is complex in terms of multiple added parameters, which would be an applicability issue during modelling.

### **1.2.1. Modelling approach in rockfall.**

Due to the variety of types of movements experienced with change in rock mass detached, modelling practices for each type of movements are also derived. These methods can be differentiated based on internally dominant processes, such as particle-particle interactions, tumbling, and fragmentation. First, discrete models or trajectory models consider the rock particles without fragmentation. The assumption here is that the rock would not break along the line of propagation and give an output based on the volume and shape of the rock block. An alternative to this approach is the continuous models for granular flows. This set of techniques considers a fragmented volume of larger particles where particle-particle interactions can be dominant. More recently, semi-structured methods use continuous particle methods (A). These models can consider both un-fragmented and fragmented flow and attempt to implement the transitional behaviour of fragmentation. Below, each of the modelling techniques is discussed.

#### **a) Trajectory models**

Trajectory models have historically been popular for hazard assessment purposes due to their ability to represent the physics of the rockfall pattern. The prediction of the rockfall mass's bounce height and kinetic energy has continued to be important outputs in damage and risk modelling (Agliardi, Crosta, and Frattini 2009). Li & Lan (2015) explained that the trajectory models could be categorized based on three groups based on the terrain and simulation properties. First, the slope could either be taken as 2D, semi 2D, or 3D terrain. Second, the rockfall could be modelled using the kinematics of various simulated objects (e.g. lumped mass, rigid body, the hybrid one, which is the combination of lumped mass and rigid body and, so forth). Third, the simulation could either be done by a probabilistic or deterministic approach.

Major uncertainties for modelling a rockfall can be given under two major headings: inherent uncertainty and epistemic uncertainty (Li and Lan 2015). The inherent uncertainty (stochasticity) in the trajectory models is mostly related to predicting the initial conditions of source location, rock properties, and so forth, which is out of bound to this research. What would be meaningful to explain is the epistemic uncertainty which deals with the rock slope interaction, fragmentation, and the availability of vegetation obstructing the trajectory of the models. A meaningful algorithm could be the way to tackle the epistemic uncertainty of the rockfall phenomena, and hence various numerical models come into play, each with their speciality. Few of them are briefly described.

Table 1 Review of trajectory models according to the modelling dimension and kinematics

Specification	Kinematics	Model	Assumptions	Reference
2D Numerical	Hybrid	Colorado rockfall simulation program (CRSP)	Surface roughness was adjusted according to the size of the simulated rockfall.	(Bartingale et al. 2009)
	Lumped mass	Rocfall	Simulated as a single independent particle. Mass of the rock not considered for the runout motion	(Rockscience Inc. 2013; Stevens 1998)
3D Numerical	Lumped mass	Stone	The size, shape, and mass of rock are not considered.	(Guzzetti et al. 2002)
		Rockfall Analyst	Input raster modelled geostatistical by simulating many trajectories	(Lan, Derek Martin, and Lim 2007)
	Hybrid	Rockyfor3D	Roughness is given as input raster in the form of Obstacle height (MOH)	(Dorren 2016)
		Picus Rock' n' Roll	Physiological principles based on patch model and stand-level production model	(Rammer et al. 2010)
	Rigid body	Rocpro3D	Rock mass parameters are derived probabilistically.	(Barnichon 2014)

**b) Flow models**

A physically-based dynamic modelling approach for flow movements is mostly used to simulate granular avalanche and debris flow. There has been considerable development of the modelling approaches over the years. Based on Pudasaini and Mergili (2019), the advancement to the models is primarily based on flow volume or material properties. Another perspective of the granular flow models is also developed, possibly overlapping the landslide phenomena (slide movements) given as single-phase granular avalanche. Further, two-phase flow simulates both the solid and liquid phase. Lastly, the three-phase flow after Pudasaini and Mergili (2019) are now given, which would model solid, fluid, and the fine-solid phase of flowing material. Few general models are listed below.

Table 2 Review of Flow models according to the modelled phases

Phase	Model	Assumptions	Reference
One-Phase	FLO-2D	Based on Voellmy fluid rheology, representing visco plastic fluid.	(Rickenmann et al. 2006)
Two-Phase	D-Claw	Depth averaged calculation, shallow water quasi-two-phase flow	(George and Iverson 2014)
	r.avaflow	Based on the three-phase mass model	(Mergili et al. 2017)
	Titan 2D	Incompressible Coulomb continuum, depth-averaged	(Sheridan et al. 2005)
	DAN3D-Flex	Both sliding of rock mass on initiation and flow equation on runout applied, making it a dynamic modelling approach	(Aaron and Hungr 2016)
	OpenLISEM hazard 1.0	Depth averaged Saint_Venant flow	(van den Bout et al. 2018)
	OpenLISEM hazard 2.0	Arbitrarily structured Mohr-Coulomb material in the set of a depth-averaged flow model	(van den Bout et al. 2020)
	RAMMS	Depth averaged, Voellmy-Salm or random kinetic energy approach.	(Christen, Kowalski, and Bartelt 2010)

### 1.3. Problem statement

The trajectory models can best describe the falling movement of a small-scale rockfall (particle fall). Here, particle-particle interactions are assumed insignificant and individual objects are rigid. The model benefits from the incorporation of the physics of bounce and fall into the modelling approach. It can predict the bounce height of individual rock fragments and the kinetic energy of moving rock blocks (Li and Lan 2015). The models for rock particle fall are mostly used on a site-specific scale for engineering design and prevention. Although recent developments can lead to regional-scale modelling, the major drawback is that the model does not consider fragmentation which is invalid in a large rock mass detachment.

The large-scale flow movement can be represented by the two-phase (solid and fluid) mass movement equations for granular flows, e.g. Pudasaini, (2012). These equations assume a continuous moving material where particle-particle interactions are dominant. Moreover, the material is perfectly mixed, and the deformation is subject to the stress-strain relationship. The equations used on a modelling platform describe the complex dynamics of the subaerial flows and sediment transport. The granular flow models for a large-scale rock avalanche are also being used and tested (Mergili et al. 2017)

Yet, as explained by Bourrier et al. (2013), the transitional phenomena, where the author expects a hybrid model to simulate the mobility between fall and flow, where things like granular mass in air trajectory could be modelled, which is extremely complicated. The best way to incorporate the transitional phenomena is thought to be achieved by semi-structured mass movement equations after van den Bout et al. (2020), which is the advancement of the two-phase flow equations from Pudasaini (2012). The semi-structured mass movement equations with the inclusion of stress-strain relationship incorporate all the parameters (angle of internal friction  $\phi$ , Cohesion  $c$ ) of a structured Mohr-Coulomb material arbitrarily into a generalized two-phase debris flow equation. Hence, giving a final equation in the depth-averaged calculation of a (semi) structured mass movement. However, the transitional phenomena best described by (van den Bout et al. 2020) have never been tested on an uncontrolled event. Thus, it is unknown how the novel semi-structured model performs when simulating real rock-fall events, particularly featuring transitional fragmentation movements between discrete movements and flows.

In summary, the model assumptions from the individual trajectory of rock blocks differ fundamentally from the assumptions of granular flow models and the semi-structured runout method. As a result, not all of these methods provide accurate predictions of rockfall or rock avalanche dynamics for all types of applications. Depending on the spatial scale of the event, the physical properties of the rock material, and the scale of the individual particles, the models' assumptions might be invalid. Implementation of rock mass movement processes within multi-hazard simulation tools requires a versatile model setup that can adapt to various types and scales of rock movements. However, the valid range of application of the various modelling methods is unknown. Progress in multi-hazard modelling involving rock mass movements, therefore, requires an analysis of the various methodologies' validity, particularly concerning the application in a multi-hazard setting. Finally, transitional phenomena such as fragmentation have only been understood to a limited extent. Application of new rock mass movement methods can increase understanding of these processes

The occurrence of a rockfall event could not just be an independent event but could be catastrophic when simulated in a multi-hazard environment. Unfortunately, there have not been many successful attempts to integrate this rockfall phenomenon into a multi-hazard approach.

The conventional ongoing methods of rockfall simulation are not designed to be integrated into a multi-hazard setting. Therefore, there is a need for a tool to be designed such that the modelling could be done in a multi-hazard setting. To sum up, the workability of the semi-structured mass movement will benefit in two ways—first, incorporation of the impacts due to rock mass fall phenomena into a multi-hazard simulation. Second, a single tool to model rockfall phenomena as a whole.



#### **1.4. Research objectives and research questions**

The main objective of this research is to assess the extent to which semi-structured granular flow models can predict the dynamics of falling rock mass movement with varying runout volumes. The research also aims to obtain a qualitative scale that helps choose the model that fits best with reality, based on the volume of the input rock mass.

Sub-Objectives and associated research questions: -

- 1. To carry out a comparative analysis of the influence of flow and trajectory assumptions in the accuracy of the rockfall runout methods.**
  - a. Which outcomes from the models are appropriate for the accuracy assessment?
  - b. How do the results of the semi-structured mass movement model compare to the trajectory or flow models?
- 2. To obtain a qualitative scale of validity for different models based on rock volume and granularity.**
  - c. How can the dissimilar model outputs from different models be used to create a standard accuracy assessment?
  - d. How to decide the volume threshold of the initiating mass for the correctness of the different models?
- 3. To identify the extent to which the assumptions underlying the model usage validate the varying granularity dimensions.**
  - e. How do the underlying assumptions of the model influence the model accuracy for the three study cases?
  - f. To what extent are these assumptions required for the derivation of the modelling methods?
- 4. To obtain a potential research direction for the improvement in multi-hazard interaction.**
  - g. Which model among the three works the best for rockfall runout? Could it be altered further for better accuracy?
  - h. In what ways can the models be enhanced for further development?
  - i. To what extent can the current models be added to the multi-hazard tool.

### **1.5. Organization of the thesis and workflow**

The thesis is divided into five chapters.

Chapter 1 describes this research's introduction and problem statements, including the associated research objectives and questions.

Chapter 2 describes the models in use, and their assumptions. Major dissimilarities among the models are discussed, focusing on where OpenLISEM (generic name used for the OPH1 and OPH2) could be improved for rockfall runout modelling.

Chapter 3 describes the methodology of the research. This part explains how the datasets from the previous studies were modified to obtain the input parameters for running the OpenLISEM model.

Chapter 4 describes the case study sites and the input parameter used in simulating each one. Lastly, the accuracies of the modelling output are given for each study site.

Chapter 5 explains how the results from the three case study sites are used in analyzing the adaptability of the semi-structured mass movement mechanism to the rockfall runout modelling. Various analysis parameters are described to validate for all three case study sites.

Chapter 6 discusses the validation of the semi-structured mass movement models for rockfall runout modelling. Further, based on the result analysis, the future research direction is delineated, which would also help improve the modelling assumptions to better fit into a multi-hazard interaction. Finally, a conclusion to summarize the results.

## 2. DESCRIPTION OF THE MODELS

Out of the three models used in this research, two (OpenLISEM hazard 1.0 and OpenLISEM hazard 2.0) are based on continuous granular flow theory, together called OpenLISEM models. There are similarities when it comes to the model input data and origin of the software. On the other hand, the Rockyfor3D (hereby called RF3D) model uses particle trajectory theory, which comes with a relatively different theoretical framework and vision. In this regard, there are major differences in the RF3D and OpenLISEM models when it comes to functionality. Here, each model is described, and finally, a conclusion is drawn regarding the major dissimilarities based on the model functionality.

### 2.1. Rockyfor3D

RF3D is chosen to represent the trajectory model because of its wide usage and good historic update (Calista et al. 2020; Dorren 2016; Sellmeier 2015). RF3D is a probabilistic process-based rockfall trajectory model. The model simulates trajectories of individual falling rock incorporating physically based deterministic algorithms with stochastic processes. Each trajectory is vector data calculating the classical parabolic freefall through the air. In addition, each trajectory calculates the bouncing of the rock on a slope and rolling (which is the short distance bouncing on pixels). Sliding phenomena are not taken into consideration in this model.

The input dimension and density of the rock block are used to calculate the inertia of the rock block if falling freely in the air. In this case, the model assumes a standard algorithm of uniformly accelerated parabolic movement. Once the block comes in contact with the slope, the incoming velocity is given further into two components- the normal velocity and tangential velocity. The incoming block causes an impact during the contact. It is calculated as penetration depth based on the following parameters 1) the normal coefficient of restitution, 2) the diameter of the block, 3) the mass of the rock, 4) the impacting velocity of the falling block.

Based on the composition and the size of the materials covering the slope, the tangential coefficient of restitution is calculated, leading to the change in velocity and rotation when further bouncing. The direction of the bounce is dependent on the aspect of the slope, and a probabilistic algorithm developed based on real-life data.

Based on the composition and the size of the materials covering the slope, the tangential coefficient of restitution is calculated, leading to the change in velocity and rotation when further bouncing. The direction of the bounce is dependent on the aspect of the slope, and a probabilistic algorithm developed based on real-life data.

Based on the composition and the size of the materials covering the slope, the tangential coefficient of restitution is calculated, leading to the change in velocity and rotation when further bouncing. The direction of the bounce is dependent on the aspect of the slope, and a probabilistic algorithm developed based on real-life data.

### 2.2. OpenLISEM Hazard 1.0

OpenLISEM hazard 1.0 (hereby called OPH1) is an open source physically based multi-hazard land surface process model. Initially started as hydrological model LISEM (Limburg Soil Erosion Model), the model is constantly under development. The model has been able to come across the interaction of hydrology with

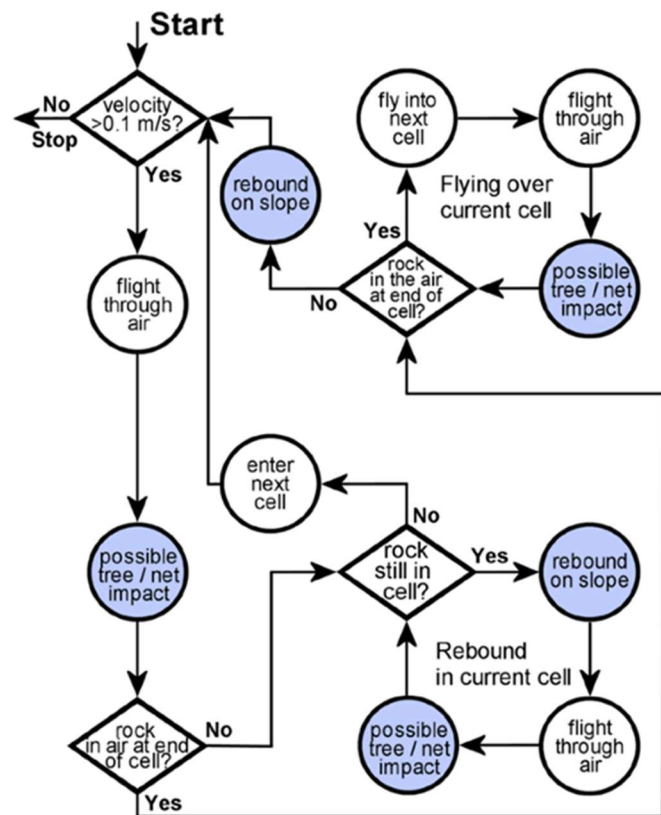


Figure 2-1 Schematic diagram of the RF3D model functionality

sediment erosion, flooding, slope stability, and further into debris flow movements. In its ability to carry out multi-hazard modelling, in this research, the flow equations will be focused as on our case study sites there are no other hazard interactions (like flooding).

The flow phenomenon is simulated by the depth-averaged description of a uniformly mixed solid and fluid on a slope. Therefore, the flow height, velocity, and slope are the first parameters used in the physically based flow equations. The primary structure of the model follows mass and momentum continuity. For both solids and fluids, momentum source terms are used based on an adapted version of Pudasaini (2012).  
Mass Conservation

$$\frac{\partial h}{\partial t} + \frac{\partial(hu_x)}{\partial x} + \frac{\partial(hu_y)}{\partial y} = R - I \quad (1)$$

Momentum Balance

$$\frac{\partial hu_x}{\partial t} + \frac{\partial(hu_x^2)}{\partial x} + \frac{\partial(hu_xu_y)}{\partial y} = gh(S_x - S_{f,x}) \quad (2)$$

$$\frac{\partial hu_y}{\partial t} + \frac{\partial(hu_y^2)}{\partial y} + \frac{\partial(hu_xu_y)}{\partial x} = gh(S_y - S_{f,y}) \quad (3)$$

Where, h=flow height,  $u_{x,y}$ =flow velocity in x and y direction, R=rainfall, I=Infiltration, g=gravitational acceleration,  $S_{x,y}$ =friction terms in x and y direction,  $S_f$ =momentum source term.

The mass conservation and momentum balance exist for solids and fluids separately, indicating the two-phase nature of the model. The interaction between the phases is based on the momentum source terms. The momentum source terms are in OPH1 are based on the work by Pudasaini (2012). The work describes the calculation of drag forces, gravitational and pressure forces, viscous forces, non-Newtonian viscosity, and Mohr-Coulomb type friction for the solid phase. The following set of equations represents the theories mentioned in momentum source terms.

$$S_{x,s} = \alpha_s \left( g \left( \frac{\partial b}{\partial x} \right) - \frac{u_s}{|\vec{u}_s|} \tan(\partial P_{b_s}) - \varepsilon P_{b_s} \left( \frac{\partial b}{\partial x} \right) - \varepsilon \alpha_s \gamma P_{b_f} \left( \frac{\partial h}{\partial x} + \frac{\partial b}{\partial x} \right) \right. \quad (4)$$

$$\left. + C_{DG}(u_f - u_s) |\vec{u}_f - \vec{u}_s|^{j-1} \right)$$

$$S_{y,s} = \alpha_s \left( g \left( \frac{\partial b}{\partial y} \right) - \frac{v_s}{|\vec{u}_s|} \tan(\partial P_{b_s}) - \varepsilon P_{b_s} \left( \frac{\partial b}{\partial y} \right) - \varepsilon \alpha_s \gamma P_{b_f} \left( \frac{\partial h}{\partial y} + \frac{\partial b}{\partial y} \right) \right. \quad (5)$$

$$\left. + C_{DG}(v_f - v_s) |\vec{u}_f - \vec{u}_s|^{j-1} \right)$$

$$S_{x,s} = \alpha_f \left\{ g \left( \frac{\partial b}{\partial x} \right) - \varepsilon \left[ \frac{1}{h} \frac{\partial}{\partial x} \left( \frac{h^2}{2} P_{b_f} \right) + P_{b_f} \frac{\partial b}{\partial x} - \frac{1}{\alpha_f N_R} \left( 2 \frac{\partial^2 u_f}{\partial x^2} + \frac{\partial^2 v_f}{\partial y \partial x} + \frac{\partial^2 u_f}{\partial y^2} - \frac{\chi u_f}{\varepsilon^2 h^2} \right) \right. \right. \quad (6)$$

$$\left. + \frac{1}{\alpha_f N_R} \left( 2 \frac{\partial}{\partial x} \left( \frac{\partial \alpha_s}{\partial x} (u_f - u_s) \right) + \frac{\partial}{\partial y} \left( \frac{\partial \alpha_s}{\partial x} (v_f - v_s) + \frac{\partial \alpha_s}{\partial y} (u_f - u_s) \right) \right) \right\}$$

$$\left. - \frac{\xi \alpha_s (v_f - v_s)}{\varepsilon^2 \alpha_f N_{R,A} h^2} \right\} - \frac{1}{\gamma} C_{DG}(u_f - u_s) |\vec{u}_f - \vec{u}_s|^{j-1}$$

$$\begin{aligned}
 S_{y,s} = \alpha_f \left\{ g \left( \frac{\partial b}{\partial y} \right) - \varepsilon \left[ \frac{1}{h} \frac{\partial}{\partial y} \left( \frac{h^2}{2} P_{bf} \right) + P_{bf} \frac{\partial b}{\partial y} - \frac{1}{\alpha_f N_R} \left( 2 \frac{\partial^2 v_f}{\partial y^2} + \frac{\partial^2 u_f}{\partial y \partial x} + \frac{\partial^2 v_f}{\partial y^2} - \frac{\chi v_f}{\varepsilon^2 h^2} \right) \right. \right. \\
 \left. \left. + \frac{1}{\alpha_f N_R} \left( 2 \frac{\partial}{\partial y} \left( \frac{\partial \alpha_s}{\partial y} (v_f - v_s) \right) + \frac{\partial}{\partial y} \left( \frac{\partial \alpha_s}{\partial y} (u_f - u_s) + \frac{\partial \alpha_s}{\partial x} (v_f - v_s) \right) \right) \right. \right. \\
 \left. \left. - \frac{\xi \alpha_s (u_f - u_s)}{\varepsilon^2 \alpha_f N_{R_A} h^2} \right] \right\} - \frac{1}{\gamma} C_{DG} (u_f - u_s) |\vec{u}_f - \vec{u}_s|^{j-1}
 \end{aligned} \quad (7)$$

Where,  $S_s$  is the momentum source terms for solids in  $m s^{-2}$ .  $\alpha_s$  and  $\alpha_f$  are the volume fraction for solid and fluid phases.  $P_b$  is the pressure at the base of the surface in  $Kg m^{-1} s^{-2}$ ,  $b$  is the basal of the flow in m.  $N_R$  is the Reynolds number.  $N_{R_A}$  is the quasi-Reynolds number.  $C_{DG}$  is the drag coefficient.  $\rho_f$  is the density of the fluid in  $kg m^{-3}$ .  $\rho_s$  is the density of the solids in  $kg m^{-3}$ .  $\gamma$  is the density ratio between the fluid and solid phases.  $\chi$  is the vertical shearing of fluid velocity  $m s^{-1}$ .  $\varepsilon$  is the aspect ratio of the model.  $\xi$  is the vertical distribution of  $\alpha_s$  in  $m^{-1}$

Finally, to incorporate all these equations into the catchment-based model, the frictional forces for the fluids are replaced with the Darcy-Weisbach equation for water flow friction. Other related parameters for flow properties that govern the debris flow dynamics are estimated based on the volumetric sediment content. The viscosity of the fluids is based on the empirical relation given by O'Brien and Julien (1993)

$$\eta = \alpha e^{\beta \alpha_s} \quad (8)$$

Where,  $\alpha_s$  is the volumetric solid content of the flow.  $\alpha$  is the first viscosity parameter, and  $\beta$  is the second velocity parameter.

The details are included in Bout et al. (2018).

### 2.3. OpenLISEM Hazard 2.0

In advancing the OPH1 model for the simulation of granular flow, OpenLISEM hazard 2.0 (hereby called OPH2) models include a semi-structured fluid-solid mass described by the runout of an arbitrarily structured two-phase Mohr-Coulomb material. A major improvement that had to be addressed from the previous version (OPH1) is the assumption of the material's fully mixed and fragmented nature (Denlinger and Iverson 2001; Pudasaini and Hutter 2003). This assumption is invalid when it comes to modelling a structured rock mass. Therefore, the previous assumption is added with the theory of a structural solid phase. These include the theories of stress tensors, internal structures, fragmentation, water partitioning, fluid stresses, and finally, the drag force and virtual mass to get the final set of depth-averaged mass conservation and momentum balanced equations. The implementation of the mentioned theories into the modelling calculation has its benefits and drawbacks. Modelling the fluid dynamics is

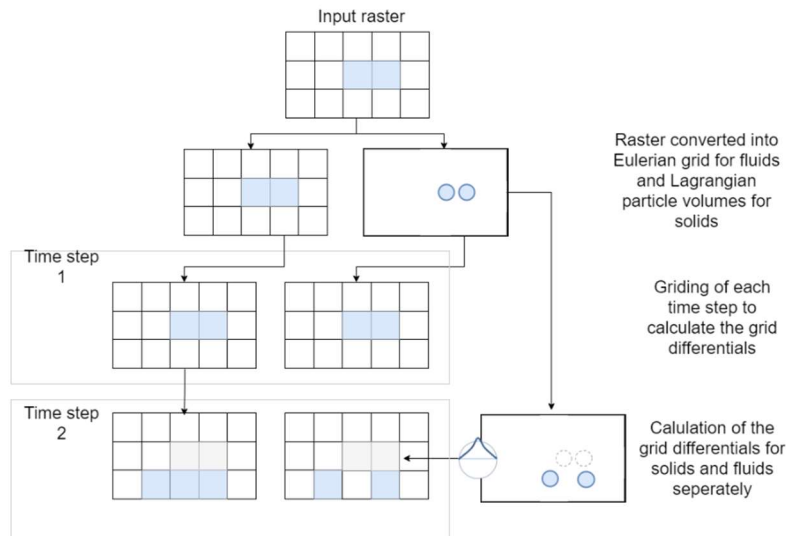


Figure 2-2 Schematic diagram of the OPH2 model functionality

solved basically by the Eulerian finite element as the diffusion and advection properties of the fluid dynamics can be well explained by these methods. However, to maintain the solid physical properties during movement, the Lagrangian finite element method or discrete element method is used. In addition, with the Lagrangian method, the advection scheme does not diffuse artificially since the calculation is based on material that is discrete particles. In OPH2, the material point method (MPM) provides the best approximations to incorporate the set of equations (Stomakhin et al. 2013). The two-phase scheme is implemented in OPH2, the fluid phase part of the equations is calculated based on the Eulerian finite element method.

The standard MPM incorporates the Eulerian and Lagrangian methods (Abe and Konagai 2016; Pastor et al. 2009). The MPM uses the framework of smooth particle hydrodynamics, where the equations are solved using discretized volumes of mass represented by kernel functions. In the case of OPH2, the use of cubic spline kernel is used, which is also used by Monaghan (2000).

The details of the advancement to the OPH2 is explained by (Aaron, McDougall, and Nolde 2019; van den Bout et al. 2020)

**2.4. Major dissimilarities seen within the flow models in respect to trajectory rockfall runout modelling**

There are several important distinctions between the considered modelling approaches. Due to the differences in their theoretical foundations, both model mechanics, their input and output data show differences. Here, we are looking at two fundamentally different modelling methods having their assumption in processing a runout of a rock mass. Whereas the previous section focused on theoretical differences, the differences in model functionalities are discussed, which would potentially impact the research objectives.

**2.4.1. Initial rock mass configuration**

Table 3 shows the major differences between RF3D and OpenLISEM in terms of rock mass configuration

Model	RF3D	OPH1 and OPH2
Initiating pixel	Single-pixel irrespective of the dimension of the rock mass. The volume calculated from d1,d2,d3 raster input maps (or entered directly into the GUI)	The Scarp zone needs to be mapped. The volume is calculated with the initial height of the rock mass, which multiplies with the pixel size.
Fluid content	Not considered	Given as Input raster map

Table 3 Differences in the initial rock mass configuration

**2.4.1. Runout Propagation**

The major difference in the RF3D and OpenLISEM model lies in the flow propagation as the RF3D does not incorporate flow into its assumptions. Here the propagation only happens as a parabolic trajectory through air and rebounds on a sloped surface. The rolling of a rock block is described by short distance bouncing off the rock block, and sliding is not incorporated. RF3D could avoid pixel travelling through air trajectory if need be, which can not be true for the flow model like OPLISEM.

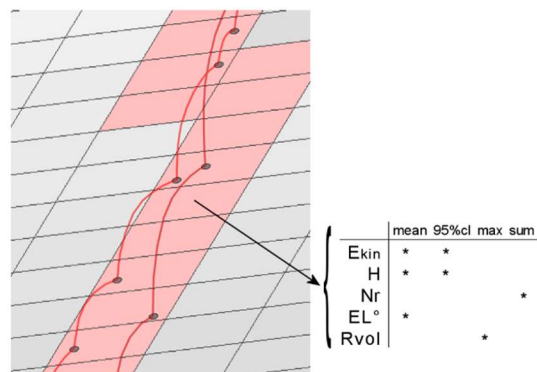


Figure 2-3 Schematic diagram showing the conversion of trajectory vector to output raster. Source- Manual RF3D

On the contrary, RF3D, upon a single simulation, may miss out on a runout path which will be a single line in a raster converted from a vector trajectory. Therefore, to make it more realistic, the software comes with a multi-simulation approach where the concept of statistics is used to draw conclusions based on the mean values or 95% confidence interval (mean+ 2\* standard deviation) values of the number of simulation conducted.

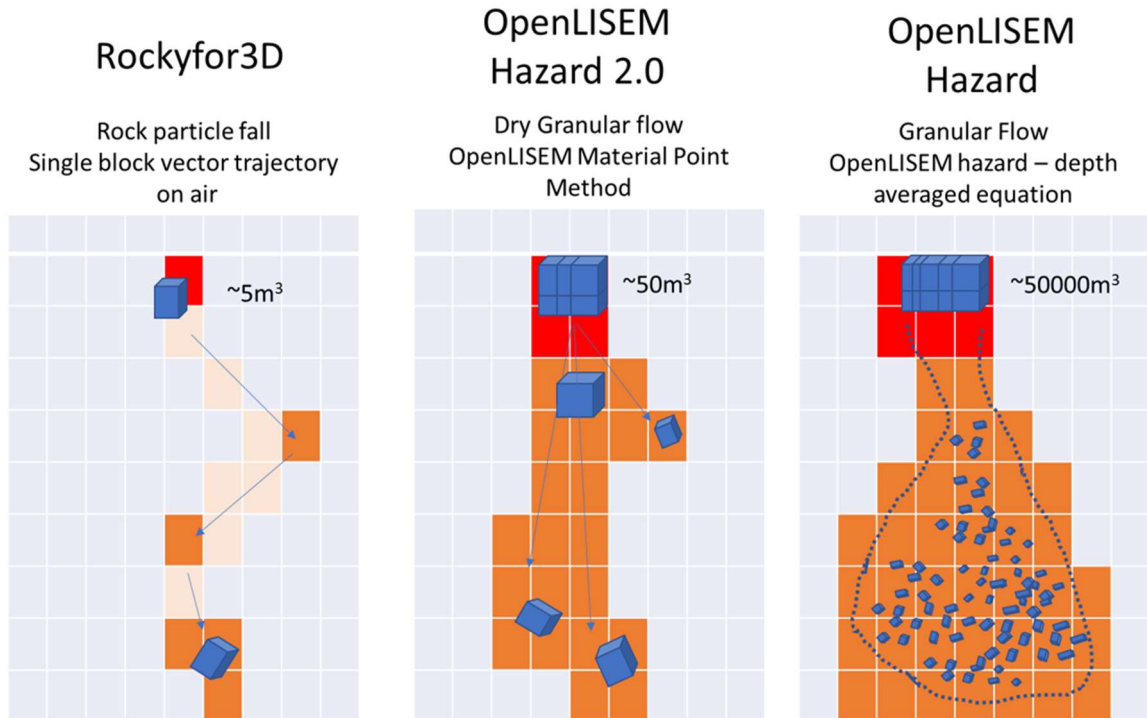


Figure 2-4 Schematic diagram showing the major model functionality. Major observations on the schematic diagram to understand the model dissimilarities include. First, the initiating pixel is given in the colour red. Second, the runout propagation for each model *i* is given in the colour orange. The rock mass structure and its tendency during runout in each modelling domain given as blue cubes. Details are described under separated headings below.

### 2.4.2. Incorporation of impact with trees

The incorporation of trees in rockfall runout modelling is taken as a vital aspect (Dorren 2016; Jazvin 2016). So, to incorporate effect of trees, the RF3D model uses four functions to calculate the energy dissipated during an impact on a tree. In addition to that, the model would incorporate the change in the runout direction based on the calculation.

#### Energy dissipation

RF3D incorporates the role of trees in a more detailed manner. Four main functions are considered when calculating the dissipation of energy. There is an associated calculation (Dorren 2016). Here only one of them is explained.

- I. The diameter of the tree, along with the breast height  
The package uses the diameter and the type of tree (coniferous or broadleaved) to calculate the energy dissipation (Dorren et al. 2005)

$$Ediss = FE \text{ ratio} * 38.7 * DBH^{2.31} \quad (9)$$

Where, Ediss= maximum amount of kinetic energy that can be dissipated by the trees (in Joule), FE ratio is the fracture energy ratio of a tree type, DBH is the stem diameter, and the breast height in cm.

- II. The impact height- the height at which the rock block hits the tree. (Dorren 2016)

- III. The position of impact on the tree- where does the block hit on the tree. Given as frontal, lateral, and scratch (Dorren et al. 2005)
- IV. Impact angle- the angle with which the block is approaching with respect to a vertically standing tree. (Jonsson 2007)

In the case of OpenLISEM, the dissipation of the energy could be in terms of

- I. The value of Mannings N- which will slow down the velocity of the moving rock mass along with the cell (Marcus et al. 1992). The velocity is directly proportional to the kinetic energy.
- II. In higher resolution DEM, the DEM with those pixels identified with trees could be added with the tree height. However, the results of this empirical way to represent trees are unknown. For example, trees precisely cannot be cubical, and the trees' strength cannot be the same at the breast height and above 5meters.

**Change in direction**

When a rock block hits a tree, there is energy dissipation and a change in direction. As mentioned in the earlier part, energy dissipation is somewhat incorporated in the modelling domain by OpenLISEM. However, change in velocity direction lack, as no point impacts are estimated for a continuous flow model. In reality, rockfall processes are significantly impacted by direction changes due to trees and other obstacles. RF3D incorporates the change in direction due to the impact on a tree based on experiments described in (Dorren et al. 2005). The deviation of a rock block is given in probability values where the deviation could be up to 76° depending on which part of the trees does the block hits.

Impact type	Probabilities (%)		
	0 – 22.5° Deviation	22.5° - 67.5° deviation	67.5° - 76° deviation
Frontal	44	50	6
Lateral	11	84	5
Scratch	72	24	4

Figure 2-5 Probabilistic assumption of the deviation in a runout trajectory (in degrees) when a runout mass collides with particular part of a tree. Source- Dorren, 2016



### 3. METHODOLOGY

Due to the COVID 19 pandemic data collection was impossible via fieldwork. Therefore, the research was designed based on previous research in order to facilitate the newly developed model. The datasets used where research had been done beforehand are, lined differently to this research. The process was helpful because of the availability of calibrated datasets from the study area, assuming that these outputs are close to reality.

The whole process of preparation of the dataset is shown in a schematic diagram in Figure 3-1. The main goal for the parameterization was to achieve the input parameters to run the OpenLISEM (OPH1 and OPH2) models based on dataset available from the previous research. Methodological details for each step are described under separated headings.

Among the three datasets, the case study of Andorra and Barcelonnette is available with the datasets where the runout is carried out in the software package RF3D. Whereas for the case study of Acheron, the output dataset is available from the software package r.avaflow (Mergili et al. 2017) and previous research done by Smith et al. (2012)

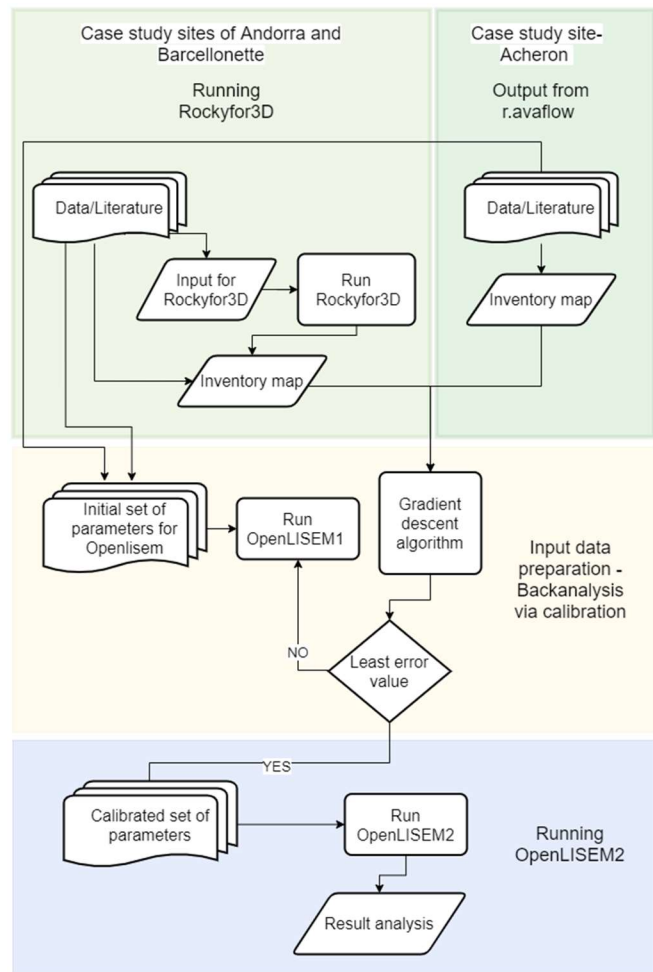


Figure 3-1 Flowchart conceptualizing the methodological details of the research

#### 3.1. Modelling

##### 3.1.1. Running RF3D

For both the cases of Andorra and Barcelonnette, extensive research has been done by others on the use of RF3D. For Andorra, three-dimensional modelling of rockfall dynamics was carried out by Baldini (2014). In addition, an investigation of the effects of protective measures and forests on rockfall dynamics was done by Jazvin (2016), which investigated both the Andorra and Barcelonnette sites to draw remarks. The previous research done before and the one being carried out here has different objectives. Therefore, several factors had to be closely observed during the process. The modelling had to be done again with the same calibrated parameter from the previous research. For example, the analysis on the case study site of Andorra was done with rockfall barrier nets (built-in command in RF3D) which is out of the scope of this research. Therefore, the modelling in RF3D had to be done again without using the nets to get comparable results. The results from RF3D with the calibrated dataset was significant as this research consider the results from the model to be the most accurate in the sense that they were based on field verification.

The input rasters for RF3D should be in ESRI ASCII format. The software functions with the input of 10 set of rasters which needs to be of the same extent and pixel size. The input datasets for this research are

prepared as per the instruction in the RF3D manual (Dorren 2016). The manual also provides an instruction guide to automatically create all the input datasets needed for the model based on GIS operation. For this, the RF3D manual provides a sample dataset consisting of the script and an organized folder setup for the input, processing, and output folders to prepare the input dataset <sup>1</sup>. The script file is a batch file (.bat) built to function with the SAGA GIS tool. The user needs to prepare the shapefile to delineate the initiation point of the rockfall source zone and enter all the attributes necessary into the attribute table. Finally, after following all the instructions properly, all the input maps are generated in the same format required for the RF3D software package to function. View the script in *Annexe 1: Script for the input data creation of RF3D*. Further, when the input maps are ready, the model run is done based on the Graphical User Interface (GUI). Primarily the working directory is set where the input dataset is present. The liberty to do the simulation, including the effect of trees, can also be selected in the GUI. Finally, the number of simulation and the block definition is set before running the RF3D model. The output will be saved on the working directory with a unique name and a detailed log file.

### 3.1.2. Running OpenLISEM

The previous version of OpenLISEM would require all the input maps into *.map* format, which is the format used in the PCRaster tool developed by the University of Utrecht for dynamic modelling applications. The latest version, OPH2, comes with this advancement that the input maps could also be a GTIFF which is generally the most commonly used format when handling rasters.

All the input maps required for this research were generated with the help of a PCRaster script in nutshell interface (windows shell for PCRaster). Similar to RF3D, OpenLISEM requires all the maps of the same extent and pixel size; therefore, building a script helps generate a consistent input dataset. View the PCRaster script *Annex 2: Script for the input data creation of OpenLISEM*

Although OpenLISEM can have as many as 23 raster input files while simulating multi-hazard modelling, the maps required in this research to simulate a rock mass runout only require seven compulsory maps mentioned in Table 4. The first four maps indicated in the table were obtained by modifying those used in previous research to fit into the OpenLISEM modelling domain. The last three maps from the table were unavailable from the previous research. New set of maps based on literature had to be made, which also had to be calibrated.

Table 4 Maps required for the OpenLISEM software package to run for this research

Input map	OpenLISEM (.map)	Description	Literature values	To be calibrated
1	Rock mass density	Pixels representing the fluid height of detaching rock mass	✓	
2	Initial solid height	Pixels representing the solid height of detaching rock mass	✓	
3	Initial fluid height	The density of the detaching rock mass	✓	
4	Rock size	Pixel showing the maximum size of a rock	✓	
5	Angle of internal friction (IFA)	Value of internal friction angle of the detaching rock mass		?
6	Cohesion	Value of cohesion of the detaching rock mass		?
7	Manning's N	Value of Mannings N given for each class		?

<sup>1</sup> [dataset for model input](#)

When the input maps are ready, the GUI will further require the run file for the software. The run file in the case of this research is modified from the one given in the manual of OPH1 (van den Bout et al. 2018). The run file generally compiles all the necessary parameters that could be changed within the GUI and saves it into a .run file format. This file generally includes the input and the output directories, the modelling settings, include/exclude processes, computational settings, and so forth. An example run file used in this study is shown in *Annexe 3: Example run file used in this research*

### 3.2. Calibration

Technically, calibration of the input parameters had to be done for the OPH1 and OPH2 models separately. However, the huge computational cost of OPH2 does not permit full calibration within the time limits of this study. In this regard, only one set of calibrated parameters were taken into the OPH1 model simulations. The details of the simulation will be further discussed per case study in the upcoming sections.

#### 3.2.1. The best estimate of the input parameter for OpenLISEM- back analysis in the form of calibration

Three input parameters that are missing, as mentioned in Table 4, are calibrated using the methodology of back analysis. The back analysis is a useful tool to predict geotechnical parameters of a problematic slope with the lack of results from laboratory testing (Hussain, Akhtar, and Stark 2012). Data from laboratory testing relies on the choice of sampling done within a study site and the number of samples taken to represent a specific unstable slope; which sometimes may not be sufficient to represent the overall rock mass. Several peer-review journals use the state of the art method to back analyse several input parameters that could not be collected in situ due to practical as well as analytical reasons (Hussain et al. 2012; McDougall 2017; Mergili et al. 2017)

In this research, back analysis was done by processing the results generated by the outputs from the software packages RF3D and r.avaflow. Then, based on this simulated inventory map (considered as “true” inventory as it was based on field-tested results), the calibration of the three unknown parameters as mentioned in Table 4 was carried out.

Calibration was started firstly with a set of parameters generated from literature as well as the previous dataset. Furthermore, these sets of parameters were simulated to generate a runout impact map. This runout impact map was assessed relative to the simulated inventory of observed processes employing the Cohens Kappa metric. As opposed to percentage accuracy, the choice for this metric is due to the complete estimate of interrater reliability. Cohens Kappa corrects for positive predictions that occur due to chance. In landslide runout assessment, this is seen to be vital as the true negative predictions among two landslide inventories generally tend to dominate the study sites as a whole (Bout et al. 2018).

A gradient descent algorithm was used to perform multi-parameter optimization efficiently. This algorithm is widely used to optimise computation on the dataset with uncertainties (Fabian 2018; Jason 2019). In this research, the objective was to minimize the value of 1-accuracy, which is an indication of total error. Gradient descent iteratively finds the gradient of the error function in n-dimensional space (with n the number of parameters used for calibration). Then, small step sizes are taken in the direction of the steepest descent. With appropriate step-sizes, determined by Armijo-backtracking, a local minimum of the objective function was found, providing a final set of parameter values. Stochastic gradient descents perform this iterative approach for numerous starting positions to find the absolute lowest minimum value.

In this research, the back calibration was done based on the OPH2 software interface, which comes with built-in functionality to write a script within the software tool. Also, there is a rich variety of toolboxes that could be used for various functionalities. For the calculation of Cohen's kappa, the function *MapContinuousCohensKappa* was used. This function returns the value of Cohens Kappa (0-1) as a reliability indicator to the two input maps that goes as the input into the function. It is generally necessary to specify a minimal flow height above which runout impact is considered, as very small flow heights (which can occur due to numerical issues) might not be visible and mapped from imagery. Thus, the continuous extension of

Cohen's kappa not only counts the presence and absence of runout impact but further considers the runout height that is incorrectly predicted in non-impacted areas.

One other crucial function used was the *OptimizeCustom* (built in in OPH2) which finds a set of parameter values for which a custom error function returns its lowest value. Here, the gradient descends/Armijo-backtracking algorithm comes into play. The gradient further was determined using a finite-difference calculation for which the learning rate and the time steps of the iteration need to be provided within the script. Lastly, the *Calibrate* function was used to assigns values to the individual parameters upon progressive iterations according to the error function being calculated by the function *OptimizeCustom*. All these functions are built-in for the OPH2 software interface. (One example script is shown in *Annex 4: Example script for calibration*)

### 3.3. Accuracy assessment

By the end of the calibration process, the three parameters to be calibrated, as mentioned in Table 4, had calibrated values that would give a certain accuracy to the OPH1 model. This accuracy calculation, meanwhile, was based on the solid heights simulated by the models. Even though solid heights are a significant parameter on runout modelling, considering the extent and sensitivity of the modelling area, the final accuracy assessment involved using spatially simulated Kinetic energy (as the reference data from RF3D provides kinetic energy). Calculating the kinetic energy values, the results of the RF3D model could be directly compared to the result from OLH1 and OLH2. Furthermore, for the large-scale events that mimic the rock avalanche behaviour, the impact was calculated as debris flow impact pressure considering the large mass of detachment and presence of fluids. For the case study of Acheron, no RF3D reference data existed, and conversion to kinetic energy was not required for inter-model comparison.

The OPH2 using the MPM was simulated based on the calibrated parameters by OPH1. The goal was to access the accuracy (based on impact pressure) of the simulation compared to the trajectory and the flow models lying into two extreme ends.

The assessment was based on calculating kinetic energy, which is not the standard output for all the models in use. Because of the model mechanics used by RF3D, model output is based on various derivatives of kinetic energy. (mean of the kinetic energies in each pixel, mean+2\* the standard deviation of kinetic energies, and so forth) But, in OpenLISEM, the kinetic energy values need to be calculated based on the mass and the velocity of each block in individual pixels.

For each pixel, the kinetic energy in OPH1 and OPH2 was calculated as follows

$$Volume = solid\ height * pixelsize^2 \quad (10)$$

$$mass = volume * density \quad (11)$$

$$Kinetic\ energy = \frac{1}{2} * mass * solid\ velocity^2 \quad (12)$$

As seen in equation 12, the energies are calculated only based on solids. Here, an assumption was made such that no energies are included associated with the height of the fluid. Since there is no much fluid in the simulation in this research, the energies are also thought insignificant.

For the flow models, the debris flow impact pressure is calculated as described by Hubl and Holzinger (Ahmadipur and Qui 2018; Hübl et al. 2003)

$$Impact\ pressure\ max = 5 * \rho V^{0.8} (gh)^{0.6} \quad (13)$$

Where,

$\rho$  – effective density of the flow mixture (water+solids)

V is the velocity, g is the acceleration due to gravity, and h is the height of the flow mixture.

Each parameter was derived from OpenLISEM output maps.

Eventually, the last step was defining a lower threshold to delineate impact due to a certain level of kinetic energies. In other words, defining the minimum kinetic energies that are required to create impact. This part

is significant as technically, the software would simulate all the kinetic energy values ranging from the maximum to the minimum, which is positive but very close to zero. However, taking all these values to map the impact would not be meaningful. Therefore, the lower cut-off was made to delineate impact, yet; these cutoff energies are site-specific and depend upon the level of protection each site is seeking. In practice, a helmet can resist the energy of 0.05KJ according to the European, Australian, and New Zealand personal protective equipment (PPE) standards. (British Standards Institution 1995; Standards Australia and Standard New Zealand 1997). In addition, when it comes to damages to the machinery, an impact of 11.6KJ is considered the threshold according to ISO 3449 (2005), and lastly, an impact of 300KJ is delineated as an impact resisted by sturdily build reinforced concrete wall (Ferrari et al. 2017; Lateltin et al. 2005; Mineo et al. 2018). Given the cutoff thresholds from various sources for the respective purpose, a lower cutoff of 0.5KJ was used here. This choice was analytically made where assumptions like individual people walking along the hazard zone are neglected. The imaginative assumption that a block of 10kgs moving as slow as 10m/s will not create impact was made in scientific terms.

A final accuracy assessment was then given by comparing the results from the OPH2 models to the kinetic energy values simulated by the RF3D models in the case study of Andorra and Barcelonnette. For the case study of Acheron, the impact pressure was calculated based on the output of the OPH1 and OPH2 model and hence compared also with the runout inventory from previous research of Mergili et al.(2017). This choice was reinforced because the previously done research on r.avaflo and OPH1 hazard share the common theoretical background- the two-phase equation from Pudasaini (2012).

## 4. CASE STUDY SITES

The three selected case study sites are selected to incorporate various scales of fall movements such as; particle fall, rock mass fall, and rock avalanche. The case studies are assigned to these movements (see Table 5) based on the unambiguous assumptions by Bourrier et al. (2013), where volume thresholds are used to categorize each movement. Figure 4-1 shows the runout distance of each study site measured through the axis of the runout. The average slope angles calculated for the runout for the three case study sites are respectively 40°, 34°, and 11° for Barcelonnette, Andorra, and Acheron. This geometrical variation helps us understand the variation in the data set, providing sufficient challenge for the models to exhibit their weaknesses and strengths.

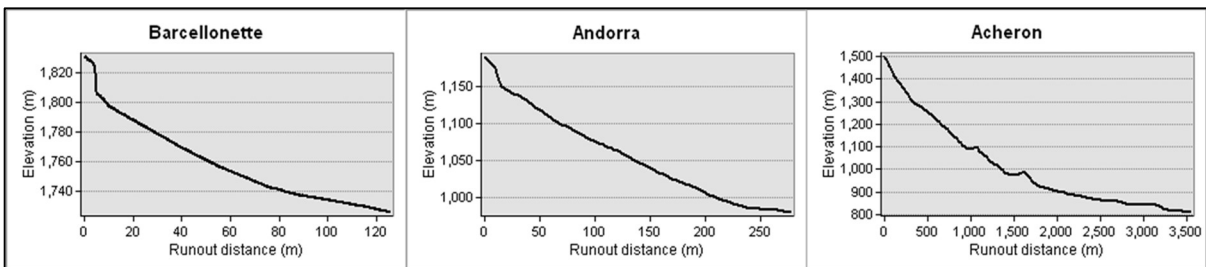
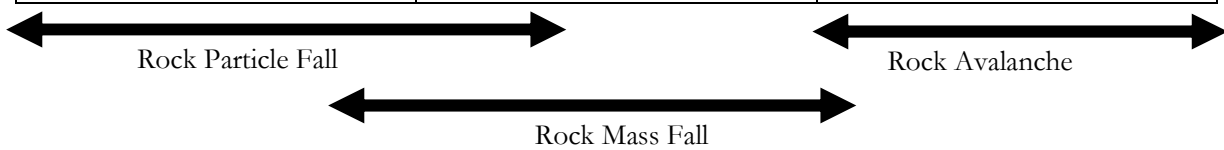


Figure 4-1 Elevation profile along the runout axis of the case study sites

Table 5 Schematic categorization of the case study sites in respect to the type of movements

The volume of detached rock mass for each case study site corresponding to the type of movement ( based on Bourrier et al. (2013))		
Barcelonnette	Andorra	Acheron
Simulations ranging from 1m <sup>3</sup> -8m <sup>3</sup> of rock mass along 7 detachments	Simulations ranging from 10m <sup>3</sup> -150m <sup>3</sup> of rock mass along 2 detachments	Simulation of 10*10 <sup>6</sup> m <sup>3</sup> of rock mass



#### 4.1. Case study 1: Acheron rock avalanche

The Acheron rock avalanche is a historical rock avalanche that occurred approximately 1100 years BP (Smith et al. 2006). The site lies in the Canterbury region, New Zealand, and is considered a large-scale rock avalanche. The source of the Acheron rock avalanche is the greywacke rock of the Mesozoic Torlesse Supergroup. The first deep-seated failure was thought to be due to an earthquake (Smith et al. 2006). The result was a massive release of 6.4 million cubic meters of rock mass, first moving east, then with a sudden turn of  $\sim 75^\circ$  towards the south, south-east following the valley (Smith et al. 2006).

The source greywacke rock consists of interbedded mudstone and sandstone steeply dipping north. Previous research also suspects that the detachment is supported due to the interbedding of the incompetent argillaceous mudstone dipping towards the north (Mergili et al. 2017; Smith et al. 2006). The cirque-shaped source resulted in a 3.5km long-runout along the valley with extreme fragmentation. The fragmentation process resulted in various geomorphological structures like levees, lateral rims, and depressions along the runout path (Smith et al. 2006). There lies a strike-slip fault almost halfway through the runout axis called the porter pass fault. The fault is later seen to be buried along the valley by the runout deposit (Smith et al. 2006)

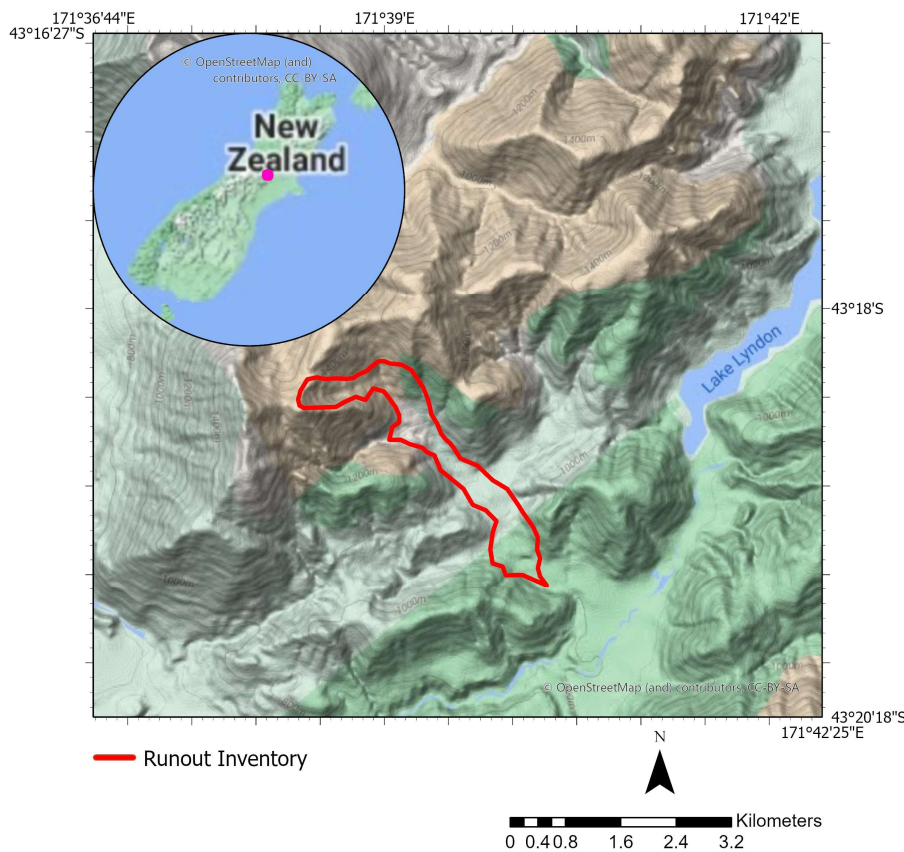


Figure 4-2 Study area of the Acheron rock avalanche, Canterbury, New Zealand.

##### 4.1.1. Input data preparation

The result raster dataset from the previous research done by Mergili (2017) generated using the software platform r.avafLOW was downloaded first, available in their repository<sup>2</sup>. Then, the dataset was downloaded as a Grass GIS zip file extracted by the Grass GIS 7.8.4 platform.

The output rasters used from the repository were the DEM with a pixel size of 20m, a total height of the rock mass to be released divided into pixels of 20m, and the runout inventory. Another dataset needed to

<sup>2</sup> [link to repository](#)



run the OpenLISEM model was extracted from the published paper (Mergili et al. 2017) and is described in Table 6.

As described in Table 6, out of the total height of the solid being detached in the 20m grid, the initial fluid height and initial solid height was separated with a ratio of 1:9. This approximation is based on the research done by Mcdonald for the physical properties of the soils in New Zealand from the greywacke parent material (Mcdonald 2012). The study results with the moisture content varied from 8.3 -25.2 % by volume for the samples. The decision to select the lower threshold (10% fluid) was applied going back to the research objective, which is to model more like a dry granular flow/ rock avalanche phenomenon. The role of fluid is considerably less, and movement of fluid-solid is thought of importance. Other missing parameters were derived from literature values. For instance, the value of cohesion was derived from a doctoral thesis looking at the rock strength and deformability of the greywacke rock in New Zealand (Stewart 2007). This value extracted from this thesis was the triaxial test results done on the parent rock. A sandstone sampled from the parent rock showed a cohesive strength of 48Mpa. This high strength of cohesion is expected not to be generalized over the whole rock mass and calibrated to a lower value. The remaining parameters like the Mannings N and rock size are used according to the OPH1 manual (van den Bout et al. 2018)

**4.1.2. Calibration results**

Calibration of the parameters, namely the IFA, Mannings N, and the initial fluid height, were initially used in calibration. However, the influence of additional fluids led to severe instabilities in the gradient descent algorithms, which could not obtain convergence. Therefore, the calibration used only the IFA and the Manning N, generating the final set of values as given in Table 6.

For the calibration, parameters for the *Optimizestom* was such that the learning rate was given at 0.01, and the time step of 0.8 was used to generate iterations. A total of 120 model iteration (as shown in Figure 4-3) finally gave the best Kappa value of 0.62 in iteration number 69. The multiplication factor achieved for the IFA was 1.02593, and the multiplication factor for Mannings N was 0.985541.

Further, since the values of Cohesion could not be calibrated from the standard method described in the Methodology part, the parameter was calibrated manually (trial and error) to find the best fit value.

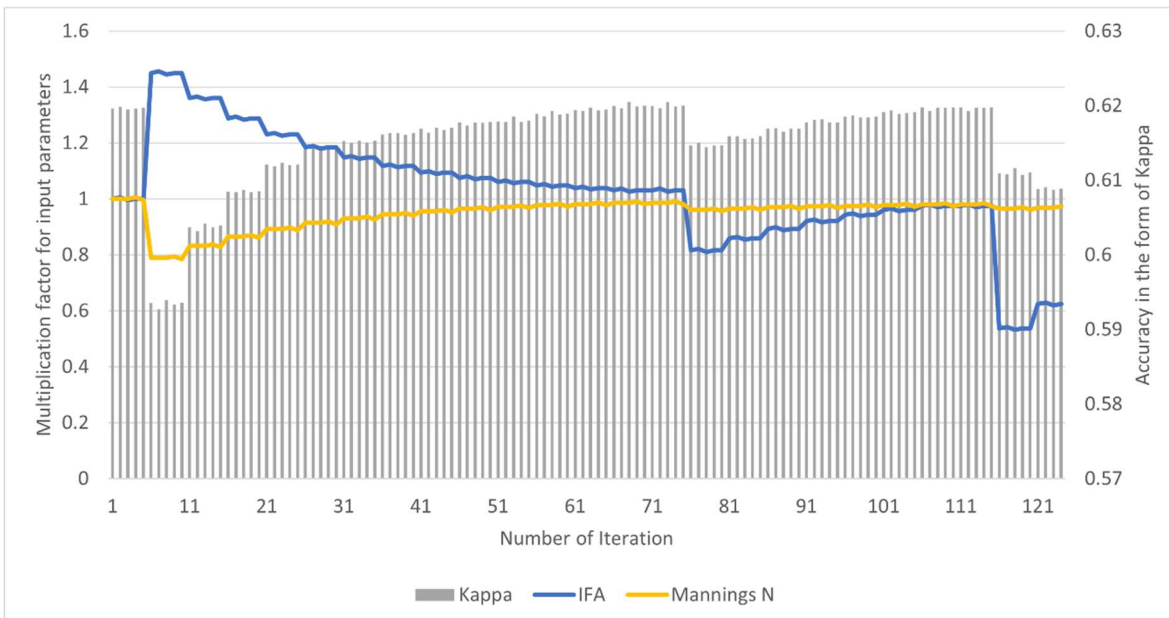


Figure 4-3 Convergence graph showing the calibration of the parameters within iterations



Table 6 Values of the calibrated parameters for the case study site of the Acheron rock avalanche.

Input map	OpenLISEM (.map)	Literature values	Values to be calibrated
1	Rock mass density	2700 kg/m <sup>3</sup> (Mergili et al. 2017)	Not calibrated
2	Initial solid height	Raster map created according to the total height of rock mass release obtained from (Mergili et al. 2017). Further fluid: solid separates as 0.1:0.9 with a general assumption to the physical properties of greywacke rock material in New Zealand (McDonald 2012; Stewart 2007)	
3	Initial fluid height		
4	Rock size		
5	Angle of internal friction (IFA)	0.39 radians (Mergili et al. 2017)	0.40 radians
6	Cohesion	48 Mpa (Smith et al. 2012; Stewart 2007)	0.014 Mpa
7	Manning's N	0.14 (van den Bout et al. 2018)	0.13

**4.1.3. Modelling results/accuracies based on impact simulated by each model**

Accuracies based on Cohens Kappa were calculated to 0.57 for OPH1 and 0.66 for OPH2. But when it comes to the transition of energies along the runout axis, OPH2 is seen to carry much more energies down the runout line although simulated with the same input parameters. The energy values for the OPH1 and OPH2 model was calculated having the output dataset. But, in the case of r.avaflow, the generic output from the repository did not contain the velocity parameters; therefore, the impact pressure simulated by the r.avaflow model could not be compared. Unfortunately, due to time limits running the LINUX based software could not be a part of this research. Further, the velocities generated by each model and its comparison to the previously done research will be discussed in section 5.

Impact map simulated by OpenLISEM models and comparing it with the output from r.avaflow

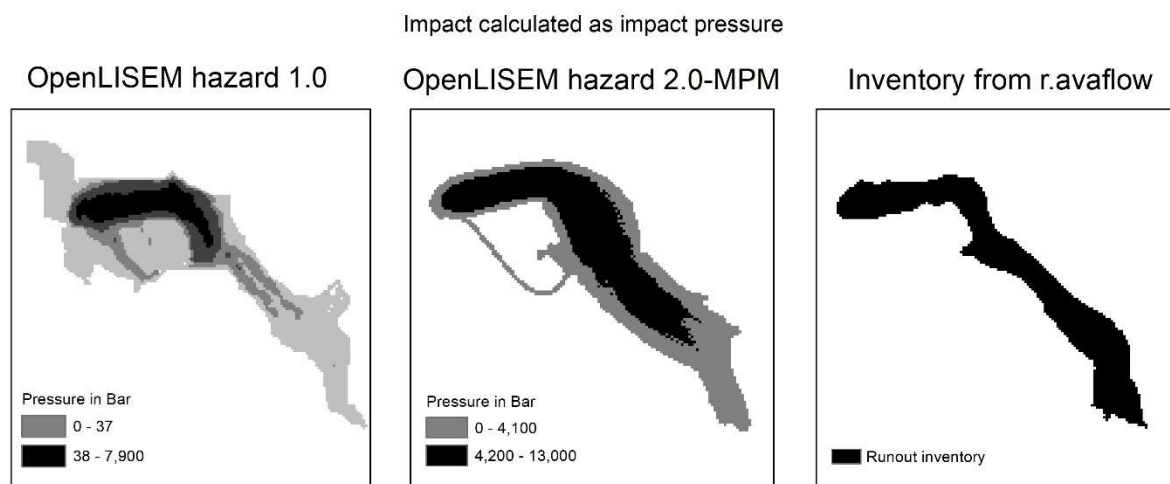


Figure 4-4 Runout inventory simulated by the three models for the case study of Acheron

## 4.2. Case study 2: Sola de Andorra

Andorra is a small country located between France and Spain. The part Solà d'Andorra is chosen for this research which lies above the capital Andorra la Vella. There have been a series of rock mass fall events in 1987, 1997, and 2008 on this site with serious damages (Andrea 2014; Mavrouli, Corominas, and Wartman 2009)

The formation of the U-shaped valley is evidence of the retreat of the Pleistocene glaciers that occurred almost 20000 years ago (Mavrouli et al. 2009). The tectonic setting around the area also leaves the area to seismicity, triggering rock mass fall. Although, the main reasons for the rockfall are thought to be the freeze-thaw action under non-seismic conditions (Andrea 2014; Mavrouli et al. 2009). The main geology of the area is granodiorite, but the area consists of sedimentary rock outcrops that are highly fractured. There have been life-threatening runout events from the past in this area with large variations in scale.

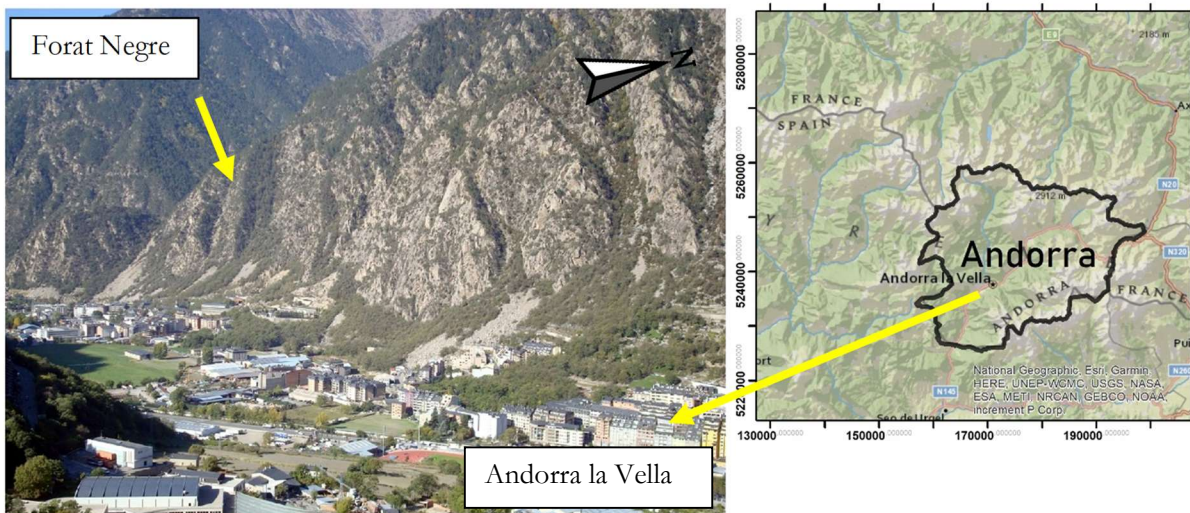


Figure 4-5 Study area of rockfall prone area in Andorra. Location map of the Forat Negre (Left). The right map gives the country's perspective lying between France and Spain to the capital Andorra La Vella. Photo- Andrea (2014)

Some important events, also mentioned before are 1987 where the runout of 50000m<sup>3</sup> of block killed three people and closed the highway, followed by the event in 2004 where 25m<sup>3</sup> of block impacted a building, and lastly, in 2008 where a 150m<sup>3</sup> block damaged a building (Andrea 2014). There have been rockfall studies based on the simulation of RF3D models where the results are validated with the historic events. Data like the runout extent, soil maps, and surface roughness will be used from the previous studies to calibrate this research (Andrea 2014; Mavrouli et al. 2009).

Similar to the method described for the Acheron case study, previous research from Andrea (2014) will be used as reference. Unfortunately, no runout inventory is available, and such an inventory is crucial in calibration. Since the trajectory models are used within the case study site for modelling in previous research, the output from the RF3D model will be used as a simulated inventory for runout impact. This simulated inventory approximates an actual inventory because the modelling output is based on a calibrated dataset using historical rockfalls.

### 4.2.1. Input data preparation

#### Input data for RF3D

Out of all the rockfall events, the rockfall events in Forat Negre were chosen. This choice was motivated by the previous research done by Andrea (2014) and Jazvin (2016) examining the forest effect and structural protective measures on the area. The previous research was seen to be crucial for the back analysis that must be done to predict the best set of input parameters for the OpenLISEM to function properly.

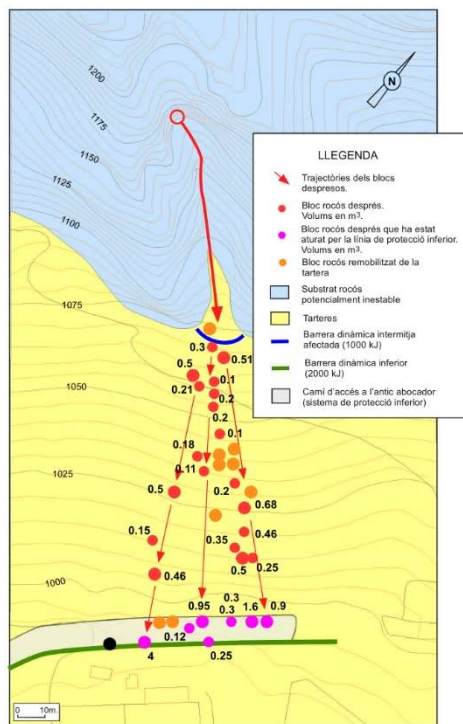
Two events in Forat Negre, namely the events in the year 2008 and 2004, were selected for modelling. There has been a detachment of 150m<sup>3</sup> of rock mass in 2008 and 25m<sup>3</sup> of rock mass in 2004. In addition to the research data, data of these two events are also available in the means of an inventory map (collected in field), where the reach of individual fragmented blocks are available as a non-digital map (PDF format as shown in Figure 4-6).

First of all, the “true” inventory map needs to be created according to the planned methodology. The largest block size of 31m<sup>3</sup> for the 2008 event and 4m<sup>3</sup> for the 2004 events was modelled in RF3D to create the simulated inventory map. Details to the simulation given in Table 7, all the parameters used are copied from the previous research done by Andrea (2014) and Jazvin (2016).

Table 7 Simulation details for RF3D for Andorra

Simulation details	2004 event	2008 event
Number of simulations	100	100
Block dimension	3*1.7*0.8	5*4.8*1.3
Block shape	Rectangular	Rectangular

Event in 2004



Event in 2008

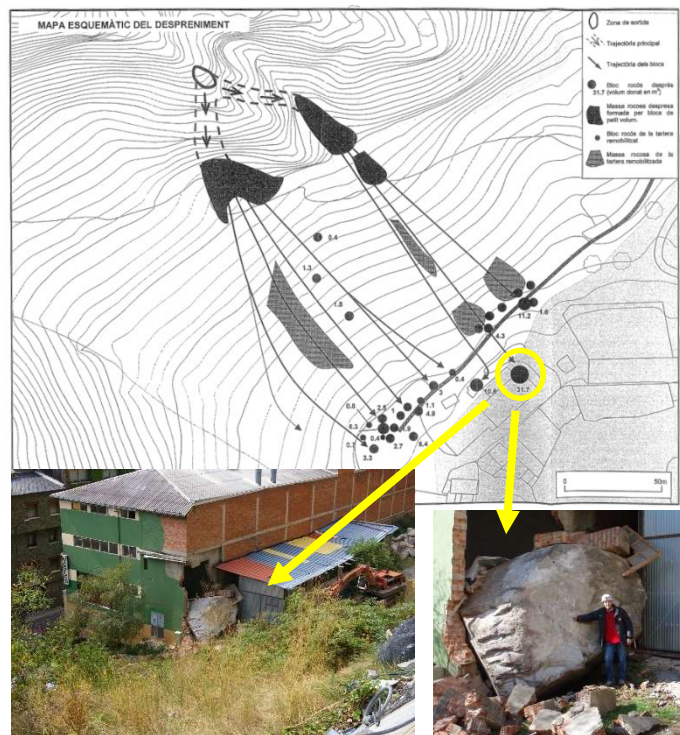


Figure 4-6 Rockfall inventory data available for the 2004 event (left) and 2008 event (right)

Other input maps (those not mentioned in Table 7) for RF3D to run were the same as used by Andrea (2014) and Jazvin (2016).

Since the output maps created by RF3D are 100 simulations of individual block trajectory, the map was masked out from the reach\_probability.asc with values less than 1.5%. This decision was based on the RF3D manual (Dorren 2016), where the author expects to consider the values lesser than 1.5% as outliers for inventory mapping.



The simulation was finally done with the inclusion of trees. The inclusion of trees into the modelling domain was in the form of an ASCII file from the previous research. In addition, the software package comes with added functionalities like the variation in rock volumes per iteration and additional fall heights during initiation, which is not used in this research.

### Input data for OpenLISEM

Based on the literature, the best fit input dataset for OPH1 was first created (see Table 8). The total solid height and fluid heights were generated according to the rockfall event of 2008 and 2004. A point location was translated into a small initiation area based on descriptions of the event and the source volumes. This way, it was made sure that the rock mass to be modelled would not be perfectly geometrical but more like a realistic rock mass. It was made sure that the total volume of the rock mass in these two events would be as same as the original detachment anticipated ( $150\text{m}^3$  for 2008 and  $25\text{m}^3$  for 2004)

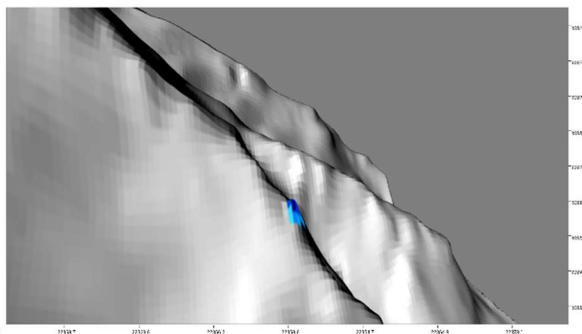


Figure 4-7 Delineation of a realistic detachment of rock mass (blue)-the image showing the hypothetical  $150\text{m}^3$  detachment occurred in 2008

Although there was no fluid associated with the trajectory modelling, for the functionality of OPH1, fluid equal to its standard moisture content was introduced into each simulation. The amount of solid to fluid ratio used in the simulation was 0.954:0.045. This ratio was derived from (Akhil and Reddy 2015) in reference to the natural moisture content (4.5% by volume) of granodiorite and hornfels. The density used was the same as that of the RF3D input file. The values of geomechanical properties, in this case, were used from research done by Mavrouli et al. (2009) where the Cohesion(c) and Angle of internal friction (IFA)( $\varphi$ ) were given as conservation estimates of joint strength based on the study done by (Barton 1974; Hoek and Bray 1981). The rock size estimate was done based on the rockfall inventory, as shown in Figure 4-6, with an idea of selecting the maximum rock size from the inventory. But since the simulations in OPH1 were done together for the 2004 and 2008 events, selecting the largest rock size within the two events would not be applicable. Hence, the largest block from the runout of the 2004 event was selected ( $4\text{m}^3$ ). Finally, the values for Mannings N was assigned based on a specific class of land use/land cover. In this process, first, digital image classification (DIG) was done from the orthophoto. DIG was done by supervised classification of the orthophoto in the software package Erdas imagine. Finally, 5 landuse/landcover classes were obtained, and these classes generated was assigned a Mannings N value from the OPH1 manual (van den Bout et al. 2018). The values are shown in Table 8.

#### 4.2.2. Calibration results

In the study case of Andorra, the set of calibrated parameters was achieved after running the algorithm for 92 iterations. The learning rate and the timestep for the *optimizrecustom* were set to 0.01 and 0.1. Hence, the final Kappa value was 0.73405, with the multiplication factor for IFA and Mannings N as 0.839833 and 0.960083, respectively. A hybrid chart is built to perceive the convergence of data change seen within the algorithms, as shown in Figure 4-8. The X-axis shows the number of iterations. The Y-axis (primary) shows the multiplication factor for each parameter delineated by the line graph and accuracy values delineated by the bar graph (secondary). SO, the final dataset then perceived by the process is shown in Table 8.

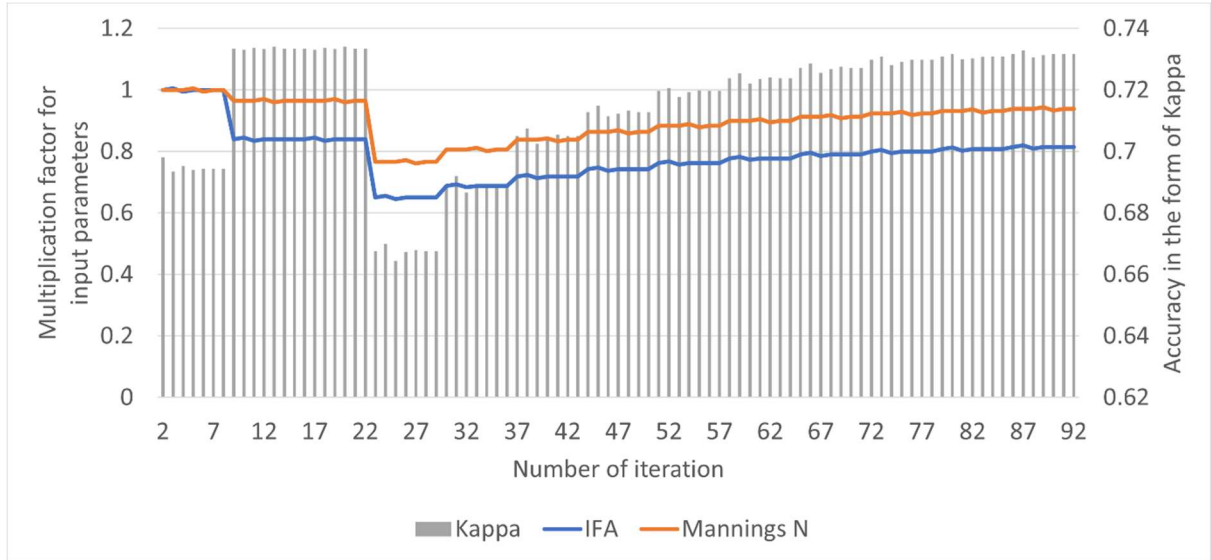


Figure 4-8 Convergence graph showing the calibration of the parameters within iterations

Input map	OpenLISEM (.map)	Literature values	Values to be calibrated		
1	Rock mass density	2200 kg/m <sup>3</sup> (Andrea, 2014; Jazvin, 2016)	Not calibrated		
2	Initial solid height	Raster with multi-value created according to the total volume and separated into two maps with a solid: fluid ratio of 0.954:0.045 (Andrea, 2014; Jazvin, 2016)			
3	Initial fluid height				
4	Rock size	4 meters (Andrea, 2014; Jazvin, 2016)			
5	Angle of internal friction (IFA)	0.53 radians (Barton 1974; Hoek and Bray 1981; Mavrouli et al. 2009)	0.44 radians		
6	Cohesion	0.20 Mpa (Barton 1974; Hoek and Bray 1981; Mavrouli et al. 2009)	0.02 Mpa		
7	Manning's N	Class	Land use type	Value	
		1	Road/building	0.05	0.048254
		2	Talus	0.1	0.096508
		3	Trees	0.5	0.482541
		4	Bush	0.3	0.289525
		5	Bare soil	0.03	0.028952

Table 8 Values of the calibrated parameters for the case study of Andorra

#### 4.2.3. Modelling results/accuracies based on impact simulated by each model

Finally, with the calibrated dataset, the simulation results for OPH2 were obtained, and the results were subjected to accuracy assessment based on the modelling outcomes of the RF3D model results.

The output of the RF3D, OPH1 and OPH2 models are calculated with impact which is calculated as kinetic energies.

### Impact map simulated by each model.

Impact calculated as Kinetic energy -Lower cutoff of 0.5 kilojoules applied

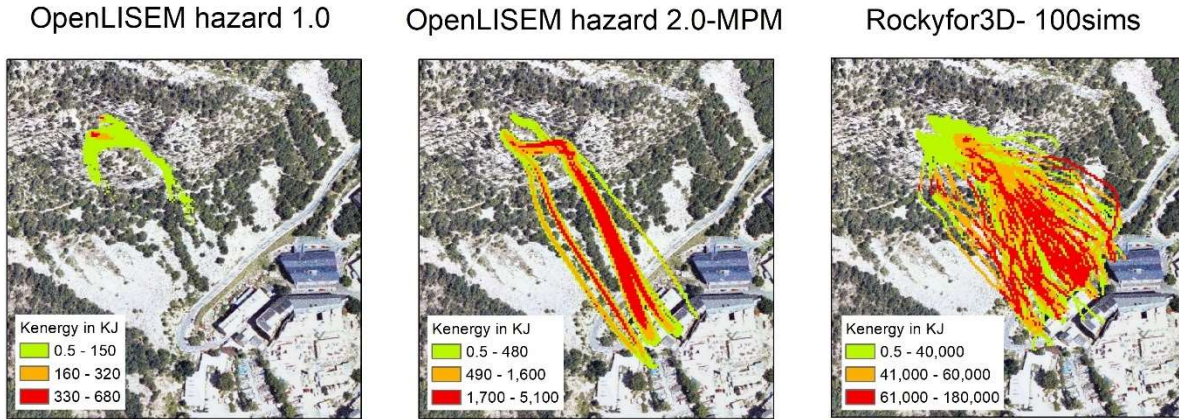


Figure 4-9 Runout inventory simulated by the three models for the case study of Andorra

As anticipated, the OPH1 model didn't function quite well when simulating a structured rock mass with the low influence of the fluid flow. But the MPM seems to have functioned reasonably well, as the reach of the rock mass simulated is relatively more accurate in comparison to the probabilistic result from RF3D (Figure 4-9). Also, the natural fragmentation behaviour of the rock mass was achieved. The fragmentation in OPH2 was non-diffusive and subject to the stress-strain forces the rock mass would experience during runout. Therefore, the rock mass fragmentation carries the partially fragmented (structured) to the runout extent, an interesting result to obtain within the flow assumption.

The OPH2 model achieves an accuracy of 0.47 in delineating the impact on this case study site. Although the model predicts fragmentation of the larger blocks released, the spread is insignificant compared to the granular flow model in OPH1. The reason for this was understood by the effect of trees and their use in simulating both models. RF3D, on the one hand, has a clear assumption regarding the deviation and impact dissipation of a rock block in the collision to trees (mentioned in 2.4). On the other hand, OPH1 and OPH2 do not contain such assumption. Instead, the OPH1 model features large spreading due to the intrinsic assumptions of granular flow models, namely non-structured cohesion-less flow. Finally, the OPH1 model uses a finite element-based solution to solve the underlying differential equations. Such numerical solutions are diffusive.

### 4.3. Case study 3: Barcelonnette

The study area is located in the French Alps along the Ubaye River valley. The geology consists of an underlying clay and shale layer with overlying competent sedimentary rocks of sandstone and limestone forming a cliff structure (Guachalla Terrazas 2016; Jazvin 2016). These sandstone blocks are subject to detachment due to weathering. A significant number of rock blocks deposited on the talus of the rock source zone along the valley is seen as evidence of the prominent rockfall in this area. The source zone is characterized by a very steep slope ( $\sim 74^\circ$ ) above a coniferous forest. Modelling done in this area was also using the RF3D software package (Guachalla Terrazas 2016; Jazvin 2016). The study results will be used extensively to parameterise the input data for the OpenLISEM models.

The study area doesn't have any significant elements at risk. Therefore, despite rockfall modelling, there has not been any other form of research in this area. Therefore, that availability in literature was scarce.

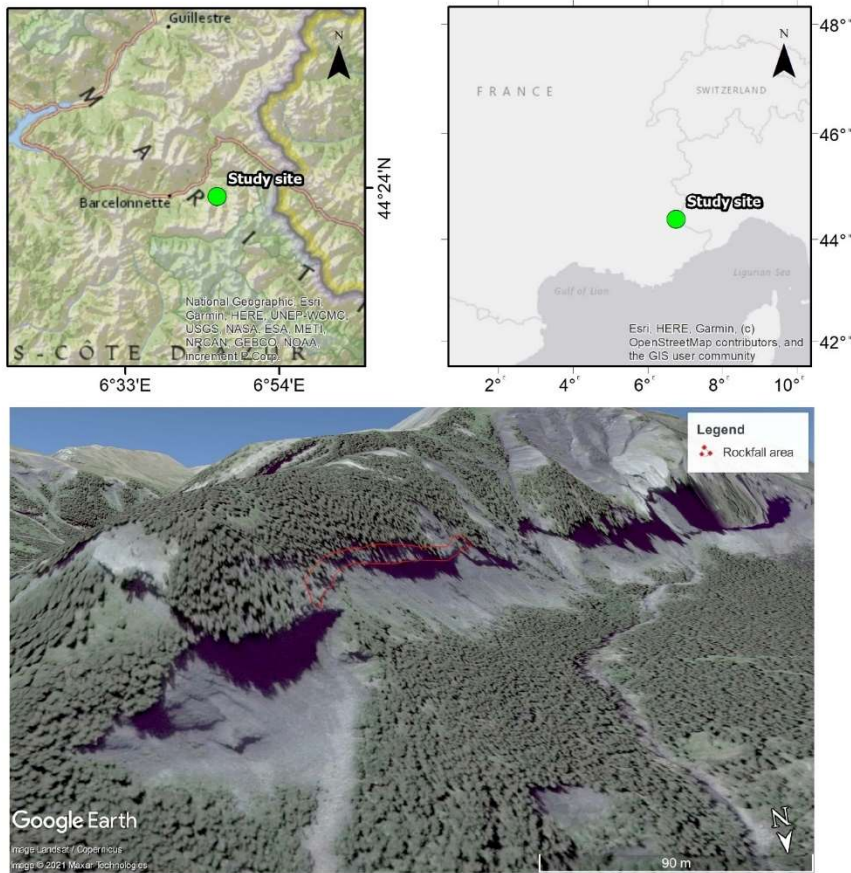


Figure 4-10 Study area of the Barcelonnette rock fall area.

#### 4.3.1. Input data preparation

##### Input data for OpenLISEM

The scale of the study site led to conduct modelling in 0.5m pixels, which previously was thought to be done in 2m resolution. Modelling done within the 2m pixels gave unclear results, which was thought to be due to the non-functionality of the flow assumption because of steepness during the initiation and large timesteps taken. The upscale of the DEM slowed down the simulation time but gave better results than that of the 2m resolution.

Detailed data like the reach extent of a boulder from the source zone, the boulder geometry, and so forth are unavailable for this case study site. The previous research analysed by delineating a hypothetical line of source along the potential rockfall area. The straight line of source is not an issue while modelling rockfall



in the RF3D package due to its assumption of separate rockfall initiation along every pixel. But the same line source was a problem during the simulation as the OPH2. OPH2 would assume this straight line of source material acted as a long connected rectangle having a height as that of the solid height map, width as

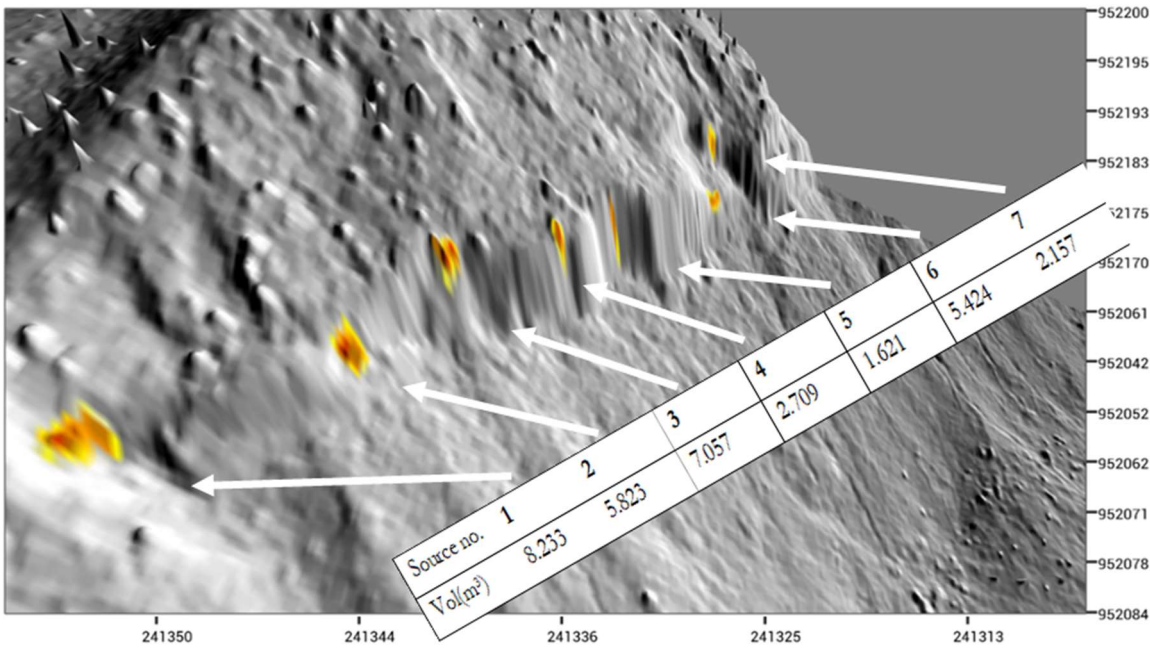


Figure 4-11 The assumed rockfall zone showing the specific volumes of detachment (in 3D)

that of the pixel size, and the length going along the length of the marked source line. Therefore, to create a much realistic and natural rock mass detachment along the source area. Rock mass detachment zones were selected manually based on the morphology of the slope and terrain condition. The seven detached rock mass have different volumes and shapes, as shown in Figure 4-11.

The parameter values for the rock physical and mechanical properties like the cohesion ( $c$ ) and IFA( $\varphi$ ) were derived from literature values. Since, the study site is with the presence of sedimentary rock, mostly limestone, the research looking at engineering properties of limestone is referred to extract values for the cohesion and IFA of the rock mass (Toševski et al. 2010). Moreover, the solid to fluid ratio is assumed based on research analysing the moisture content of rock mass (Mammen et al. 2019; Rempe and Dietrich 2018).

### Input data for RF3D

Although modelling in OPH1 and OPH2 was done in 0.5m pixel, modelling in RF3D was still decided to do in 2m pixel. This choice is motivated by the research done by Dorren and Heuvelink (2004), which concludes the proper functionality of the software lies between the resolution of 2m and 10m. The modified input maps (i.e., rockdensity.asc) are generated based on a script (.bat file) to run the SAGA GIS version 4 by Luuk Dorren in May 2017. The script is available on the website of ecorisQ.<sup>3</sup>

The identification of the pixels containing trees is generated from the software tool FINT (Dorren 2014). The tool generates the position of trees based on digital surface models based on high-resolution surface models (e.g. LIDAR). The spatial identification of trees is calculated based on the DSM and DEM, including other properties such as the tree's stem diameter and breast height. These parameters are needed for the RF3D software to run with the simulation, including trees.

Finally, the “true” inventory for Barcelonnette is generated using the RF3D. The reach\_probability.asc map is used. The preparation process and the map used are the same as mentioned in section 4.2.1. Other input

<sup>3</sup> [Input data preparation for RF3D](#)



maps for RF3D are the same as used by Jazvin (2016). Please refer to their thesis for the details of the input parameters.

Source number	1	2	3	4	5	6	7
Block dimension	2*2*2.05	2*2*1.45	2*2*1.76	2*2*0.67	2*2*0.40	2*2*1.35	2*2*0.53
Number of simulation	100						
Block shape	Rectangular						

Table 9 Simulation details (RF3D) for Andorra

### 4.3.2. Calibration

The set of calibrated parameters is achieved after running the algorithm for 70 iterations. First, the learning rate and the timestep for the *optimizecustom* are set to 0.01 and 0.05. Hence, the Kappa value is 0.713837, with the multiplication factor for IFA and Mannings N as 0.927644 and 0.997607, respectively. Finally, the final dataset, then modified by the calibration process, is shown in Table 10.

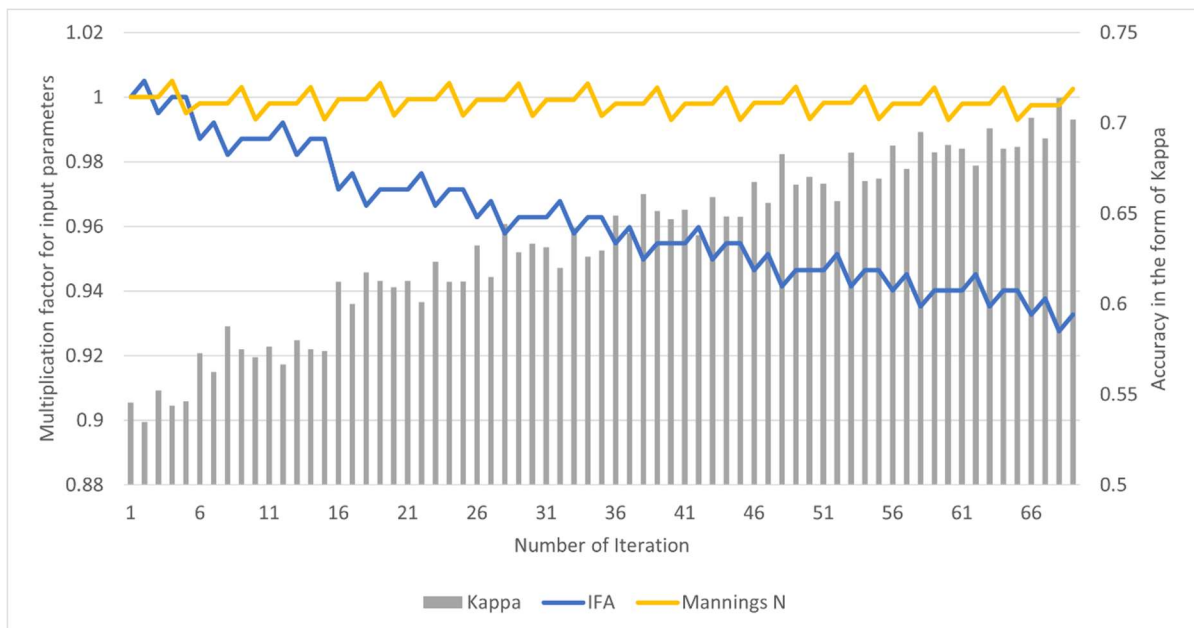


Figure 4-12 Convergence graph showing the calibration of the parameters within iterations

Input map	OpenLISEM (.map)	Literature values	Values to be calibrated
1	Rock mass density	2600 kg/m <sup>3</sup> (Jazvin, 2016)	Not calibrated
2	Initial solid height	Hypothetical values are used corresponding to the site conditions. Solid: fluid ratio 0.95:0.05 with an assumption of general moisture content in a rock mass (Mammen et al. 2019; Rempe and Dietrich 2018).	
3	Initial fluid height		
4	Rock size		
5	Angle of internal friction (IFA)	0.64 radians (Toševski et al. 2010)	0.56 radians
6	Cohesion	16 Mpa (Toševski et al. 2010)	0.02 Mpa
7	Manning's N	0.15	0.14

Table 10 Values of the calibrated parameters for the case study site of Barcelonnette

**4.3.3. Modelling results/accuracies based on impact simulated by each model**

Results here are similar to that of the case study of Andorra. The OPH1 model did not function well with a low Kappa value of 0.04. Due to terrain steepness during initiation, the solids and fluids are seen to diffuse, losing their energies upon the first few timesteps. On the contrary, the OPH2 model managed to transport the solids onto the runout extent anticipated. Hence, a Kappa value of 0.57 is achieved when comparing it with the simulated inventory as described in section 3.3. The velocity simulated by the OPH2 model is although low as compared to the RF3D simulation. The low-velocity results in low kinetic energies simulated, which are significantly different in between the RF3D and OPH2 model outputs, as seen in Figure 4-13

**Impact map simulated by each model.**

Impact calculated as Kinetic energy -Lower cutoff of 0.5 kilojoules applied

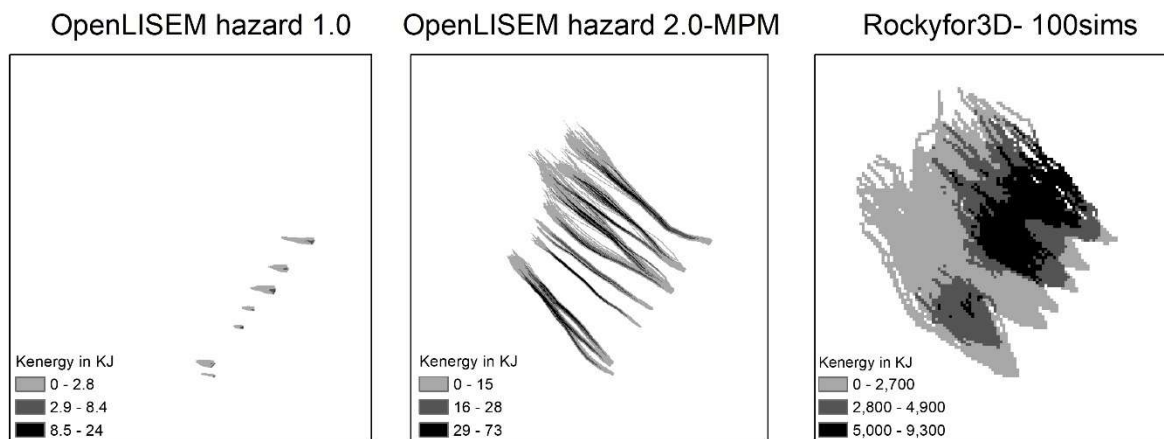


Figure 4-13 Runout inventory simulated by the three models for the case study of Barcelonnette

## 5. RESULTS

The following part is divided into analysis sections to address the research questions. Each section is thought to carry importance in the runout of a semi-structured mass.

- 5.1 aims at understanding the spatial accuracy in the means of runout extent each model would simulate.
- 5.2 will further analyse the details looking at the velocities of a rock block each model would simulate along the runout axis.
- 5.3 will quantify the amount of energy each model is simulating when it comes to a specific element at risk
- 5.4 will explain details about the fragmentation behaviour simulated by the OPH2 model and the distanced these fragmented blocks travel.

### 5.1. Analysis associated with the overall accuracy of the models based on Cohens Kappa reliability index

Based on the values of Cohens Kappa it is apparent from Table 11 that the OPH1 is not the best tool to model the rock particle fall (individual rock on-air trajectory). As anticipated, Kappa values calculated for the case study of Andorra and Barcelonnette simulated low accuracies with the OPH1 model. The lower accuracies of OPH1 are present due to shortcomings of the model, i.e., the assumption that the initiating mass would lose its structure upon the first timestep of simulation, and the mass gets disintegrated and mixed with equal portion. In theory, the impact of a rockfall is generated when a certain mass of rock would travel at a certain velocity. Therefore, disintegrated rock mass with lost structure would generate lower energies depending on the study site and might not create an impact.

Based on model outputs such as the simulated velocities and the Cohens Kappa, OPH2 is seen comparatively bearing higher accuracy and progressing upon the simulation of dry granular flow in a non-diffusive setting. This progress of the OPH2 over OPH1 is substantial and progressive in modelling the flow of a dry rock mass. Yet, aligning with the simulation done by the trajectory analysis is a challenge. The accuracy could not get better than 0.57 for the OPH2 compared to the RF3D outputs as there is still progress to run OPH2 as a software in simulating rock as an individual block.

Another observation based on Table 11 is that the case study site of Barcelonnette simulates higher accuracy than Andorra. Simulated accuracies could be explained by the role of trees, as many trees are present along the runout line in the study case of Andorra as compared to Barcelonnette. Uncertainty is added to the OpenLISEM models because the mechanism to represent trees in this

Case study sites	Values of Cohens Kappa	
	OPH1	OPH2
Acheron	0.57	0.66
Andorra	0.16	0.47
Barcelonnette	0.04	0.57

Table 11 Calculated Cohens Kappa values for each case study sites

Impact simulated by the models in use

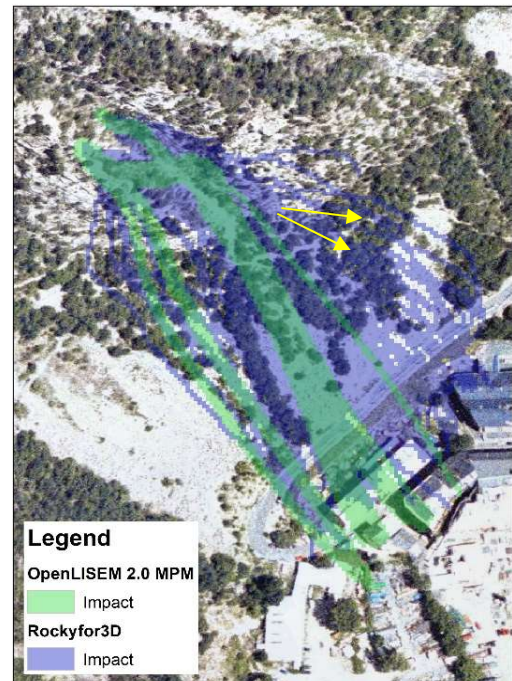


Figure 5-1 Effect of trees in modelling, yellow line showing the parts where OpenLISEM model need to fragment and spread in collision with trees.

model does not include dispersive redirections after collisions. Therefore, as seen in Figure 5-1, there could not be deviation or obstruction of the runout mass due to trees, which is possible in the case of the RF3D model and hence implemented to result in an impact map that is spread towards the end of the runout.

For the avalanche modelling (Acheron study case), both OPH1 and OPH2 simulate the phenomena accurately with a Kappa value of 0.57 and 0.66, respectively. The OPH2 using MPM is seen to have more realistic and accurate results because the OPH2 model is seen to maintain the structure of a rock mass during runout. Only during the runout with full stress-strain calculation, it is seen to disintegrate further. However, OPH1, the initiation is rather diffusive (irregular) with a streamlined flow of the material, generally true while modelling fluids.

There has to be velocity and mass to generate enough energy along the runout line to create an impact. The flow model is incapable of doing this as the mass gets disintegrated and spread over the hillslope. This unstructured diffusive type of flow is prevented by the presence of cohesive structure in the moving blocks. Such as mechanism is provided by the OPH2 model, which preserved the majority of kinetic energy generated along the runout axis.

**5.2. Analysis associated with the velocity of a rock mass along a runout axis**

The results from the three case study sites are different in terms of the rock mass detachments and slope morphology. Therefore, to construct a framework in adding all the case study sites into one analysis, some additional methods were applied that relate mostly to the model assumptions and the type of output seen under each model assumptions. The comparison was a challenge since the RF3D model does not consider the possible fragmentation of rock mass that is being detached; it rather uses a probabilistic assumption by simulation of the largest boulder seen to reach any specific slope. Therefore, to make fair comparison, the OPH2 model was prevented in fragmenting the block of rock mass during simulation. This was done by increasing the value of cohesion of the rock mass. The value of cohesion, therefore, was changed to 0.04MPa for the case of Andorra. The change in value is based on trial and error during modelling where the property of fragmentation in the simulated rock block was monitored.

Selection of sources with different volume detached in each case study sites

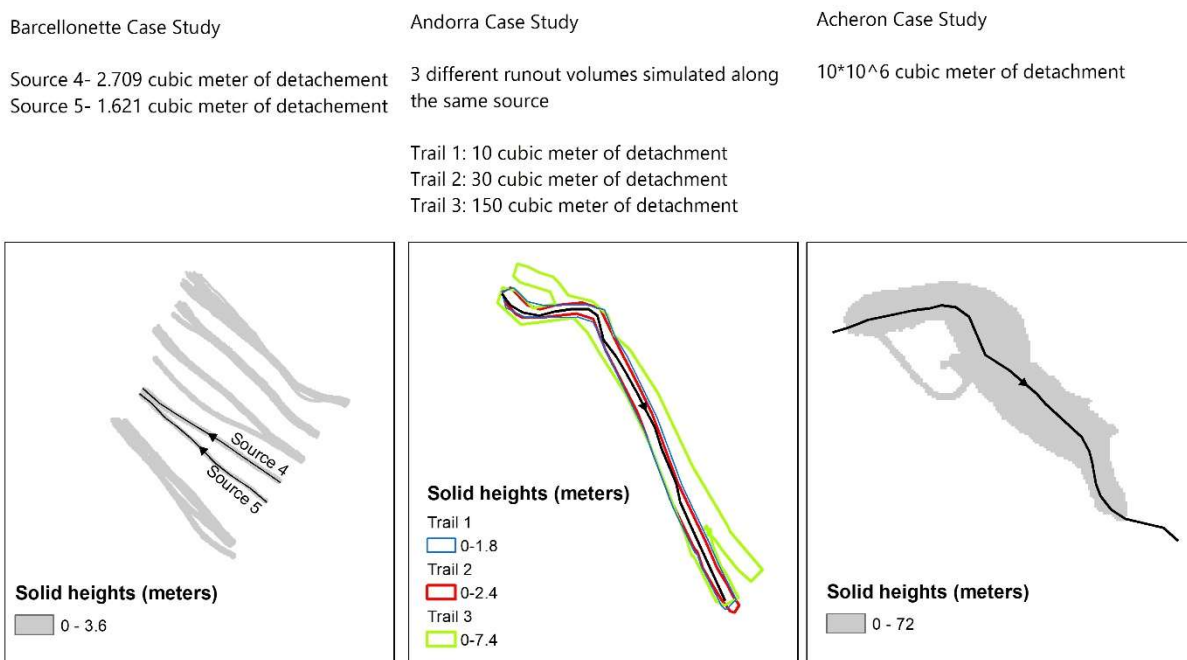


Figure 5-2 Selected runout axis for the analysis within the case study sites.

Summing up, 6 runout axis were simulated with a variation on the rock mass dimension incorporating all the case study sites using the selected models Figure 5-2. The evaluation was mostly to understand the velocity each model would predict along a designated runout line.

	Barcelonnette		Andorra			Acheron
	Source 4	Source 5	Trail 1	Trail 2	Trail 3	Source 1
Volumes in m <sup>3</sup>	2.70	1.62	10	30	150	10*10 <sup>6</sup>
<b>Name hereafter</b>	Runout 1	Runout 2	Runout 3	Runout 4	Runout 5	Runout 6

Table 12 Details of the runout axis with the given name for simplicity

As previously mentioned in section 2.4, the main issue in comparing two theoretically different models is that it will differ the output dataset significantly. In this case, the runout of the trajectory models did not match exactly with the runout of the flow model (shown in Figure 5-3). This issue was addressed according to the probabilistic nature of the RF3D package, where multiple simulations are possible.

The simulation concerned only checking the velocities along the runout axis by the OPH2, a GIS operation was implemented. This included drawing a perpendicular vector transect along the runout line,

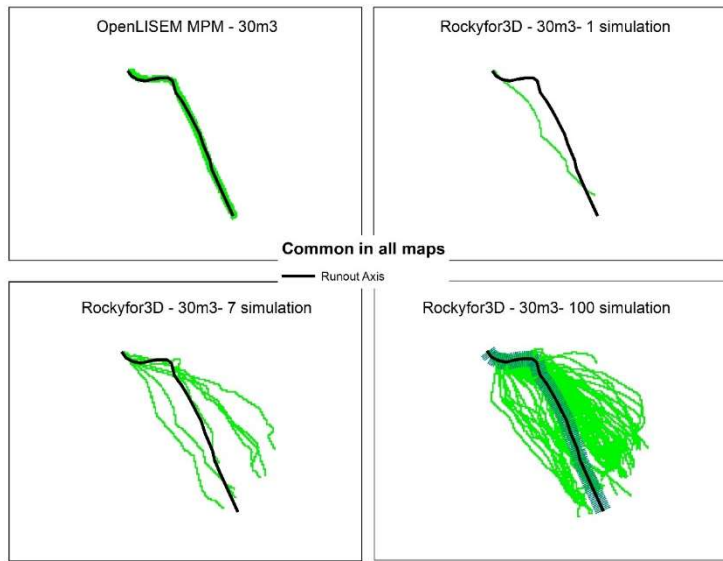


Figure 5-3 Description of the methodology to compare the model results from the trajectory models to the flow models

the transect spacing, and the width was decided as per the runout extent delineated by the OPH2 model as the main concern was in checking the applicability of the OPH2 model functionality. Then, extraction of the raster information on the vector transects was done by the zonal statistics tool in ArcGIS. These output maps show the maximum velocity in each pixel selected in the analysis. The maximum velocity values from the OPH2 model were compared with the mean value raster of the RF3D in calculating the zonal statistics along the transect. This choice was made because the maximum velocity raster created for RF3D involves several simulations (probabilistic) delineating maximum velocity along each trajectory. Therefore, selecting the maximum values from these many simulations would give the worst-case scenario among the multiple probabilistic simulations, which would not be comparable with the simulation from OPH2.

Based on this analysis, certain similarities and differences of simulating the velocities of a moving rock mass were observed. The velocities were also compared to each discrete value of slope evaluated within the transect line. Overall, the conclusion drawn from the observations is that trajectory models have sudden rise and fall of velocities, resulting from model assumptions to allow free movement, rotation, flying, and sudden impacts. Further, as shown in Figure 5-4 for each runout, there is a significant variation in the runout velocities simulated by the model for each case study sites.

For the case study site of Barcelonnette, where the volume initiated to model the runout is rock particle fall 2.70 m<sup>3</sup> (Runout1) and 1.62 m<sup>3</sup> (Runout 2), the velocities simulated by the OPH2 model decreased approximately by a factor 2 compared to the RF3D model. The simulated velocities showed a similar trend throughout the runout axis, where almost 2-fold greater velocities are simulated by the RF3D model with respect to the OPH2 models.



For the case study of Andorra, the analysis was carried out for the runout 3,4 and 5 (shown in Figure 5-2 and Table 12). The point initiation for all three runouts were the same, but there is a variation of the rock volume. Therefore, the data would show the comparison of simulated velocities by each model with change in runout volume. Here, two observations can be made. First, based on the change of results with the increase in rock volume during simulation. The simulated velocities by OPH2 in comparison to RF3D shows that the OPH2 model is less sensitive to the change in runout volumes. Although the simulation for runout 3 is  $10\text{m}^3$  of rock mass and the simulation of runout 5 is  $150\text{m}^3$ , there is no significant change in velocities simulated with the rock mass change. Perhaps, in RF3D, the sensitivity is seen relatedly higher with stiff peaks fluctuation in the velocities. Second, based on the differences in simulated velocities where, in contrast to the trend followed by runout 1 and 2, the velocities simulated along the runouts 3,4 and 5 tend to diverge less and are nearly identical when reaching transect 80 (see Figure 5-4). Before transect point 80 the value of slopes in degrees are seen to be generally greater than 40 degrees, and after transect 40 the slope values are gradually decreasing. Therefore, the results are understood in a way where the data would delineate that the functionality of the OPH2 model would be less accurate if the slope of the terrain is greater than  $40^\circ$ .

The final observation made for runout 3,4 and 5 is that the increase and decrease of the velocities are sudden and with high fluctuation for the RF3D. In contrast, for OPH2, the velocities area is steady and persistent. This way, the simulated rock block in the case of OPH2, although could not achieve as much momentum as simulated by the RF3D model, the momentum it gained was carried along further to the runout extent. In other words, the OPH2 model could not achieve the property of a rock mass falling down a cliff where a sudden increase in velocity is expected. The sudden increment in the velocity as it leaves the ground and sudden velocity lost is expected when it hits a substratum (could impact against houses, retaining structures). Finally, in runout 6 (Acheron), velocities were compared amongst the OPH1 and OPH2 models. The ground truth, in this case, was also taken from (Smith et al. 2006), where the simulation was done based on the software package DAN. The Observation from runout 6 is such that the OPH2 model is overestimating velocities in regard to the other two simulated models of OPH1 and DAN. In comparison to the OPH1 and OPH2, the OPH2 model looks more close to the results obtained by Smith et al (2006).

The results for the differences in the model come from their theoretical background. On the one hand, OPH1 and OPH2 have completely different theoretical background compared to the RF3D models. The rheology for the OPH1 and OPH2 models are based on two-phase equations with solids and fluids having separate force balances and separate but linked velocities. On the other hand, RF3D has its trajectory assumption in 3D, where a block of rock in contact with a surface would not slide but only bounce depending on the impact the block is carrying. The model generates a runout axis by short distance bouncing of the simulated rock block. Therefore, in general, the outputs from the models would still remain hugely different after the model are calibrated to the same runout inventory. Even though, the outcomes of the models are the same when it comes to reach and coverage of the runout mass yet, there is quite a difference in the dynamics of movement and associated impact during the movements.

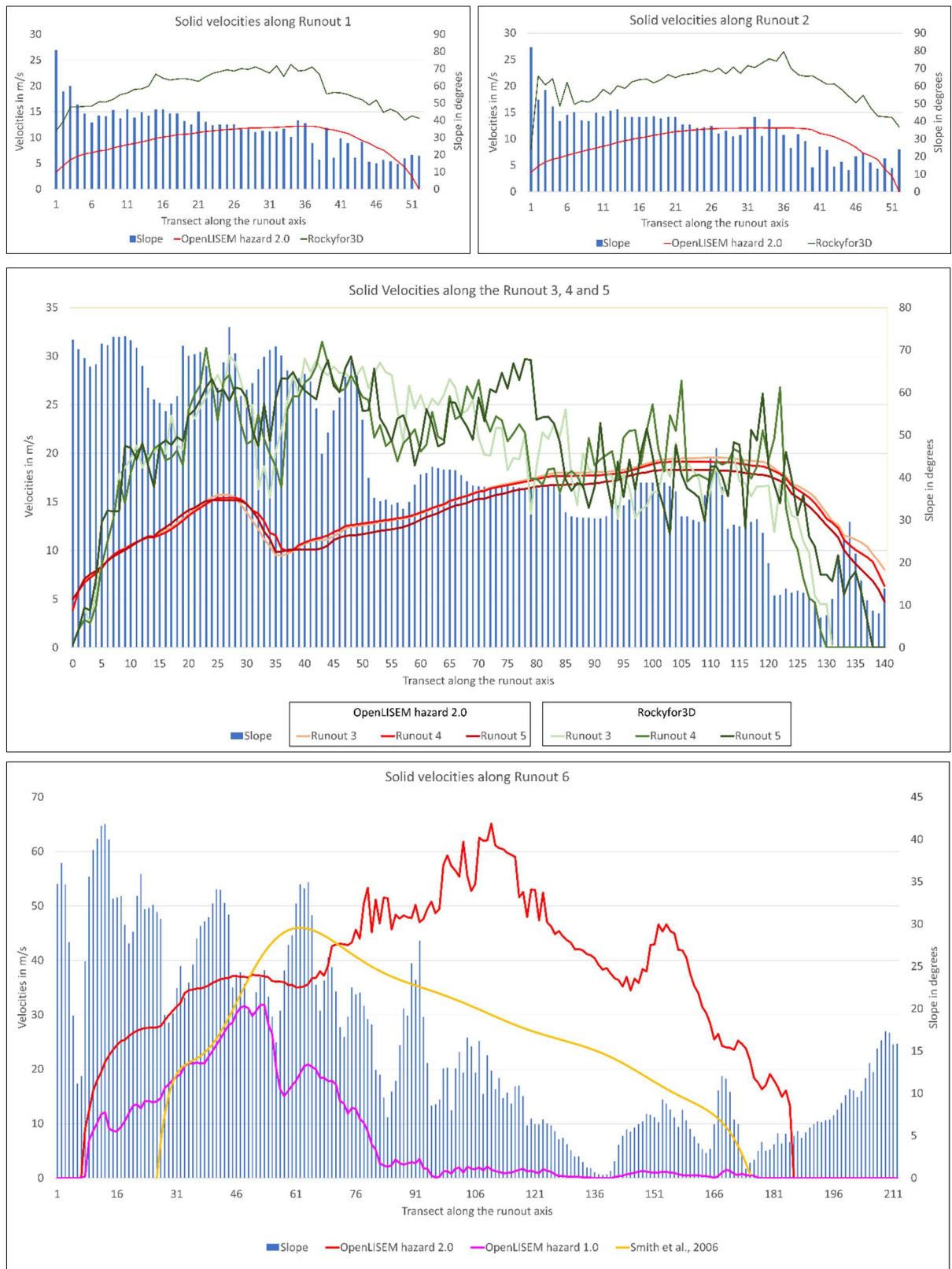


Figure 5-4 Simulated solid velocities by the representing models for each runout axis

### 5.3. Analysis associated with impact on the elements at risk

This part of the analysis concerns understanding the impact of a rockfall hazard into specific elements at risk. Here, observations were made at one specific point on the runout axis where the runout first encounters the element at risk. Fragmentation was prevented to occur for the OPH2 model in order to make a good comparison with the RF3D model. Therefore, the velocity parameter was the only concern here during the analysis. The calculated kinetic energies for the OPH2 model were based on velocity values simulated by the total rock mass within the single pixel.

Not all of the case study sites feature elements at risk. The case study of Barcelonnette lies in a forest within the French alps and does not have any settlement that might be impacted. Therefore, the quantification of impact in the case of Barcelonnette would be in regard to a hypothetically installed rockfall barrier net (Transect 27 and 28 as shown in Figure 5-5). The analysis of kinetic energies will indicate what, if such a barrier net were installed, the differences in simulated impact pressures would be.

In the case of Andorra, there lies a road along the runout axis. Therefore, the evaluation will be based on transect number 111 as mentioned in Figure 5-5.



Figure 5-5 Delineation of the elements at risk and the selected transect within the runout axis

	Selected transect	The kinetic energy in KJ		Multiplication factor for inaccuracy
		RF3D	OPH2	
Runout 1 (2.70m <sup>3</sup> )	Transect 27	3238.9	504.2	6.0
Runout 2 (1.62m <sup>3</sup> )	Transect 28	1299.8	295.0	6.4
Runout 3 (10m <sup>3</sup> )	Transect 111	10025.0	4198.6	2.3
Runout 4 (30m <sup>3</sup> )	Transect 111	38691.4	12032.8	3.2
Runout 5 (150 m <sup>3</sup> )	Transect 111	213038.9	54899.7	3.8

Table 13 Kinetic energies stimulated by the RF3D and OPH2 models.

As seen in Table 13, the kinetic energies calculated by OPH2 are substantially less than the energies simulated by the RF3D package. The underestimation is the largest in the smallest rock mass simulated, which is runout 2 with 1.62m<sup>3</sup> detachment. Overall, there seems to be at least a three-fold underestimation of kinetic energy that OPH2 simulates compared to RF3D simulations.



### 5.4. Fragmentation analysis and reach distance

Fragmentation analysis was only possible on one of the case study site of Andorra, as it featured a detailed inventory of branching impact paths during past events. The results from OPH2 were compared with the detailed inventory to highlight any value or error in the prediction of fragmentation behaviour along with

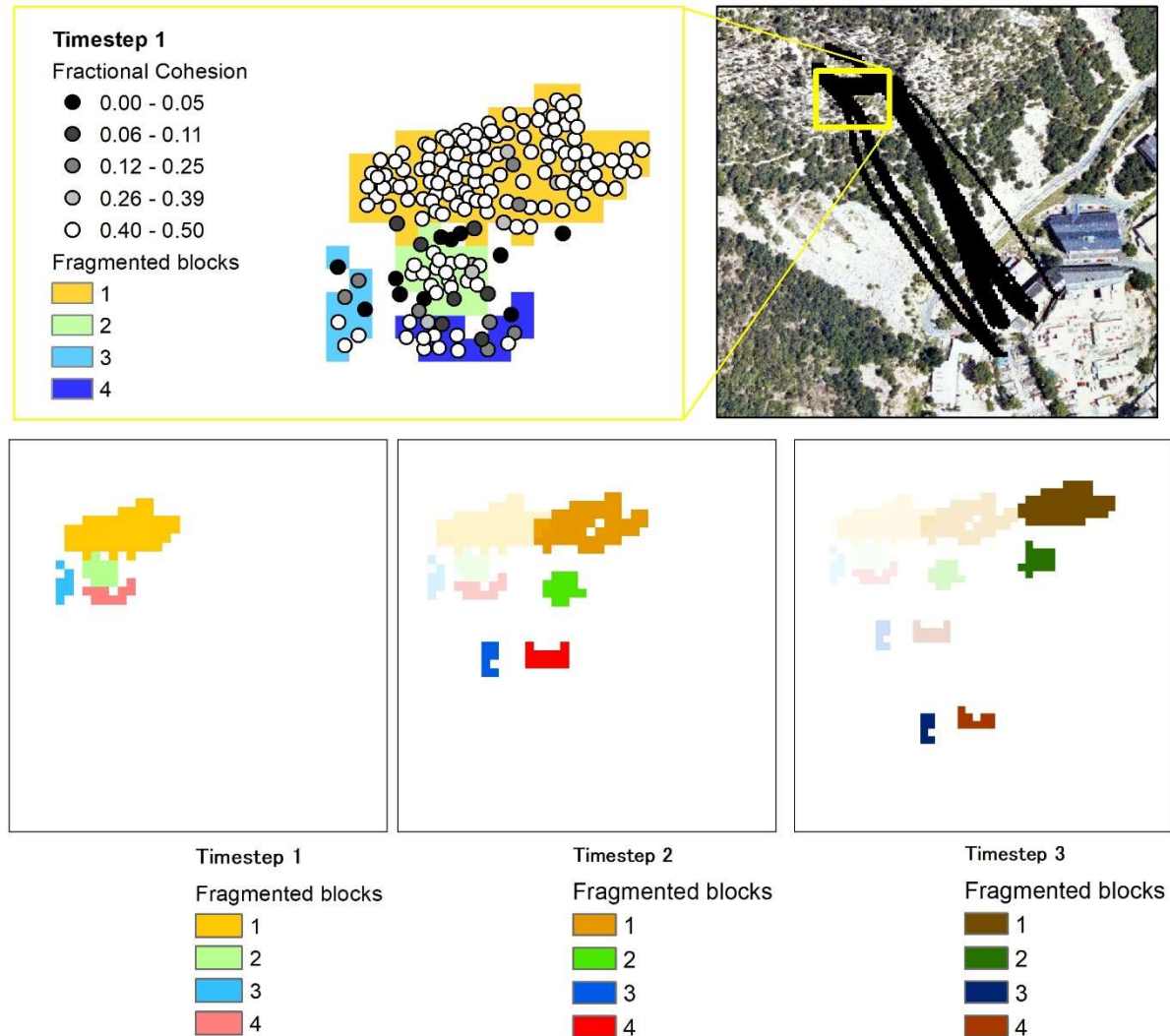


Figure 5-6 Fragmentation of the rock block during the first major collision

the runout inventory. The RF3D model, which was mostly used in this research, is not assimilated here because the model assumes that there is no fragmentation involved during the modelling process.

The output of OPH2, in addition to other standard raster outputs, also generates the particles timesteps from the Lagrangian framework. These particles come as a shapefile with the attributes related to the position, velocities, stress/strain, fractional cohesion etc., on each particle. The value of fractional cohesion was the parameter in use here.

Based on calculating the stresses on the rock mass, this parameter would give a value to delineate the fragmentation status ranging from the value of 0-1 (0 meaning completely fragmented and 1 meaning intact rock mass). These values were then used to analyse the possible blocks formed during a significant impact during runout. Here, the 2008 rockfall event where the first fragmentation of a rock mass of 150m<sup>3</sup> was analysed (yellow box in Figure 5-6). The rock mass was tentatively fragmented into 4 large rock fragments taking independent trajectories based on the impact. The blocks seem to rotate and have interaction amongst

one another during the simulation process. There is no further major collision to fragment the rock mass, and hence, the rock masses move downslope while maintaining the structure from the previous collision. The rock mass of  $150\text{m}^3$  finally resulted in several fragmented rock blocks, the largest block of  $71\text{m}^3$  as shown in red in Figure 5-7. The fragmentation and location of the final deposits do not match the observed locations. Based on the inventory, a substantially high number of rock fragments resulted from the detached rock mass. Although, there were only a few major observed towards the end of the runout axis bearing large volumes.

Many reasons might be stated for this differentiation. Rock collision and tumbling is a very chaotic process influenced by small details in elevation, obstacles and geometry of the rocks. Such details cannot yet be made a part of a deterministic model such as OPH2. Hence, the forces associated with the tumbling and free fall movements cannot be achieved by the controlled flow assumptions. Future improvements to such modelling setups might provide improvements to the actual deposit volumes and locations.

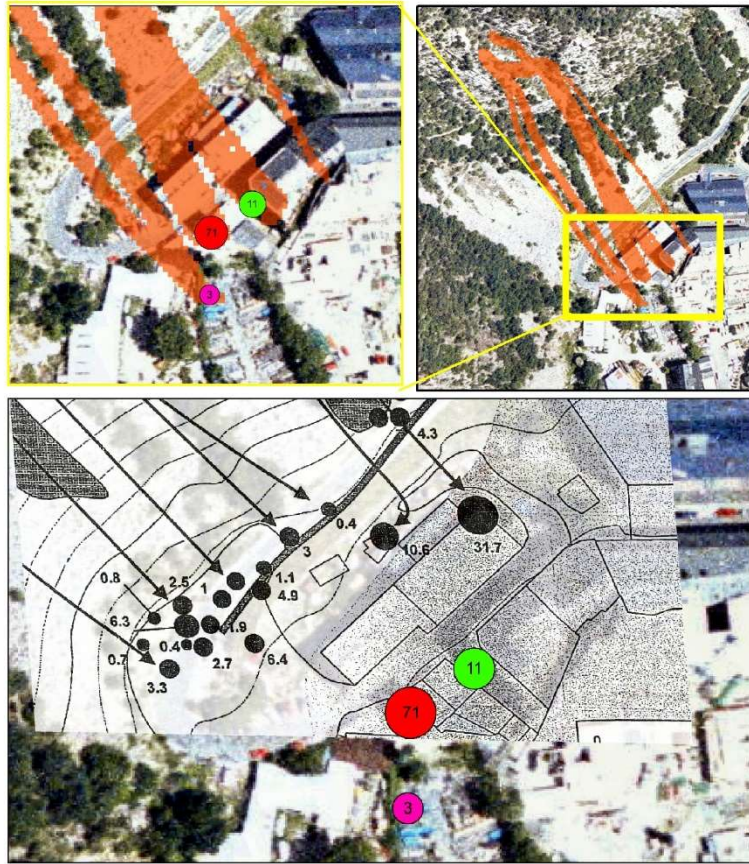


Figure 5-7 Distal end of the runout propagation showing the final deposition of the rock volume ( $\text{m}^3$ )

## 6. DISCUSSION AND CONCLUSION

### 6.1. Discussion

#### 6.1.1. Data preparation, modelling, and calibration.

Exact parameters were not available for the OpenLISEM simulations, which lead to the use of back analysis. The back analysis assisted in generating the best-estimated input data and further provided a means of investigating the sensitivity of the model. For example, the IFA was the most sensitive parameter for modelling with OpenLISEM (described in section 6.1.1.1). Based on the literature review, three parameters were anticipated to be of the highest importance in the calibration process: Mannings N, cohesion and the IFA. However, the OLH1 model does not support the runout of cohesive masses and instead assumes fully fragmented and mixed solid-fluid mixtures. Due to this assumption, the value of cohesion is insignificant upon runout modelling with OPH1 and therefore could not be calibrated. While this parameter could be used to calibrate the OPH2 model, given the computational time and amount of processing, this was not possible.

On the one hand, the calibrated dataset helped generate better accurate runout inventories; on the other hand, it also led to values of the geotechnical parameters practically very low. For example, in the study case of Acheron, the value of IFA of the rock was 0.41 radians which calibrated to 0.39 radians. Such values were similarly reported by other studies focused on back-analysis (Mergili et al. 2017). However, measured values for both the rock masses near the initiation site and the deposits are reported to be significantly higher. Thus, these values remain indicative of missing understanding in the mechanics of rock mass runout. The missing understanding could be due to the error in defining how the rock mass movement initiated (for example, sliding versus toppling detachment). In addition, the inability of a model to define a lubrication layer at the basal surface of the moving rock mass usually seen in long-distance runout (Cleary and Campbell 1993)

#### 6.1.1.1. Sensitivity analysis of the input parameters

The sensitivity analysis was carried out by extracting 6 random data plots from the convergence data obtained during calibration. The 6 samples (2 from each case study site) were selected in this analysis, as shown in Figure 6-1. The graph shows the normalized value of the accuracy (Kappa value) on the Y-axis and the multiplication factor for the change in parameter value on the X-axis. It is apparent from the graph that a change in the value of IFA results in more change in accuracy as compared to the change in Mannings N value. The lower sensitivity of Mannings N could be described by the high velocity of the rock mass being

modelled where the forces due to gravity on a steep terrain would be significant to that of the frictional terms. Also, the sensitivity of Mannings N could be due to the categorization of the Mannings N value in fewer land units. For example, there are only five land units described to have variation in the Mannings N value in the case study site of Andorra; for the case study of Acheron and Barcelonnette, a single value of Mannings N is used for the simulation.

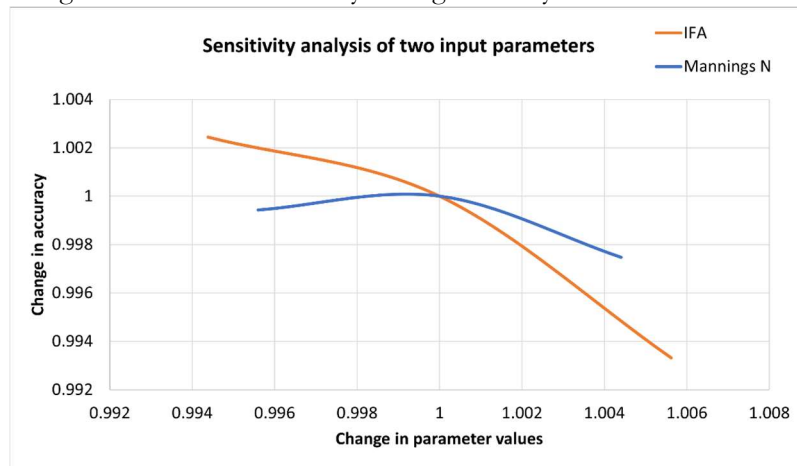


Figure 6-1 Sensitivity analysis of two input parameters- IFA of the rockmass and the value of Mannings N

### 6.1.2. Validation of the OPH2 model

OPH2 model showed increased accuracy in modelling dry granular flow movement compared to the granular flow model (OPH1). All the simulations for the case studies were done with no or very low fluid content to model a dry rock mass runout. When it comes to simulating fluids and solids and comparing it with the runout inventory generated for each case study site, the OPH1 showed near equal spatial accuracy in all case study sites. Kappa value obtained during the research are 0.62, 0.73, 0.71, respectively (described in Table 11), for the Acheron, Andorra and Barcelonnette case study sites. Since the presence of solid and fluid would not delineate impact when it comes to falling processes of rock mass, additional analysis had to be done. The analysis was further done to calculate the Kinetic energies and impact pressures for respective runout movements. The OPH1 model deviated from the reference data significantly in the case studies of Andorra and Barcelonnette with a very low kappa value. The OPH1 for Andorra gave a Kappa value of 0.16, which increased to 0.47 in OPH2. Similarly, for the Barcelonnette case, OPH1 gave a Kappa value of 0.04, which got increased to 0.57 in the case of OPH2. However, there is not much fluctuation in the Kappa values in the case of Acheron as the OPH1, and its modelling assumptions are seen to be working in granular flow movements.

#### 6.1.2.1. Advantages of the OPH2 model

Modelling the runout of a structural mass allowing fragmentation is so far the best advancement shown by the OPH2 model. The OPH2 model stands out in this case from the other two models (RF3D and OPH1) used in this study sites, which do not have this functionality. An increase in the accuracy of fragmentation might be obtained by calibrating the OPH2 model directly based on the full inventory of the area. Analysis of the reach distance done in one of the case studies described in section 5.4 would also help understand that the model would predict the runout distance accurately and progress with calibration.

There are various areas where the theoretical foundations of OPH2 limited the accuracy of the model compared with other modelling tools such as RF3D. For instance, the usage of trees and the deviation the trees could give to the spreading of the rockfall runout, which will be discussed in section 2.4.2.

#### 6.1.2.2. Disadvantages of the OPH2 model

Casualties due to rockfall are mostly due to the high impact velocity of a rock block (Corominas et al. 2019). The underestimation of velocities by the OPH1 and OPH2 models are thus major downsides, as they underestimate hazard with potentially dangerous consequences. Based on the velocity profiles, this can most likely be explained in reference to the modelling assumption that the OPH2 cannot model freely moving mass in the air. The process of free-falling mass of rock is anticipated to happen in the case studies (Andorra and Barcelonnette) discussed in this work. This research further shows that, for the presented simulations, flying and tumbling behaviour prevented accurate usage of the OPH2 models when slopes were greater than 40 degrees.

In the simulated velocities of rock blocks for elements at risk upon the three study cases, there is at least a 3-fold underestimation of the velocity values. This underestimation could be a problem if this tool is used for engineering and designing work for mitigation and adaptation. The model yet needs to be advanced in a way where blocks could be modelled to lose contact with the landscape temporarily, and during flight, ignore forces such as friction on the land surface, drag forces, and so forth. In addition, there is a sudden increase and rapid decrease of velocities when the trajectory assumption does the simulation- this is best explained as the rock block in the study cases moves in air trajectory. Currently, the simulation of flying and tumbling behaviour is not possible in OPH2. This could perhaps be one of the phenomena that need to be included in the modelling domain for rock mass fall modelling.

Another reason for the relatively lower velocities in OPH1 and OPH2 compared to RF3D is how surface friction is represented in these models. RF3D simulates distinct impacts, where the geometry of the block contacts the terrain, and an impulse is exchanged that alters the velocity of the block. The OPH1 and OPH2

models instead assume the entire bottom surface of a flowing body is always in contact with the terrain, where a friction force is active based on surface roughness parameters and the local flow velocity, density and height. This friction force provides a time-and spatial average, while RF3D provides a non-continuous implementation with discrete peaks during the collision. As a result, OPH1 and OPH2 underestimate the local impact forces on the flowing material, which results in an underestimation of fragmentation behaviour. Additionally, this means that the OPH1 and OPH2 model show velocities that alter immediately and more gradually to changes in slope and land cover type.

**6.1.3. Applicability of the OPH2 based on model performance.**

OPH2, due to its extensive sets of equations incorporated into an MPM framework, requires a long computational time for modelling. The computational time for each model is shown in Table 14. RF3D, due to its probabilistic nature, had to be run for 100 iterations. Yet, the modelling time consumption of RF3D is significantly less compared to the OPH1 and OPH2 models. Regardless of the modelling advantages, the processing time taken by OPH2 is drastically higher in comparison to the OPH1 and RF3D. The time taken could directly be related to the application of the model in various applications. For example, using simulation tools in hazard assessment, engineering application or early warning can be time-critical and require fast tools for direct results. In this case, it is better suggested to use of RF3D for all the small-scale events (<100m<sup>3</sup>) where the user would not be concerned about the rock mass's fragmentation behaviour. In addition, the input data required for both OPH1 and OPH2 are much more extensive and include soil properties, land cover parameters and geotechnical parameters. This requires preparation, either for field measurements or adapting available data to the format required by the model. Additionally, with a variety of scenarios, this can result in significant data storage.

*Table 14 Total runtime taken by each model*

Case Study sites		Acheron	Andorra	Barcelonnette	Total Runtime
Running OPH2	Runtime (approx.)	1440 mins for 1 iteration	960 mins for 1 iteration	1590 mins for 1 iteration	3990 mins
Running RF3D	Runtime (approx.)	N/A	0.5min for 100 iterations	0.3min for 100 iterations	0.8mins
Running OPH1 for calibration	Runtime (approx.)	2820 mins for 120 iterations	1260 mins for 92 iterations	1440 mins for 70 iterations	5520 mins
Total runtime		4260 mins	2220.5 mins	3030.3 mins	9510.8 mins

Also, due to the matter of large time consumption for each iteration, the calibration of OPH2 was not possible in this research. This is clearly a disadvantage over the OPH1 model. An example can be drawn out from the modelling of the case study of Andorra, where the modelling time for OPH1 is ~46mins which rockets to ~960 mins for running OPH2.

When modelling rockfall as an individual hazard, such as for engineering design, the tool OPH2 is not thought to be ideal. Not all the features of rockfall dynamics are yet captured within the modelling framework, as seen under the case study site of Barcelonnette and Andorra.

For the large-scale events similar to the study site of Acheron, the OPH2 would provide better use compared to the OPH1 model. The improved accuracy and implementation of fragmentation behaviour would benefit the analysis of the event.

When considering the capabilities for multi-hazard modelling using OPH2, there have been major advances as compared to the OPH1 package in the sense of non-diffusive transport of the solids, improved velocities during transport. Therefore, the use of OPH2 is suggested to be used as an advancement to the OPH1 model. Although, with numerous aspects to progress upon to incorporate rockfall modelling, the processes added in addition to the OPH1 model is thought to create better simulation accuracy as a whole to the multi-hazard setting. Lastly, the OPH2 software package is user-friendly in the sense that it offers fewer



input data than the OPH1 model. This functionality is progressing upon the OPH1 by streamlining input parameters in the interface and model code.

Moreover, modelling practices are useful for generating early warning systems by predictive runout simulations. Here, understanding the applicability of the OPH2 model in a predictive runout scenario is discussed. OPH2 is a deterministic model therefore, the same set of results are generated with each model iteration; this is different to the probabilistic assumptions (e.g. RF3D) where a probabilistic set of observed values are applied to generate stochastic results which are complete in terms of prediction. The better way for OPH2 to be a better predictive model is by means of training the model based on calibration. But, due to the deterministic nature of OPH2, the predictive capability is still a challenge. The complexity can, therefore, be avoided by the use of probabilistic models in predictive runout modelling.

#### **6.1.4. Potential improvements on the adaptability of the OPH2 model in multi-hazard assessment**

Based on the results and discussion section, the potential improvements to the OPH2 model are indicated in this section. Several mechanisms that were crucial in this work are described below.

##### **6.1.4.1. Modelling of free fall and tumbling behaviour of rock mass**

With the latest version of OPH2 using the MPM framework, the advancement is until the point where the translational movement of an intact rock mass could be modelled. Yet, this is not sufficient as the case studies show that the functionality of the OPH2 model is hampered when the slope of the terrain is larger than 40 degrees. By this means, the understanding is in a way where the depth-averaged (semi 2D) assumptions need to be replaced perhaps by a 3D simulation. The best solution could be modelling based on the 3D Lagrangian framework, where a mass of rock could be modelled with no surface friction if flying or tumbling behaviour is dictated. In addition, there needs to be flexibility within the model where the block of rock moves could move freely based on the contact to the terrain. This might include tumbling, rolling and rotating movements. The RF3D software package best describes all the mentioned aspects of rockfall modelling.

The implementation of a 3D Lagrangian framework could be a major challenge. The major assumptions made in the OPH1 and OPH2 models are based on a depth-averaged equation (vertical velocity ignored) where the implementation of physical equations are simplified. To process all these equations in 3D would perhaps need a completely new set of methodology/ set of derivations.

##### **6.1.4.2. Point-based impacts instead of spatially averaged friction**

OPH2 applies frictional forces in terms of the spatially averaged value calculated based on Mannings N. Therefore, friction terms are normalized into one single line of flow propagation the material simulated are moving. The averaging of forces leads to smoothening out high impact zones, which could be crucial for a rock mass moving in a high speed. Underestimation, therefore, upon a specific impact zone will be problematic while doing rockfall modelling because the impact zone could perhaps, be a house or a rockfall barrier. The calculation, therefore, must be precise without averaging the impact zones.

Generally, the trajectory models use the point-based impacts where for each simulated block, the impact during contact with the ground (represented by a single pixel) is calculated by the incoming velocity of the block and the block mass. Observed impacts are therefore seen to be higher in comparison to the flow assumptions as the trajectory models do not consider several assumptions that is seen on a standard flow model (eg, drag forces, frictional forces (no sliding), material interaction, diffusion)

##### **6.1.4.3. Redirection due to tree impact**

The effect of trees on the runout of rock mass is largely scale dependent. Trees would, of course, not play a large role in huge avalanches. A study done by Teich et al. (2012) for rock avalanches states that the runout length of 150m from the detachment to the impact into a tree is enough to break or uproot trees (Schneebeili

and Bebi 2004). Therefore, the recommendation in this research is valid only in the case of rock particle fall and for rock mass fall to a certain extent.

The first way OPH2 incorporates trees into modelling is by lowering the values of Mannings N, creating greater friction along this pixel categorized as trees. There could be a second way to use a very high-resolution model where the elevation of individual trees could be described within the elevation model. But in reality, the impact of a rock mass with trees would dissipate energy (lowered velocity) and deviate the block of rock towards extents depending on where the block hits the trees. When it comes to velocity dissipation, there could be a possibility that the OPH2 could be validated for usage (only to some extent), but the redirecting phenomena are completely left out.

### **6.1.5. Recommendation for further improvements**

#### **6.1.5.1. Improvement of the current research**

In addition to the work done in this master's thesis, possible betterment suggested to do similar research are described under the following headings: -

##### Calibration of Cohesion

OPH2 model could not be calibrated in this research because of the time taken by the software package to run. Further, with the usage of supercomputers, the advancement would be in calibrating the OPH2 model. In addition to other parameters, the cohesion of the rock mass could also be calibrated. This was unsuccessful in this research due to the associated modelling assumptions of OPH1.

##### Use of detailed inventory

Not all the case study sites had mapped inventory based on a field visit. Except for Andorra, the inventory used to delineate the accuracy was based on the output of a different model. Even though, the modelling outputs are validated, used of a detailed inventory would be encouraged to use to carry out similar studies

##### Role of fluids

In the motive of simulating dry granular flow, the OPH2 model in this research was modelled with negligible fluid during simulation. However, concerning the modelling framework, the use of fluid may generate better results. Therefore, the use of fluid in this research is unknown for the smaller rock mass detachments and could be an interesting aspect to look at further.

##### Use of hypothetical data

The shape of the rock mass for the case study sites of Andorra and Barcelonnette are completely unknown. The modelling in this research was done based on a hypothetical shape constructed based on volume of the rock mass and geomorphology. However, in advancing the current research, the shape of the initiation rock mass could be looked into with more in-depth research.

A hypothetical barrier is mapped to calculate the impact during the Barcelonnette study site analysis due to the absence of elements at risk. The hypothetical barrier placed is with superficial analysis. Therefore, further research would be encouraged to be done to improve this phenomenon.

#### **6.1.5.2. Recommendations on the usage of OPH2 model**

OPH2 is in its early development to model a structured mass movement. This research indicates that OPH2 is not an ideal model yet to simulate the rockfall phenomena, especially. Therefore, unless a researcher intends to model rockfall phenomena using OPH2 for scientific analysis, the software is not recommended for the application in engineering design and development. On the contrary, due to its unique advancements in modelling fragmentation on a rock mass the recommendation would be in further research in achieving betterment in simulating accuracies related to the velocities of the rock mass.

### 6.1.5.3. Recommendation for further improvements

During this research, the modelling framework of OPH2 is not seen working, especially on the part where there has to be a modelling of free fall tumbling and rolling behaviour of a rock mass. Therefore, the first and foremost recommendation would be to incorporate these movements into the framework.

Second, due to the speed of the movements a rock would experience during the runout, the friction parameters are overpowering, slowing down the velocity of a moving rock mass. Frictional terms played a vital role due to the assumption of spatially averaged friction behaviour in the OPH2 model. The spatially averaged friction terms are recommended to be replaced by point-based impacts during simulation to address this.

Where it comes to spatial coverage, the effect of trees is seen crucial in this research. The trees are seen as a factor where the runout spreads towards a wider extent during runout. Since the OPH2 model does not incorporate deviation (due to trees) of a runout path during the simulation, there is a strong need to incorporate these characteristics. Therefore, the recommendation lies in advancing the model with the effect of trees.

## 6.2. Conclusion

The purpose of this study was to address the applicability of the newly developed semi-structured mass movement model, namely OpenLISEM hazard 2.0. To investigate this, a comparative analysis with OpenLISEM Hazard 1.0 and Rockyfor3D was done on three rock mass movement events with different spatial scales. The names of the three case study sites in use are Acheron, Andorra and Barcelonnette. These were selected to provide enough variability to the models selected for the runout extent, initiation volumes, and slope morphology.

Comparison of the model outputs was based on the calculated rockfall impact in kinetic energies for the case study of Andorra and Barcelonnette and debris flow impact pressure for the case study of Acheron. The spatial correlation of the outputs was done by a GIS analysis based on zonal statistics along a vector transect.

Three parameters, namely the IFA, cohesion of the rock mass, and Manning's N, were calibrated by an optimization function. The accuracy was based on the simulated energies simulated within each model based on the Cohens kappa index. The accuracy calculated in reference to the validated model gave an accuracy of 0.66, 0.47 and 0.57 for the study case of Acheron, Andorra and Barcelonnette, respectively.

In order to provide a deeper analysis of the influence of model mechanics, analysis based on velocities for runout trajectories was carried out. For each of the models, output was evaluated based on the velocities and kinetic energies stimulated. There is at least a two-fold underestimation of velocities along the slope greater than 40 degrees. In addition, analysis upon specific elements at risk was done where an underestimation of at least three-fold impact was seen using the OPH2 model. These evaluations led to the conclusion that simulation for engineering design is not suitable with OPH2.

In other words, the shortcoming of the OPH2 model was perceived in simulating velocities experienced by the motion of freefall, tumbling and rolling phenomena in rock mass runout. These phenomena could not be modelled with the current theoretical background of the model and hence needs improvement.

In contrast to all the shortcomings, the OPH2 model showed precise fragmentation behaviour compared to a runout inventory. The fragmentation behaviour OPH2 showed could not be modelled with the other modelling tool used under this research.



## LIST OF REFERENCES

- Aaron, Jordan, and Oldrich Hungr. 2016. "Dynamic Simulation of the Motion of Partially-Coherent Landslides." *Engineering Geology* 205:1–11. doi: 10.1016/j.enggeo.2016.02.006.
- Aaron, Jordan, Scott Mcdougall, and Natalia Nolde. 2019. "Two Methodologies to Calibrate Landslide Runout Models." *Landslides* 16(5):907–20. doi: 10.1007/s10346-018-1116-8.
- Abe, Keita, and Kazuo Konagai. 2016. "Numerical Simulation for Runout Process of Debris Flow Using Depth-Averaged Material Point Method." *Soils and Foundations* 56(5):869–88. doi: 10.1016/j.sandf.2016.08.011.
- Agliardi, F., G. B. Crosta, and P. Frattini. 2009. "Integrating Rockfall Risk Assessment and Countermeasure Design by 3D Modelling Techniques." *Natural Hazards and Earth System Science* 9(4):1059–73. doi: 10.5194/nhess-9-1059-2009.
- Ahmadiipur, Amir, and Tong Qui. 2018. "Impact Force to a Rigid Obstruction from a Granular Mass Sliding down a Smooth Incline." *Acta Geotechnica* 13. doi: 10.1007/s11440-018-0727-5.
- Akhil, K. S., and Venkat Reddy. 2015. "Geological and Geotechnical Investigations of Calicut Granite of Kerala Geological and Geotechnical Investigations of Calicut Granite of Kerala State - A Case in Study." (March).
- Andrea, Bonini Baldini. 2014. "Three-Dimensional Modelling of Rockfalls at Sola d' Andorra (Spain)." *Universita di Bologna*.
- van Asch, Th W. J., C. Tang, D. Alkema, J. Zhu, and W. Zhou. 2014. "An Integrated Model to Assess Critical Rainfall Thresholds for Run-out Distances of Debris Flows." *Natural Hazards* 70(1):299–311. doi: 10.1007/s11069-013-0810-z.
- Barnichon, J. D. 2014. "RocPro3D." Retrieved October 2, 2020 ([http://www.rocpro3d.com/rocpro3d\\_en.php](http://www.rocpro3d.com/rocpro3d_en.php)).
- Barrantes, Gustavo. 2018. "Multi-Hazard Model for Developing Countries." *Natural Hazards* 92(2):1081–95. doi: 10.1007/s11069-018-3239-6.
- Bartingale, E. I. ..., Jerry Higgins, Richard Andrew, Alan Rock, and Runing Zhang. 2009. "Colorado Rockfall Simulation Program Version 5.0." Pp. 189–200 in *60th highway geology symposium*.
- Barton, Nicholas. 1974. "Review of the Shear Strength of Filled Discontinuities in Rock." *Norg Geotek Inst, Publ* (105):1–38. doi: 10.1016/0148-9062(75)90034-0.
- Bourrier, Franck, Luuk Dorren, and Oldrich Hungr. 2013. "The Use of Ballistic Trajectory and Granular Flow Models in Predicting Rockfall Propagation." *Earth Surface Processes and Landforms* 38(4):435–40. doi: 10.1002/esp.3372.
- Bout, B., Luigi Lombardo, C. J. Van Westen, and V. G. Jetten. 2018. "Integration of Two-Phase Solid Fluid Equations in a Catchment Model for Flashfloods, Debris Flows and Shallow Slope Failures." *Environmental Modelling and Software* 105:1–16. doi: 10.1016/j.envsoft.2018.03.017.
- van den Bout, B., Theo van Asch, and Wei Hu. 2020. "Towards a Model for Structured Mass Movements: The OpenLISEM Hazard Model 2.0a." *Geoscientific Model Development*. doi: 10.5194/gmd-2020-101.
- van den Bout, B., Victor. Jetten, Ad. De Roo, C. J. van Westen, and Coen. Ritsema. 2018. *OpenLISEM Multi-Hazard Land Surface Process Model*.
- Bozzolo, D., and R. Pamini. 1986. "Simulation of Rock Falls Down a Valley Side." *Acta Mechanica* 130:113–30.
- British Standards Institution. 1995. "Specification for Industrial Safety Helmets." *BS EN 397*.
- Broilli, Luciano. 1974. "Ein Felssturz Im Großversuch." Pp. 69–78 in *Rock Mechanics, Suppl. 3*. Springer, Vienna.
- Calista, Monia, Valeria Menna, Vania Mancinelli, Nicola Sciarra, and Enrico Miccadei. 2020. "Rockfall and Debris Flow Hazard Assessment in the SW Escarpment of Montagna Del Morrone Ridge (Abruzzo, Central Italy)." *Water (Switzerland)* 12(4):1206. doi: 10.3390/W12041206.
- Carson, M. A., and M. J. Kirkby. 1972. *Hillslope Form and Process*. Cambridge University Press.
- Christen, M., J. Kowalski, and P. Bartelt. 2010. "RAMMS: Numerical Simulation of Dense Snow Avalanches in Three-Dimensional Terrain." *Cold Regions Science and Technology* 63(1–2):1–14. doi: 10.1016/j.coldregions.2010.04.005.
- Cleary, P. W., and C. S. Campbell. 1993. "Self-Lubrication for Long Runout Landslides: Examination by Computer Simulation." *Journal of Geophysical Research* 98(B12).
- Corominas, Jordi, Gerard Matas, and Roger Ruiz-Carulla. 2019. "Quantitative Analysis of Risk from

- Fragmental Rockfalls.” *Landslides* 16(1):5–21. doi: 10.1007/s10346-018-1087-9.
- Corominas, Jordi, Olga Mavrouli, and Roger Ruiz-Carulla. 2017. “Rockfall Occurrence and Fragmentation.” Pp. 75–97 in *Advancing Culture of Living with Landslides*. Springer International Publishing.
- Cruden, David M., and David J. Varnes. 1996. “Landslides Types and Processes.” *Landslides: Investigation and Mitigation, Transportation Research Board Special Report 247, Washington D.C.* (Bell 1992):36–75.
- Davies, T. R., and M. J. McSaveney. 2009. “The Role of Rock Fragmentation in the Motion of Large Landslides.” *Engineering Geology* 109(1–2):67–79. doi: 10.1016/j.enggeo.2008.11.004.
- Delaney, Keith B., and Stephen G. Evans. 2014. “The 1997 Mount Munday Landslide (British Columbia) and the Behaviour of Rock Avalanches on Glacier Surfaces.” *Landslides* 11(6):1019–36. doi: 10.1007/s10346-013-0456-7.
- Denlinger, Roger P., and Richard M. Iverson. 2001. “Flow of Variably Fluidized Granular Masses across Three-Dimensional Terrain 2. Numerical Predictions and Experimental Tests.” *Journal of Geophysical Research: Solid Earth* 106(B1):553–66. doi: 10.1029/2000jb900330.
- Dorren, L. K. A. 2016. “Rockyfor3D (v5.2) Revealed-Transparent Description of the Complete 3D Rockfall Model.” *EcorisQ* 33.
- Dorren, L. K. A., and G. B. M. Heuvelink. 2004. “Effect of Support Size on the Accuracy of a Distributed Rockfall Model.” *International Journal of Geographical Information Science* 18(6):595–609. doi: 10.1080/13658810410001703804.
- Dorren, Luuk. 2003. “A Review of Rockfall Mechanics and Modelling Approaches.” *Progress in Physical Geography* 27(1):69–87. doi: 10.1191/0309133303pp359ra.
- Dorren, Luuk. 2014. “FINT – Find Individual Trees.” *EcorisQ*, 6.
- Dorren, Luuk, Frédéric Berger, Céline Le Hir, Eric Mermin, and Pascal Tardif. 2005. “Mechanisms, Effects and Management Implications of Rockfall in Forests.” *Forest Ecology and Management* 215(1–3):183–95. doi: 10.1016/j.foreco.2005.05.012.
- Evans, S. G., and O. Hungr. 1993. “The Assessment of Rockfall Hazard at the Base of Talus Slopes.” *Canadian Geotechnical Journal* 30(4):620–36. doi: 10.1139/t93-054.
- Evans, S. G., G. Scarascia Mugnozza, A. L. Strom, R. L. Hermanns, A. Ischuk, and S. Vinnichenko. 2006. “Landslides from Massive Rock Slope Failure and Associated Phenomena.” *Springer* 03–52. doi: 10.1007/978-1-4020-4037-5\_1.
- Fabian, Pedregosa. 2018. “The Stochastic Gradient Method.” Retrieved October 22, 2020 ([http://fa.bianp.net/teaching/2018/COMP-652/stochastic\\_gradient.html](http://fa.bianp.net/teaching/2018/COMP-652/stochastic_gradient.html)).
- Ferrari, F., A. Giacomini, K. Thoeni, and C. Lambert. 2017. “Qualitative Evolving Rockfall Hazard Assessment for Highwalls.” *International Journal of Rock Mechanics and Mining Sciences* 98:88–101. doi: 10.1016/j.ijrmms.2017.07.013.
- George, David L., and Richard M. Iverson. 2014. “A Depth-Averaged Debris-Flow Model That Includes the Effects of Evolving Dilatancy. II. Numerical Predictions and Experimental Tests.” *Proceedings of the Royal Society* 470(2170):20130820. doi: 10.1098/rspa.2013.0820.
- Guachalla Terrazas, Analia. 2016. “Ecosystem-Based Measured for Reducing Shallow Landslides Risk in Sloping Terrain.” University of Twente.
- Guzzetti, Fausto, Giovanni Crosta, Riccardo Detti, and Federico Agliardi. 2002. “STONE: A Computer Program for the Three-Dimensional Simulation of Rock-Falls.” *Computers and Geosciences* 28(9):1079–93. doi: 10.1016/S0098-3004(02)00025-0.
- Hantz, Didier, Jordi Corominas, Giovanni B. Crosta, and Michel Jaboyedoff. 2021. “Definitions and Concepts for Quantitative Rockfall Hazard and Risk Analysis.” *Geosciences (Switzerland)* 11(4). doi: 10.3390/geosciences11040158.
- Hoek, E., and J. Bray. 1981. “Rock Slope Engineering. Revised 2nd Edition, The Institution of Mining and Metallurgy, London. - References - Scientific Research Publishing.” Retrieved June 10, 2021 ([https://www.scrip.org/\(S\(351jmbntvnsjt1aadkposzje\)\)/reference/ReferencesPapers.aspx?ReferenceID=1417574](https://www.scrip.org/(S(351jmbntvnsjt1aadkposzje))/reference/ReferencesPapers.aspx?ReferenceID=1417574)).
- Hsü, Kenneth J. 1975. “Catastrophic Debris Streams (Sturzstroms) Generated by Rockfalls.” *Bulletin of the Geological Society of America* 86(1):129–40. doi: 10.1130/0016-7606(1975)86<129:CDSSGB>2.0.CO;2.
- Hübl, Johannes, Gerhard Holzinger, Michael Bacher, Markus Friedrich, Peter Mayr, Roland Mayr, Katharina Platzer, Robert Svaton, and Friedrich Zott. 2003. “Kleinmaßstäbliche Modellversuche Zur Wirkung von Murbrechern, WLS Report 50/ Band 3.” *Universität Für Bodenkultur Wien Institut Für Alpine Naturgefahren Und Forstliches Ingenieurwesen* (September 2015).

- Hussain, Manzoor, Kamran Akhtar, and Timothy D. Stark. 2012. "International Conference On." 4(3):7625.
- ISO 3449. 2005. "Falling-Object Protective Structures." *Earth-Moving Machinery*.
- Jason, Brownlee. 2019. "Gradient Descent For Machine Learning." *Machine Learning Mastery*. Retrieved October 22, 2020 (<https://machinelearningmastery.com/gradient-descent-for-machine-learning/>).
- Jazvin, Ena. 2016. *Examining the Forest Effect and Structural Protective Measures in Rockfall Prone Areas Using the Rockyfor3D Model*. Enschede, NL.
- Jonsson, M. J. O. 2007. "Energy Absorption of Trees in a Rockfall Protection Forest." (17214):209.
- Khatiwada, Durga, and Ranjan Kumar Dahal. 2020. "Rockfall Hazard in the Imja Glacial Lake, Eastern Nepal." *Geoenvironmental Disasters* 7(1):29. doi: 10.1186/s40677-020-00165-9.
- Lan, Hengxing, C. Derek Martin, and C. H. Lim. 2007. "RockFall Analyst: A GIS Extension for Three-Dimensional and Spatially Distributed Rockfall Hazard Modeling." *Computers and Geosciences* 33(2):262–79. doi: 10.1016/j.cageo.2006.05.013.
- Lateltin, Olivier, Christoph Haemmig, Hugo Raetzo, and Christophe Bonnard. 2005. "Landslide Risk Management in Switzerland." *Landslides* 2(4):313–20. doi: 10.1007/s10346-005-0018-8.
- Li, Langping, and Hengxing Lan. 2015. "Probabilistic Modeling of Rockfall Trajectories: A Review." *Bulletin of Engineering Geology and the Environment* 74(4):1163–76. doi: 10.1007/s10064-015-0718-9.
- Luna, B. Quan, A. Remaître, Th W. J. van Asch, J. P. Malet, and C. J. van Westen. 2012. "Analysis of Debris Flow Behavior with a One Dimensional Run-out Model Incorporating Entrainment." *Engineering Geology* 128:63–75. doi: 10.1016/j.enggeo.2011.04.007.
- Mammen, J, S Saydam, South Wales, P Hagan, Joseph Mammen, Serkan Saydam, and Paul Hagan. 2019. "A Study on the Effect of Moisture Content on Rock Cutting Performance." in *Proceedings of the 2009 Coal Operators' Conference, Mining Engineering, University of Wollongong*.
- Marcus, W. A., K. Roberts, L. Harvey, and G. Tackman. 1992. "An Evaluation of Methods for Estimating Manning's n in Small Mountain Streams." *Mountain Research & Development* 12(3):227–39. doi: 10.2307/3673667.
- Marzocchi, W., M. L. Mastellone, A. Di Ruocco, P. Novelli, E. Romeo, and P. Gasparini. 2009. "Principles of Multi-Risk Assessment Interaction amongst Natural and Man-Induced Risks." doi: 10.2777/30886.
- Mavrouli, O., J. Corominas, and J. Wartman. 2009. "Methodology to Evaluate Rock Slope Stability under Seismic Conditions at Solá de Santa Coloma, Andorra." *Natural Hazards and Earth System Science* 9(6):1763–73. doi: 10.5194/nhess-9-1763-2009.
- Mcdonald, D. C. 2012. "A Survey of Some Physical Properties of New Zealand Soils from Greywacke Parent Material." *New Zealand Journal of Agricultural Research* 4(2):161–76. doi: 10.1080/00288233.1961.10419930.
- McDougall, Scott. 2017. "2014 Canadian Geotechnical Colloquium: Landslide Runout Analysis — Current Practice and Challenges." *Canadian Geotechnical Journal* 54(5):605–20. doi: 10.1139/cgj-2016-0104.
- Mergili, Martin, Jan-Thomas Fischer, Julia Krenn, and Shiva P. Pudasaini. 2017. "R.Avaflow v1, an Advance Open-Source Computational Framework for the Propagation and Interaction of Two-Phase Mass Flows-Right." *Geosci. Model Dev* 10(1):553–69. doi: 10.5194/gmd-10-553-2017.
- Mineo, Simone, Giovanna Pappalardo, Michele Mangiameli, Santo Campolo, and Giuseppe Mussumeci. 2018. "Rockfall Analysis for Preliminary Hazard Assessment of the Cliff of Taormina Saracen Castle (Sicily)." *Sustainability (Switzerland)* 10(2):1–18. doi: 10.3390/su10020417.
- Monaghan, J. J. 2000. "SPH without a Tensile Instability." *Journal of Computational Physics* 159(2):290–311. doi: 10.1006/jcph.2000.6439.
- Nemčok, A., J. Pašek, and J. Rybář. 1972. "Classification of Landslides and Other Mass Movements." *Rock Mechanics Felsmechanik Mécanique Des Roches* 4(2):71–78. doi: 10.1007/BF01239137.
- O'Brien, J. S., P. Y. Julien, and W. T. Fullerton. 1993. "Two-Dimensional Water Flood and Mudflow Simulation." *Journal of Hydraulic Engineering* 244–61.
- Pastor, M., B. Haddad, G. Sorbino, S. Cuomo, and V. Dremptic. 2009. "A Depth-Integrated, Coupled SPH Model for Flow-like Landslides and Related Phenomena." *International Journal for Numerical and Analytical Methods in Geomechanics* 33:143–72. doi: 10.1002/nag.705.
- Pitman, E. Bruce, and L. E. Long. 2005. "A Two-Fluid Model for Avalanche and Debris Flows." *Philosophical Transactions of the Royal Society A: Mathematical, Physical and Engineering Sciences* 363(1832):1573–1601. doi: 10.1098/rsta.2005.1596.
- Pudasaini, Shiva P. 2012. "A General Two-Phase Debris Flow Model." *Journal of Geophysical Research: Earth Surface* 117(F3):n/a-n/a. doi: 10.1029/2011JF002186.

- Pudasaini, Shiva P., and Kolumban Hutter. 2003. "Rapid Shear Flows of Dry Granular Masses down Curved and Twisted Channels." *Journal of Fluid Mechanics* 495(495):193–208. doi: 10.1017/S0022112003006141.
- Pudasaini, Shiva P., and Martin Mergili. 2019. "A Multi-Phase Mass Flow Model." *Journal of Geophysical Research: Earth Surface* 124(12):2920–42. doi: 10.1029/2019JF005204.
- Rammer, W., M. Brauner, L. K. A. Dorren, F. Berger, and M. J. Lexer. 2010. *Evaluation of a 3-D Rockfall Module within a Forest Patch Model*. Vol. 10.
- Rempe, Daniella M., and William E. Dietrich. 2018. "Direct Observations of Rock Moisture, a Hidden Component of the Hydrologic Cycle." *Proceedings of the National Academy of Sciences of the United States of America* 115(11):2664–69. doi: 10.1073/pnas.1800141115.
- Rickenmann, D., D. Laigle, B. W. McArdell, and J. Hübl. 2006. "Comparison of 2D Debris-Flow Simulation Models with Field Events." *Computational Geosciences* 10(2):241–64. doi: 10.1007/s10596-005-9021-3.
- Ritchie, A. M. 1963. "Evaluation of Rockfall and Its Control." In *Highway Research Record 17, Stability of Rock Slopes*, Highway Research Board, National Research Council, Washington, D.C. 13–28.
- Rockscience Inc. 2013. *RocFall 5.0 Beta Program Rigid Body Impact Mechanics*.
- Schneebeili, M., and P. Bebi. 2004. "Snow and Avalanche Control." *Encyclopedia of Forest Sciences* (January 2004):397–402.
- Selby, M. J. 1993. *Hillslope Materials and Processes*. Second Edi. Oxford University Press: Oxford.
- Sellmeier, Bettina. 2015. "Quantitative Parameterization and 3D-Run-out Modelling of Rockfalls at Steep Limestone Cliffs in the Bavarian Alps." Technische Universität München.
- Sheridan, M. F., A. J. Stinton, A. Patra, E. B. Pitman, A. Bauer, and C. C. Nichita. 2005. "Evaluating Titan2D Mass-Flow Model Using the 1963 Little Tahoma Peak Avalanches, Mount Rainier, Washington." *Journal of Volcanology and Geothermal Research* 139(1–2):89–102. doi: 10.1016/j.jvolgeores.2004.06.011.
- Smith, GM, DH Bell, and TRH Davies. 2012. "The Acheron Rock Avalanche Deposit, Canterbury, New Zealand: Age and Implications for Dating Landslides." *New Zealand Journal of Geology and Geophysics* 55(4):375–91. doi: 10.1080/00288306.2012.733947.
- Smith, GM, T. R. Davies, M. J. McSaveney, and D. H. Bell. 2006. "The Acheron Rock Avalanche, Canterbury, New Zealand- Morphology and Dynamics." *Landslides* 3(1):62–72. doi: 10.1007/s10346-005-0012-1.
- Spang, R. ., and R. . Rautenstrauch. 1988. "Empirical and Mathematical Approaches to Rockfall Protection and Their Practical Applications." 1237–43.
- Standards Australia and Standard New Zealand. 1997. "Occupational Protective Helmets." *AS/NZS 1801*.
- Stevens, Warren D. 1998. "RocFall: A Tool for Probabilistic Analysis, Design of Remedial Measures and Prediction of Rockfalls." University of Toronto.
- Stewart, S. 2007. "Rock Mass Strength and Deformability of Unweathered Closely Jointed New Zealand Greywacke." *University of Canterbury* 455.
- Stomakhin, A., C. Schroeder, L. Chai, J. Teran, and A. Selle. 2013. "A Material Point Method for Snow Simula-Tion." *ACM Trans. Graph* 32. doi: 10.1145/2461912.2461948.
- Tai, Y. C., and C. Y. Kuo. 2012. "Modelling Shallow Debris Flows of the Coulomb-Mixture Type over Temporally Varying Topography." *Natural Hazards and Earth System Sciences* 12(2):269–80. doi: 10.5194/nhess-12-269-2012.
- Tang, Chao Lung, Jyr Ching Hu, Ming Lang Lin, Jacques Angelier, Chia Yu Lu, Yu Chang Chan, and Hao Tsu Chu. 2009. "The Tsaoling Landslide Triggered by the Chi-Chi Earthquake, Taiwan: Insights from a Discrete Element Simulation." *Engineering Geology* 106(1–2):1–19.
- Teich, Michaela, Perry Bartelt, Adrienne Grêt-Regamey, and Peter Bebi. 2012. "Snow Avalanches in Forested Terrain: Influence of Forest Parameters, Topography, and Avalanche Characteristics on Runout Distance." *Arctic, Antarctic, and Alpine Research* 44(4):509–19. doi: 10.1657/1938-4246-44.4.509.
- Toševski, Aleksandar, Davor Pollak, Z. . Enko, Dunja Aljinovic´d, Aljinovic´ Aljinovic´d, and Neven Tadej. 2010. "Some Engineering Properties of Limestone: Tunnel StraÅ¾ina Case Study (Croatia)." *Tunnelling and Underground Space Technology*. doi: 10.1016/j.tust.2010.08.004.
- Varnes, David J. 1978. "Slope Movement Types and Processes." Pp. 11–33 in *Special report*.
- Whalley, W. B. 1984. "Rockfalls." Pp. 217–56 in *Slope Instability*. John Wiley and Sons Ltd.

# ANNEXES

---

## **Annexe 1: Script for the input data creation of RF3D**

The included .bat files (scripts) automatically create input rasters for RF3D on the basis of template shapefiles.

The .bat file SAGA\_Rockyfor\_vector2raster\_terrain creates the required basic input rasters (rockdensity.asc, d1.asc, rg70.asc, ... etc.)

The .bat file SAGA\_Rockyfor\_vector2raster\_forest creates the required rasters for a simulation with forest rasters (nrtrees.asc, dbhmean.asc, ... etc.)

The .bat file SAGA\_Rockyfor\_vector2raster\_rockfall\_net creates the required rasters for a simulation with nets (net\_number.asc, net\_height.asc, ... etc.)

-----

### Working steps

1. Download SAGA-GIS version 4 (from [www.saga-gis.org](http://www.saga-gis.org))
2. Extract the complete directory structure from this zip file into your SAGA-GIS program directory (for example, C:\programfiles\SAGA-GIS\RF3D\_script)
3. Edit the .bat file in a text editor, such as notepad, and adapt the path of the SAGA directory in line 3: set SAGA\_FOLDER=C:\programfiles\SAGA-GIS: then save and close
4. Copy the empty shapefile templates from the directory TEMPLATES\_SHP into your working directory
5. Prepare your input data using the copied shapefile templates and copy these files in the directory INPUT. The data required for running the scripts is always dem.asc & terrain.shp, or dem.asc & forest.shp, or dem.asc & rockfall\_net.shp.
5. Next double-click on the .bat file of your choice and the input rasters for RF3D files will be created in the directory OUTPUT.

-----

### Additional info:

- the directory TEMP is empty, except during file conversion
- the shapefile, attribute and directory names in the script have to be precisely respected; if not the script does not function! Therefore, please use the empty shapefile templates from the directory TEMPLATES\_SHP in your GIS.

By courtesy of Guillaume Favre-Bulle, GeoVal (CH), who developed the basis for these scripts

Luuk Dorren, May 2017  
 Int. ecorisQ Association

## Annex 2: Script for the input data creation of OpenLISEM

```

#! --matrixtable --lddout
#####
# Model: #
# Date: #
# Version: 1.0 #
# Author: Om #
#####

binding

initial

report grad.map = sin(atan(slope(dem.map)));

report ldd.map = lddcreate(dem_test.map,1e1,1e1,1e1,1e1);
report accuflux.map = accuflux(ldd.map,1.0);

report id.map = dem.map * 0.0 + 1.0;

#channel

report channelmask.map=scalar( if(accuflux.map gt 2500,1.0,0.0));
report channelldd.map= lddcreate (-accuflux.map *if(channelmask.map gt 0.5,
1.0),1e31,1e31,1e31,1e31);
report chandepth.map= channelmask.map*2* accuflux.map ** 0.32;
report channelwidth.map= channelmask.map*1* accuflux.map ** 0.083;
report channelgrad.map = grad.map;
report chanman.map = dem.map * 0.0 + 0.075;
report channelcoh.map= coh.map;
report chanksat.map=ksat1.map;

#soilmap
    
```

```

report                                     pefile:///D:/academia/Year                2/Internship/AIT-
GIC/LISEM/SRTM_godawari/dem_30m.mapr.map=exp(-2.0*ndvi.map/(1-
max(ndvi.map,0.02)));
report lai.map=max(0.01, ln(cover.map)/(-0.4));
report luclass.map= scalar (if(soiltype.map eq 3,1,if(soiltype.map eq 4,2,if(soiltype.map eq
6,3,4))););
#report luclass.map= soiltype.map;

report n.map = lookupscale(lu.tbl,2,luclass.map);
report rr.map = lookupscale(lu.tbl,1,luclass.map);
report ch.map = lookupscale(lu.tbl,3,luclass.map);
report clay1.map = lookupscale(lu_sed.tbl,1,luclass.map);
report sand1.map = lookupscale(lu_sed.tbl,2,luclass.map);
report gravell.map = lookupscale(lu_sed.tbl,3,luclass.map);

S = sand1.map;
C = clay1.map;
OM = organic.map;
Gravel = gravell.map;

OM = OM /100*1.72;
Densityfactor = 0.9;

# multiple regression eq
M1500    =-0.024*S+0.487*C+0.006*OM+0.005*S*OM-0.013*C*OM+0.068*S*C+0.031;
#W18)
M1500adj =M1500+0.14*M1500-0.02; #X18)
M33      =-0.251*S+0.195*C+0.011*OM+0.006*S*OM-0.027*C*OM+0.452*S*C+0.299;
#Y18)
M33adj = M33+(1.283*M33*M33-0.374*M33-0.015); #Z18)
PM33    = 0.278*S+0.034*C+0.022*OM-0.018*S*OM-0.027*C*OM-0.584*S*C+0.078;
#AA18)
PM33adj = PM33+(0.636*PM33-0.107); #AB18)
SatPM33 = M33adj + PM33adj; #AC18)
SatSadj = -0.097*S+0.043; #AD18)
SadjSat = SatPM33 + SatSadj; #AE18)
Dens_om = (1-SadjSat)*2.65; #AF18)
Dens_comp = Dens_om * Densityfactor; #AG18)
PORE_comp =(1-Dens_om/2.65)-(1-Dens_comp/2.65); #AI18)
M33comp = M33adj - 0.2*PORE_comp; #AJ18)
#output
report thetas1.map = cover(1-(Dens_comp/2.65),0.5); #AH18)
PoreMcomp = thetas1.map-M33comp; #AK18)
LAMBDA = (ln(M33comp)-ln(M1500adj))/(ln(1500)-ln(33)); #AL18)

```

```

GravelRedKsat=(1-Gravel)/(1-Gravel*(1-1.5*(Dens_comp/2.65))); #AM18)
report Ksat1.map =cover(1930*(PoreMcomp)**(3-LAMBDA)*GravelRedKsat,10.0);
#AN18)
report BD1.map = Gravel*2.65+(1-Gravel)*Dens_comp; #U18
report WP1.map = M1500adj;
report FC1.map = M33adj;
report PAW1.map = (M33adj - M1500adj)*(1-Gravel);

bB = (ln(1500)-ln(33))/((ln(FC1.map)-ln(WP1.map)));
aA = exp(ln(33) + bB*ln(FC1.map));

report psi1.map = cover(max(10, aA*(FC1.map + 0.7 * (thetas1.map - FC1.map))**-bB),0.0);
report thetai1.map = (FC1.map + 0.7 * (thetas1.map - FC1.map));

report zero.map = dem.map * 0.0;
report soildensity.map = lookupscalar(lu_soil.tbl,1,luclass.map);
report soilifa_raw.map = lookupscalar(lu_soil.tbl,2,luclass.map);
report soilrocksize.map = lookupscalar(lu_soil.tbl,3,luclass.map);
report soilifa.map= soilifa_raw.map*0.0174533;
report coh.map = lookupscalar(lu_soil.tbl,4,luclass.map);
report soildepth.map= zero.map+1;

report cohadd.map=coh.map;
report aggrstab.map = zero.map + 12;
report d50.map = zero.map + 60;
report d90.map = zero.map + 90;
report litter.map= zero.map *0;

report initiationtime.map=zero.map+2;
report initialfvolume.map=scarp.map*4;
report initialsvolume.map=scarp.map*10;
report initialsrocksize.map=scarp.map*0.5;
report initialsifa.map=soilifa.map;
report initialsdensity.map=zero.map+2200;
report debrismaterial.map=zero.map+1;
report rocksize.map=zero.map+3;
report rockdensity.map=soildensity.map;
report r

```

### Annexe 3: Example run file used in this research



[[openLISEM runfile version 1.0]

[Input]

Work Directory=D:/academia/Year 2/Multi hazard/Practicals bastian/  
 Map Directory=D:/academia/Year 2/Multi hazard/Practicals bastian/FINAL ASSIG/maps/  
 Include Rainfall=1  
 Rainfall Directory=D:/academia/Year 2/Multi hazard/Practicals bastian/rain/  
 Rainfall file=  
 Include Snowmelt=0  
 Snowmelt Directory=  
 Snowmelt file=  
 [display]  
 Image Directory=D:/academia/Year 2/Multi hazard/Practicals bastian/rain/  
 Image file=  
 Mask Directory=D:/academia/Year 2/Multi hazard/Practicals bastian/rain/  
 Mask file=  
 Include Image=0  
 Include Mask=0

[Output]

Result Directory=D:/academia/Year 2/Multi hazard/Practicals bastian/res/  
 Main results file=totals.txt  
 Filename point output=hydrograph.csv  
 Report point output separate=0  
 Timeplot as CSV=1  
 Timeplot as PCRaster=0  
 Report point output for SOBEK=0  
 SOBEK date string=10  
 Rainfall map=rainfall.map  
 Interception map=interception.map  
 Infiltration map=infiltration.map  
 Runoff map=runoff.map  
 Runoff fraction map=rofraction.map  
 Channel discharge map=chandism3.map  
 Erosion map=eros.map  
 Deposition map=depo.map  
 Soilloss map=soilloss.map  
 Filename landunit output=totlandunit.txt  
 Channel detachment map=chandet.map  
 Channel deposition map=chandep.map  
 WH max level map=whmax.map  
 Flood level map=floodmax.map  
 Flood time map=floodtime.map  
 Flood start time=floodstart.map  
  
 Channel Max Q=channelmaxq.map  
 Channel Max WH=channelmaxhw.map

Flood stats=floodstats.csv  
 Maximum Debris Flow Height Map=maxdebrisflowheight.map  
 Maximum Debris Flow Velocity Map=maxdebrisflowvelocity.map  
 Debris Flow Start Map=debrisflowstart.map  
 Entrainment Map=entrainment.map  
 Slope Failure Map=slopefailure.map  
 Minimum Safety Factor Map=minimumsafetyfactor.map

[Simulation times]

Begin time=0  
 End time=100  
 Timestep=.5

[General options]

Include Rainfall=1  
 Include snowmelt=0  
 No Erosion simulation=1  
 Include Erosion simulation=0  
 Advanced sediment=0  
 Include main channels=0  
 Include channel infil=0  
 Include channel baseflow=0  
 Hard Surfaces=0  
 Include road system=1  
 Include house storage=0  
 Include raindrum storage=0

[Interception]

Use canopy storage map=0  
 Canopy storage equation=1  
 Stemflow fraction=0,050  
 Canopy Openess=0,450  
 Include litter interception=0  
 Litter interception storage=1,00

[Infiltration]

Infil Method=3  
 Include compacted=0  
 Include crusts=0  
 Impermeable sublayer=0  
 Include percolation=0  
 Table Directory=  
 Table File=profile.inp  
 SWATRE internal minimum timestep=0.01  
 Matric head files=  
 Geometric mean Ksat=1  
 Use Water Repellency=0  
 Water Repellency A=1.2

Water Repellency B=0.3  
 Water Repellency C=0.12  
 Water Repellency D=1  
 Include tile drains=0  
  
 [Surface Flow]  
 Enable Solid Phase=0  
 Enable Entrainment=0  
 Enable Deposition=0  
 Enable Compaction=0  
 Enable Seismic=0  
 Enable Slope Stability=0  
 Enable Upslope Forcing=0  
 Enable Downslope Forcing=0  
 Include Bedrock Layer=0  
 Enable Slope Failure=0  
 Minimum Safety Factor=0,90  
 Maximum Safety Factor=1,30  
 Maximum safety factor for display=3,50  
 Entrainment Coefficient=0,00012  
 Minimum Entrainment Height=1,00  
 Minimum Failure Height=0,10  
 Spatially Dynamic Timestep=1  
 Limit Cores=0  
 Core Limit=1  
 Enable Levees=0  
 Enable Barriers=0  
 Enable Flow Barriers=0  
 Flow barrier table filename=flowbarriers.txt  
 Enable Inflow=0  
 Inflow table filename=inflow.txt  
 Include Initial FluidSolid Mixture=0  
 Include Forced FluidSolid Mixture=0  
 Inclue Maximum ChannelVolume=0  
 Inclue Maximum Volume=0  
 Flow Minimum Timestep=1,000  
 Kinematic Timestep Power=2,00  
 Surface Flow Courant Factor=0,25  
 Surface Flow Scheme=2  
 Drag Power Law Coefficient=1  
 Viscosity Alpha=1,00  
 Viscosity Beta=20,00  
 Minimal Flood Water Depth=0,00  
 Minimum Debris Flow Volumetric Sediment Fraction=0,00  
 Use HLL2=0  
 Solid-Fluid Drag Coefficient=0,50  
 Suspended Viscosity=0  
 Lax Multiplier=1,00

Friction force correction=1,00  
 Erosion Cohesion Calibration=1,00  
 Erosion Grain Size Calibration=1,00

[Kinetic Energy]

KE parameters EQ1=1,28,300,0,520,0,042  
 KE parameters EQ2=0,8,950,8,440  
 KE parameters EQ3=0,7,600,0,220  
 KE time based=0  
 Detachment efficiency=1  
 Use material depth=0

[Sediment]

Advanced sediment configuration=0  
 BL method=0  
 SS method=1  
 Estimate grain size distribution=1  
 Number of grain size classes (simulated)=2  
 Read grain distribution maps=0  
 Grain size class maps=2,20,50,125,250,500  
 Use material depth=0  
 Sigma diffusion=1,00  
 Limit TC=0  
 Limit Deposition TC=

[Conservation]

Include grass strips=0  
 Grassstrip Mannings n=0.1  
 Include buffers=0  
 Buffers impermeable=0  
 Sediment bulk density=1400  
 Include Sediment traps=0

[Calibration]

Ksat calibration=1,070  
 N calibration=1,000  
 Theta calibration=1,000  
 Psi calibration=1,000  
 Channel Ksat calibration=1,000  
 Channel N calibration=1,000  
 Erosive Power Calibration=1,00  
 Transport Capacity Calibration=1,00  
 Settling Velocity Calibration=1,00  
 Internal Friction Angle=0,20  
 Dynamic Viscosity Calibration=1,00  
 Drag Force Calibration=1,00  
 Solid Phase Friction Calibration=1,00  
 Release Volume Calibration=1,00

Limit Failure=0  
 Soil Cohesion Calibration=1,00  
 Soil Internal Friction Angle Calibration=1,00  
 Soil Depth Calibration=1,00  
 Create Stable Initial Safety Factor=0  
 Minimum Safety Factor Calibration=1,00000  
 Splash Delivery Ratio=0,10  
 Particle Cohesion of Deposited Layer=0,50

[OpenGL visualization]  
 Light\_Ambient\_R=1,00  
 Light\_Ambient\_G=1,00  
 Light\_Ambient\_B=1,00  
 Light\_Ambient\_A=0,30  
 Light\_Directional\_R=1,00  
 Light\_Directional\_G=1,00  
 Light\_Directional\_B=1,00  
 Light\_Directional\_A=0,70  
 Light\_Directional\_X=-1,00  
 Light\_Directional\_Y=-1,00  
 Light\_Directional\_Z=-1,00  
 Surface\_Draw=1  
 Surface\_Micro\_Elevation\_Scale=100  
 Surface\_Mipmap\_Distance\_1=15000  
 Surface\_Mipmap\_Distance\_2=50000  
 Surface\_Vegetated\_Small\_Color\_R=0.3  
 Surface\_Vegetated\_Small\_Color\_G=0.5  
 Surface\_Vegetated\_Small\_Color\_B=0  
 Surface\_Vegetated\_Large\_Color\_R=0.06  
 Surface\_Vegetated\_Large\_Color\_G=0.1  
 Surface\_Vegetated\_Large\_Color\_B=0.04  
 Surface\_Bare\_Color\_R=0.20  
 Surface\_Bare\_Color\_G=0.16  
 Surface\_Bare\_Color\_B=0.03  
 Surface\_Roads\_Color\_R=0.1  
 Surface\_Roads\_Color\_G=0.1  
 Surface\_Roads\_Color\_B=0.1  
 Surface\_Buildings\_Color\_R=0.3  
 Surface\_Buildings\_Color\_G=0.3  
 Surface\_Buildings\_Color\_B=0.3  
 Surface\_Erosion\_Color\_R=0.15  
 Surface\_Erosion\_Color\_G=0.14  
 Surface\_Erosion\_Color\_B=0.04  
 Surface\_Erosion\_Color\_A=1  
 Surface\_Deposition\_Color\_R=0.35  
 Surface\_Deposition\_Color\_G=0.33  
 Surface\_Deposition\_Color\_B=0.13  
 Surface\_Deposition\_Color\_A=1

Water\_Draw=100  
Water\_Reflectivity=100  
Water\_Refractivity=100  
Water\_Velocity\_Scale=100  
Water\_Micro\_Elevation\_Scale=100  
Water\_Transparancy=100  
Water\_Deep\_Color\_R=0.1  
Water\_Deep\_Color\_G=0.1  
Water\_Deep\_Color\_B=1.0  
Water\_Deep\_Color\_A=0.8  
Water\_Shallow\_Color\_R=0.8  
Water\_Shallow\_Color\_G=0.6  
Water\_Shallow\_Color\_B=1.0  
Water\_Shallow\_Color\_A=0.05  
Water\_Sediment\_Color\_R=0.15  
Water\_Sediment\_Color\_G=0.14  
Water\_Sediment\_Color\_B=0.04  
Water\_Sediment\_Color\_A=1.0  
Roads\_Draw=0  
Rain\_Draw=0  
Clouds\_Draw=0  
Roads\_Distance=2000  
Buildings\_Draw=0  
Buildings\_Distance=200000  
Trees\_Draw=0  
Trees\_Distance=200000  
Trees\_Instances=1000000  
Trees\_Increment=1500  
Grass\_Draw=0  
Grass\_Distance=10000  
Grass\_Instances=200000  
Grass\_Increment=200  
Grass\_Vertical\_Scale=100.0

[Output maps]

Runoff maps in l/s/m=  
Timeseries as PCRaster=0  
Erosion map units (0/1/2)=0  
Regular runoff output=1  
Output interval=1  
User defined output=0  
Output times=0  
CheckOutputMaps=0,0  
CheckOutputMapsNUT=  
CheckOutputMapsMC=  
CheckOutputMapsGUL=

[Texture classes]

ClassMu=

[map names]

[OutputBASIC]

OUTRUNOFF=ro

OUTCONC=conc

OUTWH=wh

OUTRWH=roc

OUTTC=tc

OUTEROS=det

OUTDEPO=dep

OUTSOILLOSS=sloss

OUTVELO=velo

OUTINF=inf

OUTSS=sstor

OUTCHVOL=chvol

OUTTILED=Qtile

OUTHMX=hmx

OUTQF=qf

OUTVF=vf

OUTHMXWH=hmxwh

OUTSED=sed

OUTSAFETYFACTOR=safa

OUTSLOPEFAILURE=slfa

OUTDFHEIGHT=dfh

OUTDFV=dfv

OUTFPH=fph

OUTSPH=sph

OUTENTRAINMENT=entr

OUTTIMESTEP=ts

[Rainfall]

ID=ID.map

[Catchment]

dem=dem.map

grad=grad.map

ldd=ldd.map

outlet=outlet.map

outpoint=outpoint.map

watershed=ws.map

[Landuse]

landunit=landunit.map

cover=per.map

litter=litter.map

lai=lai.map



ch=ch.map  
road=roadwidt.map  
grasswidth=grasswid.map  
smax=smax.map

[Surface]

rr=rr.map  
manning=n.map  
stonefrc=stonefrc.map  
crustfrc=crustfrc.map  
compfrc=compfrc.map  
hardsurf=hardsurf.map

[Erosion]

coh=coh.map  
cohadd=cohadd.map  
aggrstab=aggrstab.map  
d50=d50.map  
d90=d90.map  
detmat=detmat.map  
sedmixdepth=sedmixdeth.map

[Slope Stability]

[Slope Stability]

soildensity=soildensity.map  
soilifa=soilifa.map  
soilrocksize=soilrocksize.map  
failuremask=failuremask.map  
soilstructured=soilstructured.map  
[Bottom layer Slope Stability]  
soildensity2=soildensity2.map  
soilifa2=soilifa2.map  
soilcohesion2=soilcohesion2.map  
soilrocksize2=soilrocksize2.map  
soilstructured2=soilstructured2.map

[Seismic Trigger]

pga=pga.map  
pgatiming=pgatiming.map

[Entrainment]

debrismaterial=debrismaterial.map  
rocksize=rocksize.map  
rockdensity=rockdensity.map  
rockifa=rockifa.map

[Infiltration]

[Swatre]

profmap=profile.map

profcrst=profcrst.map  
 profwltr=profwltr.map  
 profgras=profgras.map  
 inithead=inithead  
 repelcell=repel.map  
 [1st layer Green&Ampt/Smith&Parlange]  
 ksats1=ksats1.map  
 psi1=psi1.map  
 thetas1=thetas1.map  
 thetai1=thetai1.map  
 soildep1=soildep1.map  
 [2nd layer Green&Ampt/Smith&Parlange]  
 ksats2=ksats2.map  
 psi2=psi2.map  
 thetas2=thetas2.map  
 thetai2=thetai2.map  
 soildep2=soildep2.map  
 [Ksat subtraction]  
 ksats1simple=ksats1.map  
 [Special surfaces]  
 ksatscrst=ksatscrst.map  
 ksatscomp=ksatscomp.map  
 ksatsgras=ksatsgras.map  
  
 [Channels]  
 [Channel properties]  
 lddchan=lddchan.map  
 chanwidth=chanwidth.map  
 chanside=chanside.map  
 changrad=changrad.map  
 chanman=chanman.map  
 chancoh=chancoh.map  
 chandetmat=chandetmat.map  
 chansedmixdepth=chansedmixdeth.map  
 [Channel Infil]  
 chanksat=chanksat.map  
 [Channel BaseFlow]  
 baseflow=baseflow.map  
 inflowidCh=inflowidch.map  
 inflowid=inflowid.map  
  
 [Surface Flow]  
 [Flow barriers]  
 barriers=barriers.map  
 flowbarrierindex=flowbarrierindex.map  
 maxvol=maxvolume.map  
 [Flow Limiting]  
 chandepth=chandepth.map

```

chanlevee=chanlevee.map
channelmaxvol=channelmaxvolume.map
channelconnected=channelconnected.map
[Initial Volume]
initiationtime=initiationtime.map
initialfvolume=initialfvolume.map
initialsvolume=initialsvolume.map
initialsdensity=initialsdensity.map
initialsrocksize=initialsrocksize.map
initialsifa=initialsifa.map
[Forced Volume condition]
forcedfvolume=forcedfvolume.map
forcedsvolume=forcedsvolume.map
forcedsdensity=forcedsdensity.map
forcedsrocksize=forcedsrocksize.map
forcedsifa=forcedsifa.map
[Flow cell boundary based Barriers]
flowbarrierindex=flowbarrierindex.map
flowbarriercrit=fbcrit.map

```

```

[Snowmelt]
SnowID=snowid.map

```

```

[Houses]
housecover=housecover.map
roofstore=roofstore.map
drumstore=drumstore.map

```

#### **Annex 4: Example script for calibration**

```

array<double> paramvalues;
array<double> paramvalues2;
array<double> paramvalues3;

array<double> errorvalues;

double Calibrate(array<double> params)
{
//write to list
paramvalues.Resize(paramvalues.length() + 1);
paramvalues[paramvalues.length()-1] = params[0];
paramvalues2.Resize(paramvalues2.length() + 1);
paramvalues2[paramvalues2.length()-1] = params[1];
paramvalues3.Resize(paramvalues3.length() + 1);
paramvalues3[paramvalues3.length()-1] = params[2];

RunModel("true_calibration_acheron.run","Initial          Solid          IFA_cal_mult="+
ToString(params[0]) +"|" + "Manning_cal_mult="+ ToString(params[1])+"|" + "Initial Fluid
Height_cal_mult="+ ToString(params[2]));

```

```

Map impact = LoadMap("try/hsmax.map");
Map inventory = LoadMap("maps/impact.tif");
double errorval = MapContinuousCohensKappa(inventory,impact,0.5);
errorvalues.Resize(errorvalues.length() + 1);
errorvalues[errorvalues.length()-1] = (errorval);

Print("PV-IFA:" + ToString(params[0])+ "PV-Mannings N:"+ToString(params[1])+" Kappa "
+ ToString(errorval)+ "Initial Fluid Height:"+ToString(params[2]));
Table t;
t.SetSize(paramvalues.length(),4);
for(int i =0; i < paramvalues.length(); i = i+1)
{
t[i,0] = paramvalues[i];
t[i,1] = paramvalues2[i];
t[i,2] = paramvalues3[i];
t[i,3] = errorvalues[i];
}
//write table to disk
paramvals_final_cal1_acheron.tbl = t;
return (1-errorval);
}

void main()
{
paramvalues = {};
OptimizeCustom({1.0,1.0,1.0},@Calibrate,0.01,0.8);
}

```